

Aus dem Max-Planck-Institut für Kolloid- und Grenzflächenforschung  
Abteilung Grenzflächen

---

**Multilayer capsules with stimuli-sensitive properties:  
pH-response and carbohydrate-sensing**

Dissertation  
zur Erlangung des akademischen Grades  
"doctor rerum naturalium"  
(Dr. rer. nat.)  
in der Wissenschaftsdisziplin Physikalische Chemie

eingereicht an der  
Mathematisch-Naturwissenschaftlichen Fakultät  
der Universität Potsdam

von  
Tatjana Mauser  
geboren am 30. Mai 1978 in Mannheim

Potsdam, den 28. August 2006

**Vorsitzender:** Prof Dr. Bechmann

**Gutachter:** Prof. Dr. Möhwald, Prof. Dr. v. Klitzing, Prof. Dr. Zemb

**Beisitzer:** Prof. Dr. Möhwald, Prof. Dr. v. Klitzing, Prof. Dr. Sukhorukov, Prof. Dr. Strauch, Prof. Dr. Beuermann, Dr. habil. Tauer

**Tag der mündlichen Prüfung:** 13.02.2007

## Abstract

Polyelectrolyte microcapsules containing stimuli-responsive polymers have potential applications in the fields of sensors or actuators, stimuable microcontainers and controlled drug delivery. Such capsules were prepared, with the focus on pH-sensitivity and carbohydrate-sensing.

First, pH-responsive polyelectrolyte capsules were produced by means of electrostatic layer-by-layer assembly of oppositely charged weak polyelectrolytes onto colloidal templates that were subsequently removed. The capsules were composed of poly(allylamine hydrochloride) (PAH) and poly(methacrylic acid) (PMA) or poly(4-vinylpyridine) (P4VP) and PMA and varied considerably in their hydrophobicity and the influence of secondary interactions. These polymers were assembled onto  $\text{CaCO}_3$  and  $\text{SiO}_2$  particles with diameters of  $\sim 5 \mu\text{m}$ , and a new method for the removal of the silica template under mild conditions was proposed. The pH-dependent stability of PAH/PMA and P4VP/PMA capsules was studied by confocal laser scanning microscopy (CLSM). They were stable over a wide pH-range and exhibited a pronounced swelling at the edges of stability, which was attributed to uncompensated positive or negative charges within the multilayers. The swollen state could be stabilized when the electrostatic repulsion was counteracted by hydrogen-bonding, hydrophobic interactions or polymeric entanglement. This stabilization made it possible to reversibly swell and shrink the capsules by tuning the pH of the solution. The pH-dependent ionization degree of PMA was used to modulate the binding of calcium ions. In addition to the pH-sensitivity, the stability and the swelling degree of these capsules at a given pH could be modified, when the ionic strength of the medium was altered. The reversible swelling was accompanied by reversible permeability changes for low and high molecular weight substances. The permeability for glucose was evaluated by studying the time-dependence of the buckling of the capsule walls in glucose solutions and the reversible permeability modulation was used for the encapsulation of polymeric material. A theoretical model was proposed to explain the pH-dependent size variations that took into account an osmotic expanding force and an elastic restoring force to evaluate the pH-dependent size changes of weak polyelectrolyte capsules.

Second, sugar-sensitive multilayers were assembled using the reversible covalent ester formation between the polysaccharide mannan and phenylboronic acid moieties that were grafted onto poly(acrylic acid) (PAA). The resulting multilayer films were sensitive to several carbohydrates, showing the highest sensitivity to fructose. The response to carbohydrates resulted from the competitive binding of small molecular weight sugars and mannan to the boronic acid groups within the film, and was observed as a fast dissolution of the multilayers, when they were brought into contact with the sugar-containing solution above a critical concentration. It was also possible to prepare carbohydrate-sensitive multilayer capsules, and their sugar-dependent stability was investigated by following the release of encapsulated rhodamine-labeled bovine serum albumin (TRITC-BSA).

# Contents

<b>1</b>	<b>Introduction</b>	<b>1</b>
<b>2</b>	<b>Literature review</b>	<b>3</b>
2.1	Polyelectrolytes in solution . . . . .	3
2.1.1	Conformation of polyelectrolytes . . . . .	3
2.1.2	Weak and strong polyelectrolytes . . . . .	5
2.2	Polyelectrolyte complexes . . . . .	6
2.3	Adsorption of polyelectrolytes at interfaces . . . . .	6
2.4	Layer-by-layer electrostatic self-assembly . . . . .	7
2.4.1	Assembly of thin films on flat substrates . . . . .	7
2.4.2	Preparation of hollow capsules . . . . .	9
2.5	Interactions within multilayers . . . . .	11
2.5.1	Electrostatic interactions . . . . .	11
2.5.2	Hydrophobic interactions . . . . .	12
2.5.3	Hydrogen-bonding interactions . . . . .	13
2.5.4	Specific interactions . . . . .	13
2.6	Stimuli-responsive multilayer thin films . . . . .	13
2.6.1	Incorporation of stimuli-sensitive polymers into multilayers . . . . .	13
2.6.2	Weak polyelectrolytes for pH-sensitive multilayers . . . . .	14
2.6.3	Multilayer films for saccharide-sensing . . . . .	17
2.7	Permeability of polyelectrolyte capsules . . . . .	19
2.7.1	Permeability for low and high molecular weight compounds . . . . .	19
2.7.2	Capsules as encapsulation vehicles . . . . .	20
<b>3</b>	<b>Methods</b>	<b>22</b>
3.1	UV-VIS Spectroscopy . . . . .	22
3.2	Fluorescence Spectroscopy . . . . .	22
3.3	Confocal Laser Scanning Microscopy . . . . .	23
3.4	Infrared Spectroscopy . . . . .	25

---

3.5	Measurement of the electrophoretic mobility . . . . .	26
3.5.1	The electric double layer . . . . .	26
3.5.2	Determination of the $\zeta$ -potential . . . . .	27
3.6	Single Particle Light Scattering . . . . .	28
3.7	Quartz Crystal Microbalance . . . . .	28
3.8	Atomic Force Microscopy . . . . .	29
3.9	Scanning Electron Microscopy . . . . .	30
<b>4</b>	<b>Experimental Section</b>	<b>31</b>
4.1	Materials . . . . .	31
4.2	Syntheses . . . . .	32
4.2.1	Labeling of PAH and BSA . . . . .	32
4.2.2	Labeling of PMA . . . . .	32
4.2.3	Coupling of 3-aminophenylboronic acid to poly(acrylic acid) . . . . .	33
4.2.4	Coupling of dithiodiglycolic acid to 3-aminophenylboronic acid . . . . .	33
4.2.5	Synthesis of CaCO <sub>3</sub> microparticles . . . . .	34
4.2.6	Synthesis of BSA-CaCO <sub>3</sub> microparticles . . . . .	34
4.3	Capsule preparation . . . . .	35
4.3.1	LbL assembly on colloidal particles . . . . .	35
4.3.2	Core dissolution . . . . .	36
4.3.3	Encapsulation of FITC-dextran . . . . .	36
4.4	Measurement conditions . . . . .	37
4.4.1	pH-measurements . . . . .	37
4.4.2	Potentiometric titrations . . . . .	37
4.4.3	Elemental analysis . . . . .	37
4.4.4	Nuclear Magnetic Resonance . . . . .	38
4.4.5	Confocal Laser Scanning Microscopy . . . . .	38
4.4.6	Determination of the osmotic deformation . . . . .	38
4.4.7	Determination of the capsule concentration . . . . .	39
4.4.8	UV-VIS Spectroscopy . . . . .	39
4.4.9	Fluorescence Spectroscopy . . . . .	39
4.4.10	Infrared Spectroscopy . . . . .	39
4.4.11	Single Particle Light Scattering . . . . .	40
4.4.12	Measurement of the electrophoretic mobility . . . . .	40
4.4.13	Quartz Crystal Microbalance . . . . .	40
4.4.14	Atomic Force Microscopy . . . . .	41

---

4.4.15	Scanning Electron Microscopy . . . . .	41
4.4.16	Energy-Dispersive-X-ray analysis . . . . .	41
<b>5</b>	<b>Weak polyelectrolyte capsules</b>	<b>42</b>
5.1	Introduction . . . . .	42
5.2	PAH/PMA capsules templated on CaCO <sub>3</sub> . . . . .	43
5.2.1	Titration experiments . . . . .	43
5.2.2	Capsule preparation . . . . .	44
5.2.3	pH-dependent stability of (PAH/PMA) <sub>2</sub> capsules . . . . .	45
5.3	PAH/PMA capsules templated on SiO <sub>2</sub> . . . . .	48
5.3.1	Dissolution of SiO <sub>2</sub> with HF . . . . .	48
5.3.2	pH-dependent stability of (PAH/PMA <sub>75kDa</sub> ) <sub>4</sub> capsules . . . . .	51
5.3.3	pH-dependent stability of (PAH/PMA <sub>790kDa</sub> ) <sub>4</sub> capsules . . . . .	52
5.3.4	Influence of ionic strength on (PAH/PMA <sub>790kDa</sub> ) <sub>4</sub> capsules . . . . .	54
5.3.5	Investigation of the role of calcium-ions on the multilayer stability . . . . .	55
5.4	P4VP/PMA capsules . . . . .	58
5.4.1	Formation of P4VP/PMA multilayers on silica templates . . . . .	58
5.4.2	Formation of capsules . . . . .	61
5.4.3	pH-dependent behavior of P4VP/PMA capsules . . . . .	64
5.4.4	Influence of ionic strength on the pH-dependent stability . . . . .	67
5.4.5	Permeability of (P4VP/PMA) <sub>4</sub> capsules for low molecular weight compounds . . . . .	69
5.4.6	Permeability of (P4VP/PMA) <sub>4</sub> capsules for polymers at pH 8 . . . . .	74
5.5	Theoretical model for pH-dependent capsule swelling . . . . .	76
5.5.1	Development of the theoretical model . . . . .	76
5.5.2	Modeling the experimental data . . . . .	80
<b>6</b>	<b>Carbohydrate-sensitive multilayers</b>	<b>84</b>
6.1	Introduction . . . . .	84
6.2	Polymers used in the multilayer assembly . . . . .	84
6.3	Sugar-sensitive multilayers on flat substrates . . . . .	85
6.3.1	Formation of multilayers as a function of pH . . . . .	85
6.3.2	Stability of multilayers with increasing sugar concentration . . . . .	88
6.3.3	pH-dependent stability of multilayers with increasing fructose concentration . . . . .	90
6.4	Sugar-sensitive capsules . . . . .	91
6.4.1	Preparation of capsules . . . . .	91

6.4.2	Stability of capsules with increasing sugar concentration . . . . .	93
<b>7</b>	<b>Summary and conclusion</b>	<b>95</b>
	<b>Bibliography</b>	<b>99</b>
	<b>List of publications</b>	<b>108</b>
	<b>Acknowledgements</b>	<b>109</b>

# 1 Introduction

The interaction of materials with their environment depends on the properties of their surfaces. By modifying the surface characteristics these interactions can be altered. One possibility of a specific modification and functionalization is given by the layer-by-layer (LbL) technique. This method was developed in the 1990s by Decher et al. for the assembly of multilayers of polyelectrolytes and has received increasing interest, as it provides nanoscale control of the deposition of composite materials [1]. Although these multilayers are most frequently formed by electrostatic interactions between polycations and polyanions, the LbL process has also been carried out using H-bond interactions [2] or specific recognition between molecules for the deposition of multilayers, e.g. biotin - avidin and sugar - lectin interactions [3,4].

In addition to the assembly of thin films on flat substrates, the LbL deposition can also be used for the coating of colloidal particles, and by subsequent dissolution of the template this procedure leads to the formation of hollow polyelectrolyte capsules [5,6]. The properties of these thin membranes can be tuned by the polymers that are adsorbed onto the colloids. Multilayer shells combine the advantages of a high surface area with nanoscale control of the chemical composition of the film.

For many future applications of polyelectrolyte capsules, such as stimuable microdevices, fabrication of sensors or actuators, and controlled delivery or release of chemicals and drugs, it is desirable to regulate the multilayer wall in response to various external stimuli, like temperature, pH, ionic strength, light, magnetic field, and chemical stimuli. The responses can vary from a tunable permeability to morphological and size changes. For many applications of stimuli-responsive systems the reversibility of modifications is a key parameter [7,8].

Compared to traditional responsive materials like hydrogels and polyelectrolyte complexes these multilayers have the advantage of combining specific response characteristics with the versatility and flexibility of the LbL technique. The aim of this work was the development of stimuli-responsive microcapsules, with the focus on pH-sensitivity and carbohydrate-sensing.

pH-responsive properties of multilayer thin films can be observed when polyelectrolytes with weak acid and base functionalities are incorporated within the layers, as the magnitude of



electrostatic and secondary interactions within these assemblies can be tuned through variation of the polyelectrolyte charge density by changing the solution pH. At extreme pH, multilayers composed of weak polyelectrolytes can be destroyed, as the pH-induced imbalance of charges overcompensates the attractive polymer-polymer ionic binding. pH-induced variations in the stability of polyelectrolyte multilayers have potential applications in medicine and biotechnology, as the amount of ion pairs is related with changes in the permeability of the capsule membrane that can be controlled by solution pH. Alterations in permeability can be used for the uptake and release of drugs and chemicals and this is of particular interest when the changes in the capsule wall stability occur in the neutral pH range, which is mandatory for many biomolecules.

Whereas many stimuli-responsive multilayers have been prepared that change characteristic properties in dependence on temperature, pH and ionic strength, only few examples can be found that respond to chemical stimuli. A challenging class of chemical stimuli are carbohydrates, because of the outstanding role these substances play in medicine and biology as well as in industrial processes. The concentration of these molecules in solution can be monitored, when the decomposition of a polyelectrolyte multilayer is triggered by a specific recognition event. Such recognition and replacement reactions open rich possibilities for future applications and explorations of polyelectrolyte membranes for the release of bioactive molecules in response to biological or chemical stimuli.

In this work, a systematic investigation of different possibilities to stabilize weak polyelectrolyte capsules by attractive forces like entanglement, hydrophobic and H-bonding interactions was carried out. For this purpose two different weak polyelectrolyte combinations were selected that vary considerably in their hydrophobic stabilization, capsules composed of poly(allylamine hydrochloride) (PAH) and poly(methacrylic acid) (PMA) and capsules composed of poly(4-vinylpyridine) (P4VP) and PMA. The influence of pH variations and ionic strength on the stability, size and permeability of these capsules was investigated and the pH-dependent changes in permeability were used for the encapsulation of polymers. Furthermore, a theoretical model for the pH-dependent size variations was proposed.

Carbohydrate-sensitive multilayers were assembled by the formation of a reversible covalent ester-bond between a polysaccharide and a phenylboronic acid moiety that was grafted onto poly(acrylic acid) (PAA), and the sensitivity of the resulting multilayer films to several carbohydrates was investigated.

## 2 Literature review

### 2.1 Polyelectrolytes in solution

#### 2.1.1 Conformation of polyelectrolytes

Polyelectrolytes combine the basic concepts of polymers and electrolytes. The main difference to other polymeric systems is, that a fraction or all of the monomeric units consist of ionizable functional groups. When polyelectrolytes are dissolved in polar solvents like water, the ion-pairs dissociate, resulting in charges that are fixed to the polymeric backbone, and small counterions that are released into the solution. Polyelectrolytes are very common in nature and prominent examples are proteins, nucleic acids and charged polysaccharides. Depending on the ionic groups present in the macromolecule, it is possible to distinguish cationic and anionic polyelectrolytes, which carry positive and negative charges, respectively. Furthermore one can distinguish strong and weak polyelectrolytes. Strong polyelectrolytes have permanent charges and are ionized over the whole pH range, whereas weak polyelectrolytes are only ionized in a limited pH range. Examples of the different types of polyelectrolytes are given in Figure 2.1. Strong polyelectrolytes are e.g. the polyanion sodium poly(styrene sulfonate) (PSS) and the polycation poly(diallyldimethylammonium

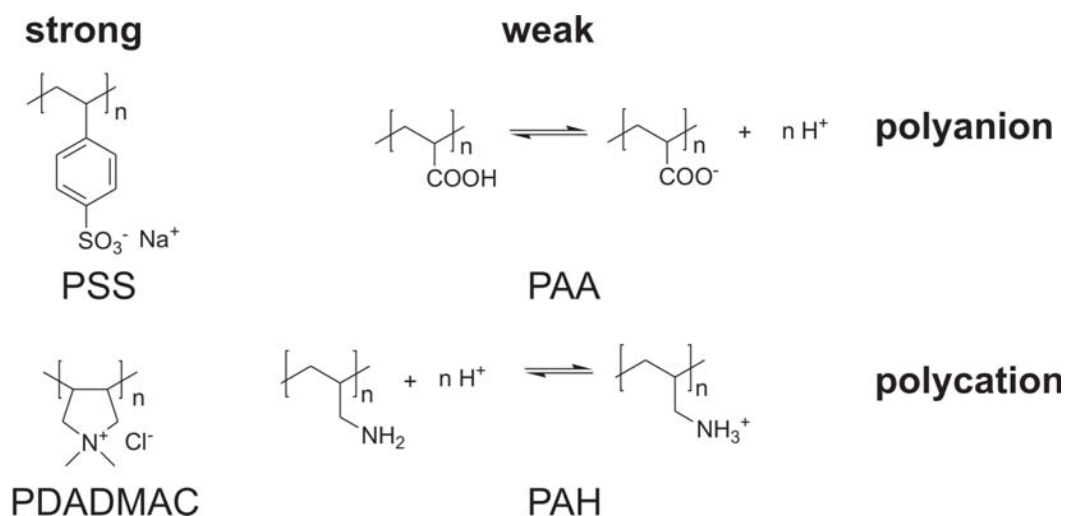


Figure 2.1: Examples of strong and weak polyelectrolytes.

chloride) (PDADMAC). PAH is an example of a weak polybase (polycation), whereas PAA is a weak polyacid (polyanion).

It is also possible to integrate cationic and anionic groups into one single macromolecule, resulting in polyampholytes. These systems are often composed of weakly acidic and basic groups, so that the sign and the magnitude of the net charge depends on the pH. At a characteristic pH value, the isoelectric point, no free net charge exists.

The conformation of a polyelectrolyte in solution depends on the polymer concentration, the interactions with the solvent and the chain length. Furthermore it depends on the acid or base strength of the ionic groups, the linear charge density, as well as the charge distribution along the chain and the nature of the counterions. The importance of these parameters is given by the repulsive electrostatic interactions between the charges along the polymeric backbone, which result in a stretched chain conformation in aqueous medium or in electrolyte solutions with low ionic strength. The stiffness of a polymer can be described by the persistence length  $q_p$ , which is the length over which the chain remains stretched. The persistence length of polyelectrolytes is given as the sum of the steric persistence length  $q_0$  that an uncharged polymer would have and the electrostatic contribution  $q_e$ ,

$$q_p = q_0 + q_e \quad . \quad (2.1)$$

The electrostatic contribution to the persistence length is given by

$$q_e = \frac{l_B}{4} \left( \frac{\kappa^{-1}}{l_{\text{eff}}} \right)^2 \quad (2.2)$$

with the Bjerrum length  $l_B$ , the Debye length  $\kappa^{-1}$  and the effective distance between charges  $l_{\text{eff}}$  [9]. The Bjerrum length relates the electrostatic interaction energy with the thermal energy according to

$$l_B = \frac{e^2}{4\pi\epsilon kT} \quad (2.3)$$

with the elementary charge  $e$ , the dielectric constant of the solvent  $\epsilon$  and the thermal energy  $kT$ . The Bjerrum length is defined as the distance between charges at which the electrostatic interaction equals the thermal energy, which is  $l_B = 0.7$  nm at room temperature for water. The distribution of counterions depends significantly on the interaction strength among the charged units. Counterion condensation occurs, if the distance between charges on the chain is smaller than the Bjerrum length (Manning condensation).

The electrostatic interactions can be influenced by the charge density of the polyelectrolytes and by the screening of charges due to electrolytes in solution. When the ionic strength of a solution is increased, the charges along the polymeric backbone are screened. This can promote a change from a rodlike to a coiled conformation of the polyelectrolyte [9–11]. The

ionic strength of the solution is related with the electrostatic potential of a charge by the Debye length  $\kappa^{-1}$ , which is defined as

$$\kappa^{-1} = (8\pi l_B c_n)^{-\frac{1}{2}} \quad (2.4)$$

with the number concentration of salt molecules per unit volume  $c_n$ . The Debye length is the characteristic length of the exponential decay of the electrostatic potential of a charge with increasing distance. A more detailed description of the behavior of polyelectrolytes in solution is given in [10–12].

### 2.1.2 Weak and strong polyelectrolytes

For strong polyelectrolytes the charge density along the chains is given by the density of dissociable groups. For weak polyelectrolytes the charge of the chain is not fixed but the degree of dissociation of the ionizable groups is determined by the external pH. For a weak polyacid (as well as for the conjugate acid of a weak polybase) the charge density is governed by the acid-base equilibrium



with the uncharged polyelectrolyte segment HA, the negatively charged segment  $\text{A}^-$  and the proton  $\text{H}^+$ . In contrast to dilute solutions of monoacids or monobases, in weak polyelectrolytes each functional group is influenced by all other groups of the polymer due to their electrostatic interactions. In principle, each binding site for a proton has a different equilibrium constant, depending on the surrounding. Furthermore, the acidity of polymeric acids decreases during the dissociation because of the electrostatic effect of the increasing charge of the polymeric anion, that depends largely on the distance between the acid groups of the polymer. The overall equilibrium of the dissociation is summarized in one single apparent equilibrium constant  $K_{\text{app}}$ , that is given by

$$K_{\text{app}} = \frac{[\text{H}^+][\text{A}^-]}{[\text{HA}]}, \quad (2.6)$$

and the degree of dissociation  $\alpha$  is usually defined as

$$\alpha = \frac{[\text{A}^-]}{[\text{A}^-] + [\text{HA}]} . \quad (2.7)$$

The apparent dissociation constant is generally expressed as its negative base-10 logarithm  $\text{p}K_{\text{app}}$ , which is given by a modified Henderson-Hasselbach equation that takes into account the electrostatic interaction along the chain by an empirical parameter  $n$  [13, 14],

$$\text{p}K_{\text{app}} = \text{pH} - n \cdot \log \left( \frac{\alpha}{1 - \alpha} \right) . \quad (2.8)$$

The  $pK_{app}$  depends on the dissociation degree  $\alpha$ , the pH and the ionic strength of the solution. On the other hand, the intrinsic equilibrium constant  $pK_i$  corresponds to the intrinsic strength of the acid groups of the polymer, i.e. in the limiting value for zero degree of ionization and is independent of pH and ionic strength.

## 2.2 Polyelectrolyte complexes

Polyelectrolyte complexes are formed when a solution of a polycation is mixed with a polyanion solution. The complexation results in precipitation of the polyelectrolytes. A 1:1 stoichiometry is often found for strong polyelectrolytes. In addition to Coulombic interaction the driving force of this reaction is the gain in entropy from the release of counterions of the individual polyelectrolytes. The formation of polyelectrolyte complexes depends on the electrostatic interaction of oppositely charged groups. Screening of these moieties by increasing the ionic strength of the solution results in a decrease of the ionic interactions. The structure of the complex is given by the conformation of the polyelectrolytes in solution, as rearrangements of the chains after the formation of a complex are only possible to a certain extent. At higher salt concentrations, the first fast formation step can be followed by slower rearrangements, as the polymer chains are less strongly bound to each other due to the increased screening of charges. Two different models for the structure of polyelectrolyte complexes have been proposed: The *ladder-like structure* with a conformation of the polymer chains parallel to each other, which is favored when the individual polyelectrolytes have a rod-like conformation in solution, and the *scrambled egg model* with an increased interdigitation of the chains. In fact, there is often a mixture of both structures observed. A detailed description of polyelectrolyte complexes can be found in [12, 15, 16]

## 2.3 Adsorption of polyelectrolytes at interfaces

The adsorption of polyelectrolytes onto a surface is governed by several parameters including the charge density of the polyelectrolyte, the surface charge density as well as the relative sign of the charges of both, the ionic strength and for weak polyelectrolytes the pH of the solution. The structure of the adsorbed polymers is influenced by their conformation in solution. When they are adsorbed from aqueous solution or an electrolyte solution of low ionic strength, the stretched chains keep their elongated conformation and form a thin film of polyelectrolyte rods. In contrast, the adsorption from a solution with increased ionic strength results in a coiled structure of the polyelectrolytes on the surface. A schematic presentation of the adsorption of a polyelectrolyte coil onto a surface is given in Figure 2.2.

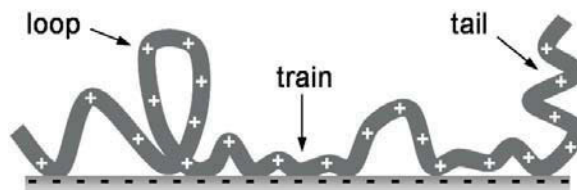


**Figure 2.2:** Schematic presentation of the adsorption of a polyelectrolyte chain onto a substrate.

Within the adsorbed coils it is possible to distinguish between different polymer segments. *Trains* are segments in direct contact with the substrate, *tails* are chain-ends that dangle into solution and *loops* are segments that have no contact with the substrate and connect two *trains*. Several studies of the adsorption of polyelectrolytes onto charged surfaces have shown that the surface charge can be reversed during the adsorption step. One explanation for this behavior can be found in the existence of *loops* and *tails*, as charges along these segments of the polyelectrolyte chain are not able to bind onto the substrate and therefore lead to an inversion of the surface charge [17]. The adsorption of weak polyelectrolytes is complicated by their variable degree of dissociation  $\alpha$ . Close to a surface, these polymers self-adjust their degree of ionization to effectively neutralize the surface charge. Segments adsorbed to an oppositely charged surface are more dissociated than in the bulk solution [18]. A more detailed treatment of the adsorption of polyelectrolytes onto surfaces is given in some comprehensive reviews [9, 10, 17].

## 2.4 Layer-by-layer electrostatic self-assembly

### 2.4.1 Assembly of thin films on flat substrates

The layer-by-layer (LbL) technique is based on the alternating adsorption of cationic and anionic substances onto a charged substrate via electrostatic interactions. One of the prerequisites for the formation of multilayers is the charge reversal after each adsorption step. In 1966 Iler prepared multilayers by electrostatic interactions between colloidal anionic and cationic particles [19]. But it was not until 1991, that Decher et al. systematically developed the electrostatic LbL technique [1] and since then the preparation of multilayers has been used for diverse applications [20, 21]. The LbL assembly was first developed for the coating of flat substrates. The principle of the alternating adsorption of polycations and polyanions is schematically described in Figure 2.3. During the LbL assembly a negatively charged substrate is exposed to a solution of a polycation for several minutes. The polyelectrolytes adsorb on the surface and the excess of polymer is eliminated by washing steps. The adsorption of the polycation results in an overcompensation of the surface charge, leading to charge

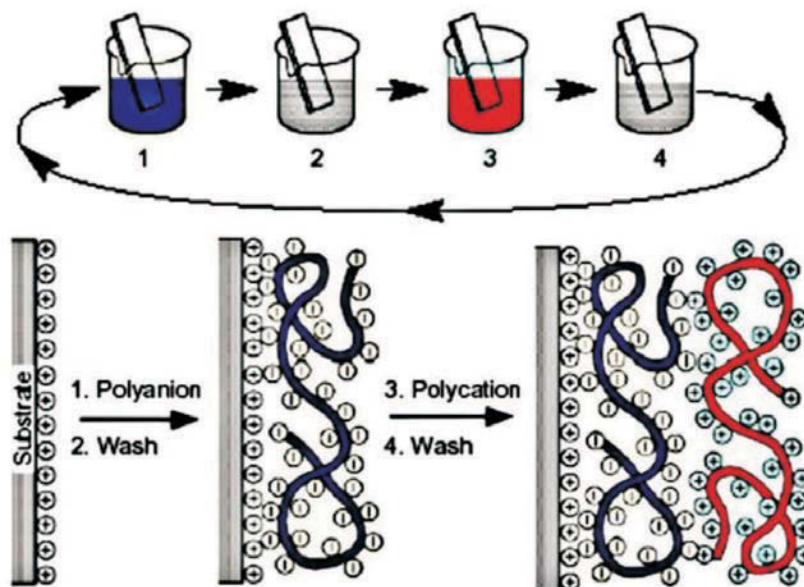


**Figure 2.3:** Simplified scheme for the construction of a multilayer of polyelectrolytes by the successive adsorption of a polyanion and a polycation by the repetition of the cycle. Steps 1 and 3 represent the adsorption of a polyanion and polycation, respectively, whereas steps 2 and 4 are washing steps [22].

reversal. After the washing step the now positively charged substrate is immersed into a solution of polyanions, which adsorb onto the surface, resulting in a negatively charged substrate. Again the polymer excess is removed with a washing step. This procedure can be followed by consecutive circles, allowing for a stepwise growth of the architecture of a film of polyelectrolytes.

Although the LbL technique is based on electrostatic attraction between positively and negatively charged species the primary driving force is probably not enthalpy but entropy, as complexation of the polyions by a charged surface liberates undissociated counterions, thus increasing the entropy of the system. An additional gain in energy can occur due to secondary interactions, like hydrogen-bonding or hydrophobic interactions between the polyelectrolytes [20,23].

In contrast to polyelectrolyte complexes, the stepwise layering process provides control about the structure, thickness, composition and interdigitation of different polyelectrolyte layers. The sequence of different components in the film is given by the charge and the sequence of the adsorption. Nearly all sorts of planar surfaces as well as colloidal particles can be used as substrates for the layering. In addition, there are nearly no restrictions concerning the materials in such films, as long as it is possible to adsorb them onto a surface and the new surface that results during the adsorption step bears functionalities that allow for the adsorption of the next layer. The LbL technique has been developed far beyond the polyelectrolyte system and a wide range of application was found in the assembly of synthetic functional

polymers with conductive, photo reactive, light emitting and redox active functionalities, as well as liquid crystalline polyelectrolytes and polymers that allow for molecular recognition. Furthermore, different functional organic pigments as well as dendrimers were used for the self-assembly. Charged nanoobjects like metal oxides, polyoxometalates, nanoparticles, fullerenes and metal colloids were also applied. In addition to synthetic polymers and colloidal particles many biological macromolecules such as proteins, enzymes, DNA and charged polysaccharides, lipids as well as viruses were assembled by the LbL technique to produce multicomposite materials [21,24].

The film thickness increases with increasing number of adsorption cycles. Several studies demonstrated that neighboring layers are not separated but exhibit an interpenetrated structure [22]. X-ray reflectometry only showed Kiessig fringes, that arise from the interference of the X-ray beams that are reflected from the film-air interface and the substrate-film interface [1, 25]. Neutron scattering experiments also showed only Kiessig fringes when all polyanion layers were labeled with deuterium. However, Bragg peaks that are characteristic for an internal layer structure were observed when only specific layer positions within the films were deuterated [26,27].

The growth of the layer thickness is not always linear with the number of cycles. It is possible to distinguish films with linear and with exponential growth. Films that show linear increase in thickness are constructed in conditions in which the polyelectrolyte solution only interacts with the polyelectrolytes of opposite charge at the external surface of the film. Linear growth is usually observed for strong polyelectrolytes, however, there are several reports showing that the film thickness can increase more than linearly with the number of deposited layers [28, 29]. Exponential growth was reported for several weak polyelectrolytes, particularly for multilayers that consisted of biopolymers [30, 31] and it was associated with an assembly process involving the diffusion of at least one of the polyelectrolytes through the whole film at each bilayer deposition step [32].

#### **2.4.2 Preparation of hollow capsules**

The LbL technique was also successfully applied for the adsorption of polyelectrolytes onto colloidal particles [33]. The adsorption steps are similar to those for flat substrates, but the removal of the excess of polyelectrolyte in solution has to be accomplished either by ultrafiltration or centrifugation of the particles [34]. When centrifugation is used, the supernatant is removed and the colloidal particles are redispersed in a washing solution. This washing step is repeated several times before the next layer is adsorbed. In addition, it was shown that it is also possible to assemble a multilayer by adding just the amount of polymer that is needed to observe a surface charge reversal, thus allowing the assembly of multilayers



without intermediate washing steps [5]. Hollow polyelectrolyte capsules can be obtained by core dissolution after the deposition of several layers [5,6]. The multilayer assembly as well as the core dissolution step are schematically described in Figure 2.4.

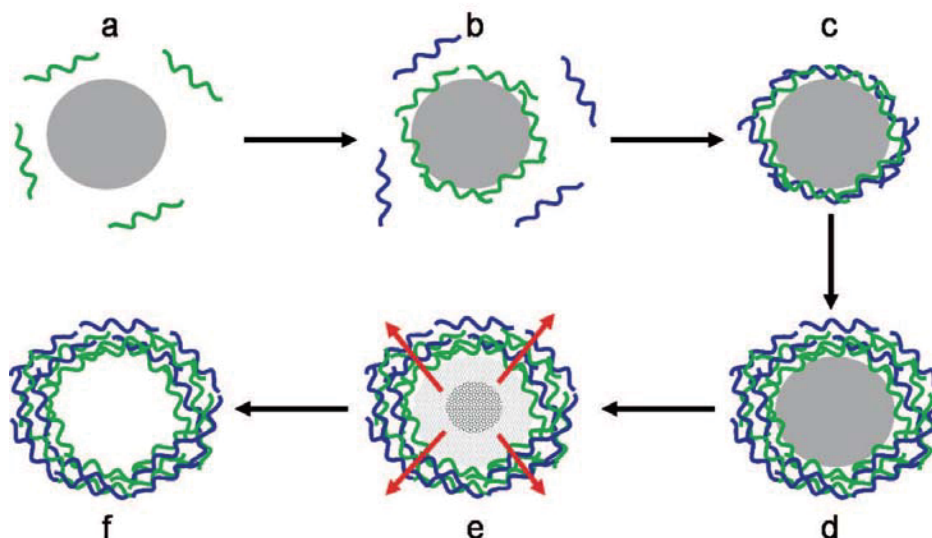


**Figure 2.4:** Scheme of the LbL deposition process on colloidal particles followed by core removal. The step-wise film formation by repeated exposure of the template to differently charged polyelectrolytes is illustrated in (a - d), and (e) shows the core dissolution, resulting in hollow polyelectrolyte capsules (f).

Many different templates have been used for the preparation of hollow polyelectrolyte capsules [35]. Originally, weakly crosslinked melamine formaldehyde (MF) particles were applied that can be removed by treatment with HCl ( $\text{pH} < 1.6$ ) or with dimethyl sulfoxide (DMSO) or N,N-dimethylformamide (DMF) [36]. However, recent research results showed that the molecular weight of the MF oligomers, products of acidic hydrolysis, depends on the age of the MF particles and varies from 4 to 14 kDa [37]. Such high molecular weight compounds can affect the integrity of the capsule wall during the dissolution process. Furthermore, MF oligomers are positively charged because of the amino groups of melamine and can form a complex with negatively charged wall components, making the amount of MF bound to the capsule wall hard to control. These properties of the core material can interfere with the stability and characteristics of polyelectrolyte capsules. The incomplete elimination of MF oligomers formed during dissolution and their biological incompatibility have strongly limited the use of this core material.

Another frequently used organic core material is polystyrene (PS), which is normally removed with either tetrahydrofuran (THF) or DMF. It was shown lately that the organic solvents used for the dissolution process lead to a structuring effect of the multilayer, thus also changing the stability of the polyelectrolyte membranes [38].

Examples of inorganic core materials are  $\text{SiO}_2$  and several carbonates [39].  $\text{SiO}_2$  particles were only used for the preparation of polyelectrolyte capsules that are stable in acidic conditions [40–44], because of the core dissolution with HF. Spherical  $\text{CaCO}_3$  microparticles are another frequently used inorganic template [45]. They are biocompatible and can be dissolved with ethylenediaminetetraacetic acid (EDTA) in neutral conditions, which is a prerequisite for a variety of bioactive substances. Therefore, this core type is often used for biological and medical applications. Scanning Electron Microscopy (SEM) pictures of  $\text{SiO}_2$  and of  $\text{CaCO}_3$  microparticles with mean diameters around  $5 \mu\text{m}$  are shown in Figure 2.5.

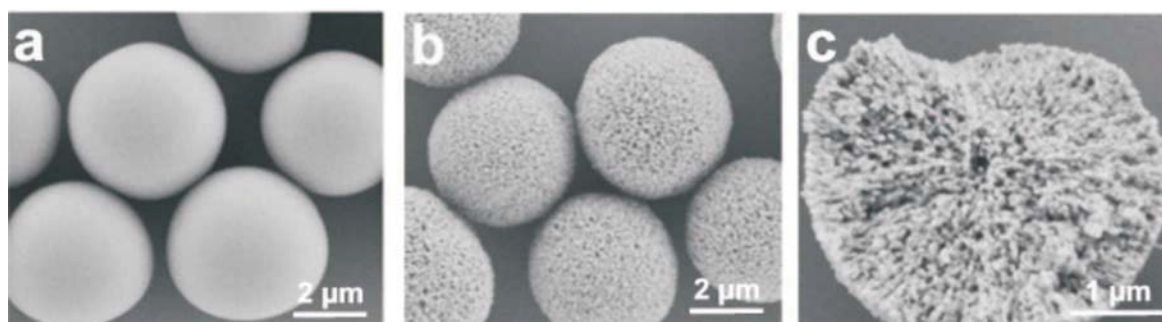


**Figure 2.5:** SEM micrographs of  $\text{SiO}_2$  (a),  $\text{CaCO}_3$  (b) and a broken  $\text{CaCO}_3$  particle (c).

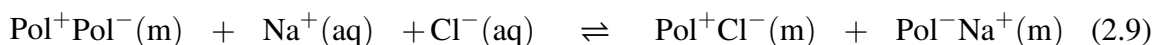
Silica particles are rather monodisperse and have a smooth surface. In contrast,  $\text{CaCO}_3$  microparticles are polydisperse and have a porous structure that leads to a huge inner surface, which can clearly be seen for a broken particle (see Figure 2.5 c). This porous structure promotes the assembly of multilayers in the pores resulting in matrix-like polyelectrolyte capsules that can have negative effects on some applications [45].

## 2.5 Interactions within multilayers

### 2.5.1 Electrostatic interactions

When multilayers are assembled by electrostatic interactions, compounds that bear a minimum charge are required. Many publications have shown that there is a critical minimal charge density below which no LbL assembly is possible [46–49]. However, in some cases it was also shown that a multilayer can be formed when only a small fraction of charges are present [50]. Thus, Laschewsky and coworkers proposed that the matching of charges is more important for a regular growth than a critical charge density of the polymers [24, 51]. For combinations of strongly dissociating polyelectrolytes, charges between the polymers are generally well matched, excluding small salt ions from the bulk of the film [27, 52]. As electrostatic interactions are screened in solutions containing salt, the ionic strength has a

huge influence on the assembly of multilayers as well as on the stability of preformed films. The screening effect of salt ions is used to change the polymer conformation and thus tunes the thickness of the assembled multilayer films [53, 54]. But a higher salt concentration can also promote the dissolution of the layers. In addition to the adsorbed amount, the structure of the films also depends on the salt concentration, resulting in rougher surfaces when the ionic strength is increased [29]. Furthermore, there is an effect of increasing ionic strength on preformed multilayers. Without additional salt, charges within a multilayer are mainly compensated by polyelectrolytes of the opposite charge. When the ionic strength of the solution is increased, the amount of segments that are charge compensated by salt counterions increases and the amount of polyelectrolyte ion pairs decreases according to the following relation [55],



with (m) denoting the multilayer and (aq) the surrounding solution. This results in a swelling and smoothing of polyelectrolyte multilayers adsorbed on flat substrates [55, 56].

Polyelectrolyte capsules, in contrast, show a pronounced shrinking effect upon addition of salt. Higher salt concentrations are known to enhance the mobility of charge-paired polyelectrolyte chains, thus allowing them to adopt a thermodynamically preferred conformation. It is assumed that the driving force of the shrinking of polyelectrolyte capsules is the reduction of the surface energy [57, 58].

## 2.5.2 Hydrophobic interactions

Kotov analyzed the contribution of hydrophobic interactions during the LbL adsorption. In this analysis the free energy of the adsorption of a polycation on top of a surface of a polyanion has several independent contributions, namely the liberation of counterions, the partial disappearance of the hydration sphere around the polyelectrolyte, the complexation of the polyelectrolytes and short-range van der Waals interactions. This analysis suggests, that without the participation of hydrophobic interactions no polyelectrolyte adsorption could be observed [23]. Dubas et al. investigated the influence of the hydrophobicity of counterions of polyelectrolytes on film parameters [54]. Laschewsky and coworkers examined the role of hydrophobic interactions for applications of the LbL technique. They showed that hydrophobic polyelectrolytes, which are associated in solution, can be separated upon adsorption on a charged surface and form stable multilayers [59].

### **2.5.3 Hydrogen-bonding interactions**

In addition to electrostatic and hydrophobic interactions, hydrogen-bonds can also play an important role in the formation of multilayers. Intermolecular hydrogen-bonds occur between H atoms, that are covalently bound to electronegative atoms like oxygen or nitrogen, and free electron pairs of other strongly electronegative atoms of a neighboring molecule. In 1997 Stockton and Rubner first demonstrated that these interactions can be used for the LbL assembly [2]. Since then several pairs of polymers have been successfully used in the self-assembly process [60,61]. H-bonded multilayers were also assembled using weak polyacids at low pH, followed by pH changes to induce charges within the layers. Moreover, it was recently shown that hollow capsules made from H-bonding multilayers can be obtained [44]. These applications of thin films stabilized by hydrogen-bonding interactions will be discussed in detail in Section 2.6.2.

### **2.5.4 Specific interactions**

Multilayers cannot only be formed by electrostatic interactions, but it is also possible to use specific recognition between molecules for the assembly of multilayers. This can be achieved by means of biological affinity including biotin-avidin and sugar-lectin interactions. The interaction between the proteins avidin or streptavidin and biotin was applied in several studies for the assembly of multilayered thin films [3, 62, 63]. The binding of carbohydrates by lectins, e.g. concanavalin A (Con A) was also used for the assembly of multilayers that were not stabilized by electrostatic interactions. Con A possesses four binding sites for its ligand D-glucose and allows for the binding of glycogen (branched polyglucose) [4].

## **2.6 Stimuli-responsive multilayer thin films**

### **2.6.1 Incorporation of stimuli-sensitive polymers into multilayers**

Stimuli-sensitive multilayers have gathered major scientific interest in different areas such as drug delivery, diagnostics and sensing. Many different polymer films and capsules that are responsive to a variety of external stimuli such as pH, ionic strength, light, temperature and magnetic field have been reported [7, 8]. The following two sections will concentrate on pH-responsive multilayers that are stabilized by electrostatic and / or H-bonding interactions and on one example of chemical stimuli, namely saccharide-sensing, as the stimuli-sensitive microcapsules presented in this work are examples of pH- and sugar-responsive systems.

## 2.6.2 Weak polyelectrolytes for pH-sensitive multilayers

### *Electrostatically stabilized multilayers*

Multilayers that are composed of weak polyelectrolytes show many different pH-dependent properties, since the linear charge density along the polymer chain is a function of the pH. As polyelectrolyte multilayers are permeable for protons [64], the electrostatic interactions between the layers can be tuned by changing the pH of the solution. In dependence on the local surrounding a weak polyelectrolyte can adjust its charge to maximize the charge compensation in a film, resulting in changes of the  $pK_{app}$  within polyelectrolyte multilayers [64–68]. Xie and Granick investigated the ionization degree of a weak polyacid beneath a multilayer of strong polyelectrolytes. Depending on the presence of polycation or polyanion outer layers, the fraction of charged groups oscillated between 30 and 85 % to compensate for the additional charge introduced by the top layer. The oscillations persisted with a decay length that far exceeded the Debye length of the aqueous solution, suggesting that this long range electrostatic coupling stemmed from the presence of polyanions and polycations that were fixed in space within the multilayer assembly rather than mobile [69, 70].

A well studied weak polyelectrolyte pair in literature is that of PAA and PAH. This polymer combination was investigated in detail on flat substrates and examples of properties that change with pH are layer thickness and roughness [71], film morphology and surface wettability [72]. By changing the pH of the polyelectrolyte solutions during layer assembly Shiratori et al. systematically changed the thickness of the adsorbed PAH and PAA layers. These studies also showed that the roughness of the substrate can have an influence on the thickness of the adsorbed layers. The pH-sensitive organization and thickness of adsorbed layers was related to the pH-dependent charge density of the polyelectrolytes [71].

Micro- and nanoporosity in PAH/PAA multilayers was observed upon treatment by low pH solutions [73] or changes in the ionic strength [74]. The pH-gated porosity transition was used for tunable Bragg reflectors and humidity sensors, when layers of PAH/PAA were confined between PAH/PSS layers [75]. PAH/PAA multilayers were also used to control the transport of ions through membranes, and the ion transport selectivity could be enhanced by an increase in the fixed charge density of the multilayers [76].

Uncompensated carboxylate groups within multilayers that were obtained by post-assembly pH changes were also used as anchoring points for the assembly of nanoparticles within weak polyelectrolyte films [77–79]. But not only multilayers composed of PAH and PAA were studied for their pH-sensitive properties. Barrett and co-workers investigated the swelling behavior of films composed of hyaluronic acid / PAH. Depending on the assembly conditions these multilayers were found to swell as much as 8 times their dry thickness [80].

There are many reports about the pH-dependent behavior of weak polyelectrolytes on flat substrates, but only little is known about covered colloids or microcapsules with weak polyelectrolyte shells.

Burke et al. studied the local dissociation constants of PAH and PAA in multilayer thin films adsorbed onto colloidal silica particles [81] and the properties of these polyelectrolyte multilayers adsorbed on PS and MF templates were investigated by Kato et al. [82]. They found that film growth as well as colloidal stability depend on the pH and ionic strength during the adsorption steps, as the dissociation degree of both polyelectrolytes plays an important role for regular multilayer growth. In addition, when PAH/PAA multilayers were assembled onto MF particles, the template could be dissolved, resulting in hollow weak polyelectrolyte capsules [82]. Gao et al. also focused on PAH/PAA capsules templated on MF templates, finding that the stability of the capsules was a function of the exposure time to 0.1 M HCl [83]. Schütz and Caruso studied multilayers of weak polyelectrolytes adsorbed on PS and SiO<sub>2</sub> cores [84], but in this case the template was only removed after the multilayers were covalently crosslinked.

The above mentioned studies concentrated on polyelectrolyte multilayers that were assembled of two weakly charged polyelectrolytes. But pH-responsive properties could also be obtained when only one of the polyelectrolytes had a pH-dependent degree of ionization. A well known example is PAH/PSS [85,86], a polymer combination that was also used in many studies of polyelectrolyte capsules. Déjournat et al. investigated the pH-dependent swelling characteristics of PAH/PSS capsules depending on the template as well as on the molecular weight and number of layers [38]. Vinogradova and coworkers examined the effect of pH on the osmotically induced swelling and the stability of PAH/PSS capsules that were filled with a strong polyanion and presented a theoretical model to explain the stable swollen state [87].

### ***Multilayers stabilized by hydrogen-bonds***

Electrostatically associated polymer multilayers and hydrogen-bonded films with weak polyacids or polybases show a reverse effect on internal ionization of the self-assembled weak polyelectrolyte. Electrostatic interactions between a weak polyacid and a polycation lead to a significant increase in the acid's ionization due to extensive electrostatic pairing. Hydrogen-bonding interactions, in contrast, stabilize the protonated form of a weak polyacid, resulting in the suppression of ionization of the acid embedded within the film [88]. Furthermore, unlike electrostatic interactions, hydrogen-bonding is not driven by a charge compensation mechanism and an upper critical ionization degree can be found, above which self-assembled films are not stable. This is complementary to the lower critical charge density in electrostatically stabilized multilayers.

The assembly of the weak polyacids PAA and PMA with uncharged polymers capable of undergoing hydrogen-bond interactions, e.g. poly(ethylene oxide) (PEO), poly(acrylamide) (PAAm) and poly(N-vinylpyrrolidone) (PVPON) was studied in detail. With these polymer combinations stable multilayers could be obtained in the acidic pH range and the resulting films were sensitive to pH changes because of the generation of electrostatic repulsion between the layers within the films [88–90]. As for electrostatically stabilized multilayers of weak polyelectrolytes, post-assembly pH changes could induce uncompensated negative charges. These were used for adsorption and release studies of positively charged dyes [91] and for the preparation of nanoparticles within thin films [92]. Multilayers of P4VP and PAA resulted in microporous films when they were exposed to basic solutions [93].

Some recent publications also reported on hydrogen-bonded hollow capsules that were prepared from polymer combinations of PMA with PVPON and PEO by templating them on silica, AgCl and CdCO<sub>3</sub> particles [43, 94, 95]. The stability of these capsules was shown to be in the same range as for the corresponding flat multilayers. Enhanced stability in neutral and basic conditions could be obtained by introducing covalent crosslinks within the multilayer wall [94]. Furthermore, hollow hydrogel capsules composed only of PMA could be obtained when PMA layers within hydrogen-bonded shells were crosslinked with ethylenediamine and exposed to high pH solutions [96]. Rubner and coworkers prepared microcapsules based on hydrogen-bonded multilayers of PAA and PAAm that were subsequently crosslinked [92]. These crosslinked PAA and PAAm multilayers have recently shown much promise for biomedical applications as they exhibited resistance toward cell adhesion [97].

### ***Multilayers stabilized by H-bonds and electrostatic interactions***

The interplay between electrostatic and hydrogen-bond interactions for the generation of stable multilayered films was studied with quarternized poly(4-vinylpyridine) (QP4VP) with different alkylation degrees ranging from 12 to 98 % and PMA [66]. The stability of multilayers of QP4VP and PMA in salt solution was investigated with different ionization degrees of QP4VP, and the multilayer growth was also correlated with phase separation in solution [98, 99]. Kharlampieva et al. stabilized hydrogen-bonded films at neutral pH by combining centers for electrostatic and H-bond interactions in a copolymer of acrylamide and dimethyldiallylammonium chloride and layering it with PMA [100]. The incorporation of P4VP/PAA layers in PAH/PAA flat multilayers resulted in H-bonded film domains that were sandwiched between electrostatically stabilized ones and led to changes of the pH-dependent destruction of the films [101]. When PAA was self-assembled with blends of P4VP and PAH, the selective removal of P4VP at high pH resulted in the formation of nanopores in the range of 10 to 50 nm [102].

## 2.6.3 Multilayer films for saccharide-sensing

### *Glucose-responsive multilayers*

Many stimuli-responsive multilayers that change characteristic physicochemical properties in dependence on various types of stimuli like temperature, pH, ionic strength, light and magnetic field have been prepared. However, only few examples can be found that use the response to chemical stimuli, i.e. concentration changes of certain molecules in the environment. A challenging class of such chemical stimuli that may have a great impact on medical applications and industrial processes are carbohydrates.

The enzymatic reaction of glucose with glucose oxidase (GOD) to gluconic acid and  $H_2O_2$  has been used for the sensing of glucose by the incorporation of GOD within polyelectrolyte multilayers on flat surfaces [103, 104], as well as on colloidal particles [105, 106].

When multilayers were assembled with the specific interaction between glycogen and Con A (see Section 2.5.4), the competitive binding of glucose and glycogen with Con A could be used to decompose the thin films [107]. Förster Resonance Energy Transfer was used to study the displacement of fluorescein labeled dextran from rhodamine labeled Con A within the shells of microcapsules, when glucose was added to the solution [108].

Recently De Geest et al. prepared glucose-sensitive capsules by the assembly of a copolymer of dimethyl-aminoethyl-acrylate and acrylamidophenylboronic acid with PSS. The authors presented a concept that proposed a glucose-induced change in the electrostatic interactions between the polyanion and the phenylboronic acid containing polycation [109].

### *Interactions between boronic acid and saccharides*

The formation of multilayers by the binding of phenylboronic acid moieties to a polysaccharide will be studied in Chapter 6. Therefore, this section describes the mechanism of the binding between boronic acids with diols and some applications of this reaction in the field of saccharide sensing.

In 1959, Lorand presented a quantitative study of the esterification of various diol-containing substances with arylboronic acids [110] and since then applications of this reversible reaction have been investigated in organic synthesis. Boronic acids are Lewis acids and the trigonal boronic acid can react with hydroxide ions to form tetrahedral boronate ions. Boronic acids react with 1,2- or 1,3-diols to form five- or six-membered cyclic esters in aqueous solution. Although covalent bonds are formed, the reaction that produces the esters is reversible, which makes it an ideal interaction in sensor design. The mechanism of the diol binding is given in Figure 2.6. The formation and dissociation of cyclic boronic acid esters with diols is believed to follow the mechanism that is indicated by the large arrows. Upon addition of



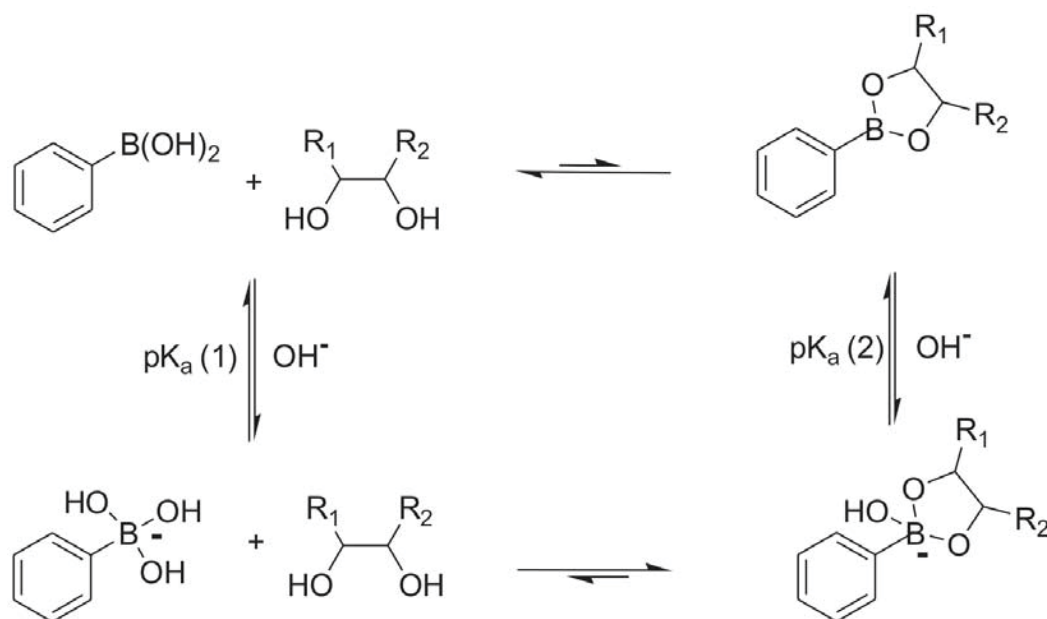


**Figure 2.6:** Equilibria between phenylboronic acids and diols in aqueous solution.

a diol, the charged phenylboronate can build a stable complex through the formation of a reversible covalent bond, whereas the complex between the uncharged phenylboronic acid and the diol is quite unstable with a high susceptibility to hydrolysis. The complexation between molecules containing planar diols and two of the hydroxyls on the boronate stabilizes the charged form of the Lewis acid. This leads to an apparent shift in the Lewis acids  $pK_a$  in the acidic direction, therefore  $pK_a(2)$  is 2 - 4 units lower than  $pK_a(1)$  [110, 111].

The pH of the environment strongly affects the sensitivity of phenylboronic acid compounds to carbohydrates, as the amount of the tetrahedral boronate ion increases with pH, however, the equilibrium position strongly depends on the structure of the boronic acid and the diol. A systematic examination of the binding between boronic acids with various diols was conducted by Springsteen et al. [111]. The affinity of phenylboronic acids to different diols depends on their structural features, especially the O-C-C-O dihedral angle.<sup>1</sup>H- and <sup>13</sup>C-NMR studies revealed a five-membered ring containing 1,2-cis-hydroxyls involved in the complexation of D-glucose and D-fructose corresponding to the  $\beta$ -furanose form of D-fructose and the  $\alpha$ -furanose form of D-glucose [112]. These findings suggest that complexation occurs preferentially with the cis-hydroxyls and the anomeric hydroxyl under neutral conditions and that the geometry of the five-membered ring is important.

Therefore, the selectivity of the boronic acid complexation for various saccharides is partly influenced by their isomeric composition in aqueous solution. When a saccharide is dissolved in water, mutarotation, which can occur on a time scale of minutes, leads to an equilibrium mixture of four forms,  $\alpha$ -pyranose,  $\beta$ -pyranose,  $\alpha$ -furanose and  $\beta$ -furanose.

The equilibrium distribution of D-glucose in neutral conditions is 39.4, 60.2, 0.2 and 0.21 %, respectively, and the distribution for D-fructose is 2.0, 68, 6.0, 23 % [113].

Detailed studies have shown that the selectivity of 1,2-diols decreases in the order five-membered-cis > six-membered-cis > six-membered-trans isomers [113]. Monoboronic acids have a higher affinity for the binding of fructose over glucose, diboronic acid compounds with the proper distance and orientation that are complementary to the two pairs of diols on glucose bind glucose with high affinity and selectivity [114].

The reaction between boronic acid moieties and diols has led to the development of a vast variety of sensor systems for carbohydrates. The achievements in the design of these sensors have been covered by several review articles [114–118]. In addition to the achievements in the design of low molecular weight boronic acid sensors, these moieties were also incorporated into hydrogels as sensing matrices for glucose [119]. The degree of swelling of the hydrogels upon binding of glucose was used for the quantitative analysis of this carbohydrate. Additionally, hydrogels combining centers for carbohydrate-sensing with temperature responsive moieties were reported [120].

## 2.7 Permeability of polyelectrolyte capsules

### 2.7.1 Permeability for low and high molecular weight compounds

The permeability of different types of capsules for compounds with low and high molecular weight has been studied in detail, and an overview is given in several review articles [121, 122]. Polyelectrolyte multilayer capsules show a semipermeable behavior. They are permeable for small molecules like fluorescent dyes, whereas polymers with higher molecular weight are excluded from the capsule interior [123, 124]. The determination of diffusion coefficients through the capsule wall depends on the conditions used for the dissolution of the core material. The core dissolution step is known to affect the properties of the capsule shell, so that different template materials change the permeability properties of the resulting capsules. For example, capsules composed of 8 layers of PAH and PSS templated on MF cores have shown a permeability of around  $8 \cdot 10^{-7}$  m/s [125], which is several orders of magnitude higher than the one observed for flat multilayers of the same polyelectrolyte pair [126]. These differences were attributed to the formation of pores during the core dissolution process. The permeability of polyelectrolyte microcapsules templated on MF was reduced by the adsorption of additional layers after the core removal [125] or increasing temperature [127]. The permeability of PAH/PSS multilayers was also studied by using fluorescein particles at low pH as a template for the adsorption of multilayers, followed by the

dissolution of this dye in neutral pH conditions. Also in this case the permeability of the multilayer for fluorescein decreased with the assembly of additional layers [128]. An increase of the ionic strength led to an increased permeability of the multilayer for fluorescein due to structural changes of the polyelectrolyte membrane [129]. Moreover, the permeability of polyelectrolyte capsules for small polar molecules could be significantly reduced when lipid membranes [130] and cholesterol were assembled on top of the polyelectrolyte capsules [131].

The semipermeability of polyelectrolyte multilayers can be used to reversibly switch the permeability for macromolecules depending on several stimuli. Examples are the increased permeability of PAH/PSS multilayers to polycations like PAH with increased ionic strength [124] or the permeability changes for macromolecules observed by changes in solvent polarity [132].

When multilayers are assembled with a weak polyelectrolyte like PAH, post-assembly pH shifts can induce additional charges within the multilayers, resulting in changes in the shell morphology and permeability. pH-induced permeability changes were studied in detail for PAH/PSS capsules templated on MF particles and several carbonates [133, 134], as well as on PS cores [135]. Recently, Tong et al. reported on stable weak polyelectrolyte microcapsules composed of poly(ethyleneimine) (PEI) and PAA that were crosslinked with glutaraldehyde, leading to permeability changes at low pH [136]. The pH-controlled permeability of hydrogen-bonded capsules was investigated by Kozlovskaya et al. [137].

In the work conducted here, the pH-dependent stability of weak polyelectrolyte capsules was investigated and the multilayer stability was related to permeability changes of the capsule wall for glucose as an example of a low molecular weight compound.

### **2.7.2 Capsules as encapsulation vehicles**

Different approaches have been used for the loading of polyelectrolyte capsules with substances of low and high molecular weight [122]. One possibility is the formation of microparticles of the substance to be encapsulated, followed by the assembly of polyelectrolyte multilayers. This strategy was followed for several drug [138] and dye microcrystals [128, 139], as well as protein aggregates [140].

The porous structure of  $\text{CaCO}_3$  templates was also used for the physical adsorption of polymers and proteins into the pores prior to multilayer formation [141, 142]. In addition,  $\text{CaCO}_3$  particles could also be used for the coprecipitation of several biomolecules during the particle fabrication process [143].

Radtchenko et al. assembled polyelectrolyte capsules that consisted of a decomposable inner shell and a stable outer wall. The inner shell could selectively be destroyed after decompo-

sition of the core material, resulting in encapsulated polymers [144]. It was either formed by the alternate assembly of multivalent ions with oppositely charged polyelectrolytes or by surface-controlled precipitation on the colloidal particles [145].

Another encapsulation technique that uses the semipermeable properties of polyelectrolyte membranes was shown by Dähne et al. [146]. They encapsulated polymeric material by a polymerization reaction inside microcapsules. Whereas the monomeric units can diffuse through the membrane of the capsules, the polymeric product is trapped in the capsule interior.

The possibility to switch the permeability of the capsule wall for macromolecules provides another method for the encapsulation and release of various substances. Following this strategy, many polymers were encapsulated by changes in pH, temperature, ionic strength or dielectric constant of the surrounding medium [132–136].

In this work, the reversible permeability changes with pH were used for the encapsulation of FITC-dextran in the neutral pH-range.

## 3 Methods

### 3.1 UV-VIS Spectroscopy

Molecules absorb energy in the ultraviolet or visible range ( $\lambda = 200 - 800$  nm), if the energy of the radiation coincides with the energy difference between the electronic ground state and an electronic excited state of the molecule. If light with an intensity  $I_0$  gets into contact with an absorbing medium, there is some loss in intensity due to scattering and reflection. In addition, the transmitted light has a reduced intensity  $I$  due to absorption ( $I_{abs}$ ) in the medium,

$$I = I_0 - I_{abs} \quad . \quad (3.1)$$

In dilute solutions, if reflexion and scattering effects can be neglected, the relationship between  $I$  and  $I_0$  can be described by the Lambert-Beer-Law,

$$A(\lambda) = \log \frac{I_0(\lambda)}{I(\lambda)} = \varepsilon(\lambda)cd \quad (3.2)$$

with the measured absorbance  $A(\lambda)$ , the intensity of the incident light at a given wavelength  $I_0(\lambda)$ , the transmitted intensity  $I(\lambda)$ , the path length through the sample  $d$ , the concentration of the absorbing species  $c$  and the molar extinction coefficient  $\varepsilon$ . For each species in a given solvent at a certain temperature,  $\varepsilon(\lambda)$  is a constant. Due to the linear relationship between the absorbance and the concentration of a substance, it is possible to evaluate the concentration of an absorbing species with its UV-VIS spectrum [147, 148].

### 3.2 Fluorescence Spectroscopy

In Fluorescence Spectroscopy, the emission of radiation from molecules in their electronic excited states can be measured. The absorption of light in the UV-VIS range excites a molecule in different vibrational states of a higher electronic state. This molecule can relax by various competing pathways. It can, e.g. take part in a chemical reaction, transfer an electron to a neighboring molecule, or undergo non-radiative relaxation, in which the energy is dissipated to surrounding molecules in form of rotational, vibrational or translational energy. First of all, this results in a vibrational relaxation (VR) of the excited molecule to the

vibrational ground state of an excited electronic state. The energy of the electronic transition can be lost either by non-radiative relaxation (internal conversion, IC) or by the emission of a photon (fluorescence). The wavelength of this photon depends on the vibrational state of the electronic ground state where the transition finishes. Therefore the structure of the emission spectrum depends on the vibrational states of the electronic ground state. The shift in the wavelength of the fluorescence light compared to the excitation wavelength is due to non-radiative energy losses in the excited electronic state. Figure 3.1 illustrates the different processes that can occur after the absorption of light in a Jablonski diagram.

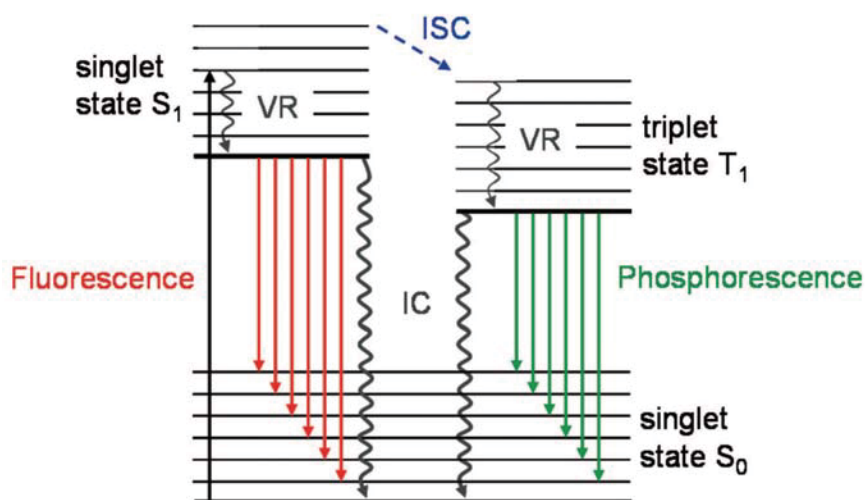


**Figure 3.1:** Jablonski diagram of the absorption and subsequent radiative and non-radiative decay pathways for an electronically excited molecule (VR: vibrational relaxation, ISC: intersystem crossing, IC: internal conversion).

In addition to fluorescence, intersystem crossing (ISC) that changes the spin multiplicity from singlet to triplet is also shown. The excited triplet state can either relax through internal conversion or emission of a photon (phosphorescence). In contrast to fluorescence, phosphorescence changes the spin multiplicity of the system. Like in UV-VIS absorption the fluorescence intensity is proportional to the concentration of the fluorophores over a wide range of concentrations [148, 149].

### 3.3 Confocal Laser Scanning Microscopy

Confocal Laser Scanning Microscopy (CLSM) is an important method for obtaining high resolution images and 3D-reconstructions of biological samples. The key feature of CLSM is to reject out-of-focus light, which results in blur-free images of thick specimen at various depths. A scheme of the CLSM is given in Figure 3.2. In a confocal microscope, light from a laser passes through a small pinhole and is reflected by a beam splitter onto an objective

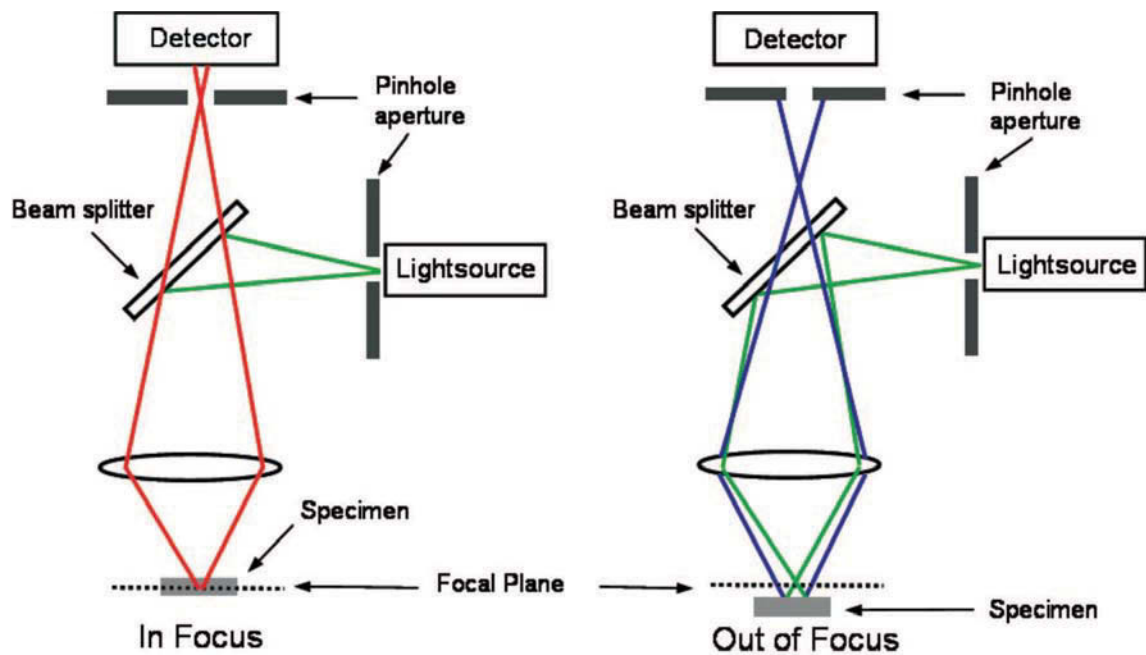


**Figure 3.2:** Schematic presentation of a confocal microscope with two different positions of the sample, in focus (left) and out of focus (right).

lens. The objective lens focuses the laser beam onto a fluorescing sample. Fluorescence light and reflected laser light from a small volume of the sample passes through the objective and is separated by a beam splitter, that reflects the laser light and transmits fluorescent light of larger wavelength to the detector. The fluorescence light is focused through a second pinhole onto the detector. The sample is located in the focal plane of both pinholes, thus only allowing light from a small focal volume of the sample to pass through to the detector and rejecting out of plane light. Light rays from below the focal plane focus in front of the detector pinhole, whereas light reflected from above the focal plane focus behind the pinhole. In this way most light from out of focus planes is blocked from reaching the detector. Only one point of the sample is illuminated and detected at the same time, so that the image is scanned point-by-point and reconstructed by a computer. Information from different depths of the sample can be obtained by changing the height of the specimen. The advantages of a confocal microscope compared to a normal fluorescence microscope are the higher axial and lateral resolution and the decreased background noise. Due to the high axial resolution pictures at various depths of a sample can be taken and reconstructed to 3D images [150].

### 3.4 Infrared Spectroscopy

Infrared (IR) Spectroscopy is based on the measurement of vibrational transitions between the ground state and an excited state in a molecule. The changes in vibrational energy are due to radiation in the spectral region of mid infrared (400 - 4000  $\text{cm}^{-1}$ ). The absorption or emission of an infrared wave changes the vibrational energy of a molecule,

$$\Delta E = E_2 - E_1 = h\nu = hc\tilde{\nu} \quad (3.3)$$

with the initial and final energy  $E_1$  and  $E_2$ , the Planck constant  $h$ , the velocity of light  $c$ , the frequency of the vibration  $\nu$  ( $\text{s}^{-1}$ ) and the wavenumber  $\tilde{\nu}$  ( $\text{cm}^{-1}$ ). A polyatomic molecule with  $N$  atoms has  $3N - 6$  normal modes of vibration ( $3N - 5$  for a linear molecule), each mode of vibration having a defined vibrational frequency. In order for a vibrational mode in a molecule to be IR active, it must be associated with changes in the dipole moment.

The vibrations can be understood with the model of the harmonic oscillator, in which the covalent bond is represented by a spring binding two masses. For a diatomic molecule the frequency of the vibration of such an oscillator depends on the mass of the atoms and the force of the binding, which is represented by the force constant  $k$ ,

$$\nu = \frac{1}{2\pi} \sqrt{\frac{k}{\mu}} \quad (3.4)$$

where  $\nu$  is the fundamental frequency and  $\mu = \frac{m_1 m_2}{m_1 + m_2}$  is the reduced mass of the oscillator between the masses  $m_1$  and  $m_2$ . One consequence of this relation is that the vibration of heavy atoms in comparison to light atoms occurs at smaller wavenumbers.

The characteristic vibrations of covalent bonds can be classified in two distinct groups:

1. stretching vibrations, which change the bond length:
  - a) symmetric stretching
  - b) asymmetric stretching
2. bending vibrations, which change the angle between two bonds:
  - a) wagging vibrations
  - b) scissoring vibrations
  - c) rocking vibrations
  - d) twisting vibrations

The vibrational spectrum of a molecule is a fingerprint of this substance. In addition, different functional groups of a molecule have characteristic vibrational frequencies, which can be assigned to absorption bands in the IR spectrum [147, 148].



## 3.5 Measurement of the electrophoretic mobility

### 3.5.1 The electric double layer

The ionic environment of a surface organizes itself to maintain electroneutrality in the system. Therefore, ions with opposite charge to the ones on the surface are attracted by Coulomb interactions and identically charged ions are repelled. Due to thermal motion, charges are not fixed but form a cloud near the interface. The electric potential varies as a function of the distance to the surface. Different models have been applied for the description of the double layer [151].

#### *Gouy-Chapman model*

The theory of the double layer was initially proposed by Gouy and Chapman. They suggested a diffuse layer in the vicinity of a charged surface with properties different from those of the bulk. In this diffuse layer the distribution of ions is determined by the electrostatic interactions with the surface and the thermal motion of the ions. For low potentials (Debye-Hückel approximation) the potential  $\Psi$  decays exponentially from its value at the surface to the value in the bulk of the solution, defined as zero,

$$\Psi = \Psi_0 \exp(-\kappa x) \quad (3.5)$$

with the potential at the surface  $\Psi_0$ , the normal distance to the surface  $x$  and the Debye length  $\kappa^{-1}$ . The decay of the electrostatic potential depends on the amount of free charges in solution (see p. 5). In this model, ions are considered to be point charges. In the vicinity of the charged surface this hypothesis is not satisfying, so that a model that takes into account the finite size of ions has been developed.

#### *Stern model*

In the model that was introduced by Stern, the solid / liquid interface is assumed to be composed of two different parts. In the inner compact layer with a thickness  $d$  (Stern-Layer) the ions have a fixed distance to the surface, and the characteristics of the outer diffuse layer are the same as in the Gouy-Chapman model. This results in a potential  $\Psi$  with a linear and an exponential part. A scheme of this model is given in Figure 3.3.

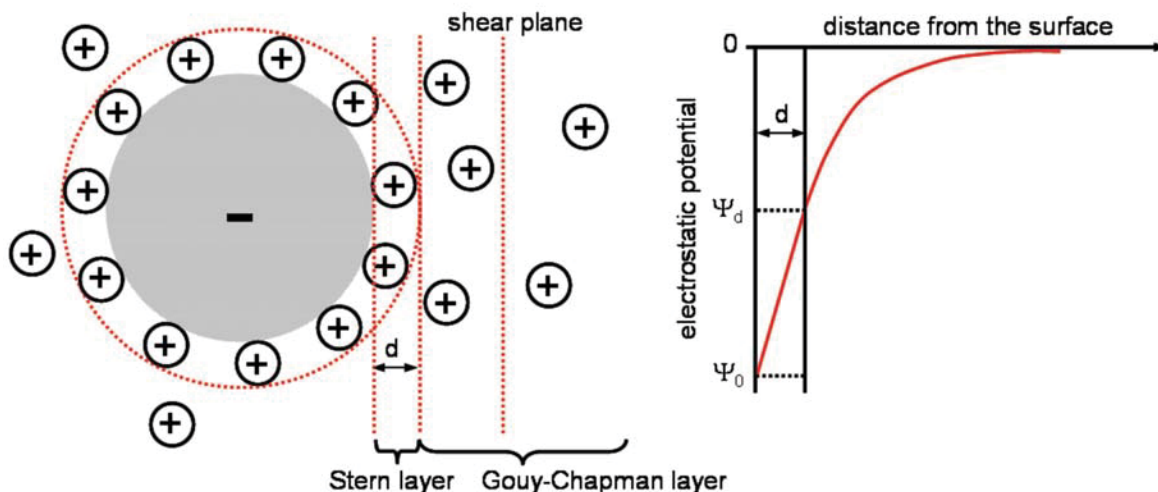


**Figure 3.3:** Scheme of the Stern model (left), including the Stern and Gouy-Chapman layer, as well as the shear plane. The diagram on the right shows the electrostatic potential as a function of the distance to the surface.

### 3.5.2 Determination of the $\zeta$ -potential

The surface charge of a colloidal particle can be determined by the electrophoretic mobility of this particle in an electric field. In solutions, charged particles are surrounded by a thin layer of solvent molecules and ions (Stern layer and Gouy-Chapman layer) that compensate the surface potential of the particles. Depending on the velocity of the movement of the particles, the diffuse Gouy-Chapman layer is partially removed. It is not possible to measure the potential at the surface directly, instead the effective surface potential at the shear plane of the colloidal particle is measured, which is the sum of the surface potential of the particles and the potential of the surrounding ions and solvent layer. The shear plane is defined as the plane between the solution, which is moved relative to the surface and the fixed ion and solvent layer on the surface (see Figure 3.3). The  $\zeta$ -potential is defined as the potential at the shear plane. The  $\zeta$ -potential can be determined with microelectrophoresis from the movement of colloidal particles in an electric field. The electrophoretic mobility  $u$  of the particles in a given electric field  $E$  can be transformed into the  $\zeta$ -potential using the Smoluchowski equation, if the viscosity  $\eta$  and the dielectric constant  $\varepsilon$  of the solvent are known,

$$\zeta = \frac{u\eta}{\varepsilon E} \quad . \quad (3.6)$$

### 3.6 Single Particle Light Scattering

Single Particle Light Scattering (SPLS) is a static scattering method based on the measurement of individual particles. It allows for the determination of both the particle size distribution and the concentration of particles in a dispersion. As it is possible to measure small differences in the size of particles with diameters in the range from 300 nm to 1  $\mu\text{m}$ , this method can be used to determine the increase in multilayer thickness during the adsorption steps. For the measurement, a particle suspension is confined into a narrow stream by means of a capillary and hydrodynamic focusing. Laser light is focused onto this particle stream, and the intensity distribution of forward scattering within an angle of 5 - 10° is recorded. A beam stop blocks the primary beam. Scattered light of single particles is measured with a photomultiplier and registered by a multichannel analyzer. The mean layer thicknesses of polyelectrolyte multilayers on colloidal particles can be determined with the Mie-Theory from the maximum of the intensity histogram with a precision of  $\pm 1$  nm [152].

### 3.7 Quartz Crystal Microbalance

The technique of Quartz Crystal Microbalance (QCM) is an ideal tool for studying the adsorption of substances onto a surface. It commonly provides mass measuring sensitivity in the nanogram range. A QCM uses the principle that a piezoelectric quartz crystal changes its oscillation frequency when mass is deposited onto or depleted from the crystal surface. On both sides of the quartz plate a small layer of gold is deposited, which serves as an electrode. In applying a difference in potential between the two electrodes, an oscillating movement is induced. The QCM allows to measure changes in the fundamental frequency  $F_1$  of the quartz plate and at all its odd harmonics  $F_\nu$  (with  $\nu$  being a positive odd integer). According to the Sauerbrey equation the frequency changes  $\Delta F_\nu$  can be related to the mass adsorbed onto the crystal [153],

$$\frac{\Delta F_\nu}{\nu} = -\frac{2F_1^2}{A\sqrt{\mu_q\rho_q}}\Delta m \quad (3.7)$$

with the change in resonance frequency  $\Delta F_\nu$ , resulting from a change in mass  $\Delta m$ , the shear modulus of quartz  $\mu_q$  ( $2.947 \cdot 10^{10} \text{ kgm}^{-1}\text{s}^{-2}$ ), the density of quartz  $\rho_q$  ( $2648 \text{ kgm}^{-3}$ ) and the electrode area  $A$ . This relation is valid for the deposition of a rigid material in contact with vacuum. The oscillation behavior of a QCM in liquids does not only depend on the properties of the quartz and the deposited material but also on the density and viscosity of the liquid medium. In liquid phase, the Sauerbrey equation does often not predict the adsorbed mass correctly [154]. When a viscoelastic material like a polymer film is deposited onto the quartz crystal, the response is even more complicated. Then, the frequency change is also

influenced by the viscosity and the elasticity modulus of the deposited substance. When the adsorbed material on the crystal is in contact with a fluid, the oscillating mass does not only include the deposited material that builds the film, but also the fluid that is present within the layers. By collecting both the dissipation and the resonance frequency of a quartz crystal it is possible to extract the viscoelastic properties of the film by modeling [155, 156].

### **3.8 Atomic Force Microscopy**

With Atomic Force Microscopy (AFM) surface topographies and surface structures can be characterized with a resolution in the nanometer range. The method was developed in the 1980s by Binnig et al. and uses the interactions between a tip and a sample for surface analysis [157]. The interactions between the tip and the sample include attractive van der Waals interactions and capillary forces, repulsive steric forces and Coulomb interactions that can be either attractive or repulsive. A combination of these different interactions is observed with AFM. During an AFM experiment, the sample surface is scanned with a sharp tip that is mounted on the end of a cantilever. The force on the tip can be measured as a deflection of the cantilever, which is optically detected by the movement of a focused laser beam on the back of the cantilever. The sample is placed on a piezo-element and approaches the tip until there is an interaction between the tip and the surface that results in a deflection of the cantilever. Due to the horizontal movements of the piezo-elements the sample surface is scanned, and the force between the tip and the surface is kept constant with a feedback mechanism and converted in a height profile of the sample.

In contact mode AFM the tip is in continuous contact with the surface and mainly short range repulsive interactions are detected. Thus, high tip to sample forces and the presence of lateral forces can lead to mechanical deformation of the surface. Because of this disadvantage, soft materials, like polymer surfaces, are usually studied in tapping mode AFM. In this mode the sample is investigated with an oscillating tip and the short intermittent contacts minimize the inelastic deformations of the surface. Here, the cantilever is excited near its resonance frequency to a sinusoidal oscillation. When it approaches the surface of the sample, the interactions between the tip and the sample dampen the amplitude of the oscillation. The height profile is recorded by keeping this damping constant [158, 159].

### 3.9 Scanning Electron Microscopy

Scanning electron microscopy (SEM) provides information about colloidal particles and dried capsules, as well as the structure and morphology of the capsule wall. The sample is illuminated with electrons that are accelerated in an electric field with a voltage  $U$ . The kinetic energy  $E_{\text{kin}}$  of the electrons is given by

$$E_{\text{kin}} = eU = \frac{1}{2}m_e v^2 \quad (3.8)$$

with the velocity  $v$  of the electrons, their mass  $m_e$  and the elementary charge  $e$ . The velocity of a material particle can be transformed into a wavelength  $\lambda$ ,

$$\lambda = \frac{h}{m_e v} \quad (3.9)$$

with the Planck constant  $h$ . Depending on the velocity of the electrons, the resolution of an electron microscope is increased by several orders of magnitude compared to the resolution of a light microscope. To obtain such a high resolution, electron microscopes are usually operated in vacuum to avoid the collision of electrons with gas molecules. In scanning electron microscopy (SEM) the sample surface is scanned with a focused electron beam. The interactions of the electrons with the sample lead to back-scattered electrons and scattered secondary electrons as well as X-rays. For microscopic applications, the scattered secondary electrons are detected [149].

# 4 Experimental Section

## 4.1 Materials

Poly(allylamine hydrochloride) (PAH) (Mw = 70 kDa), poly(methacrylic acid sodium salt) (PMA) (Mw = 75.1 kDa and Mw = 790 kDa), mannan (from *Saccharomyces cerevisiae*), poly(4-vinylpyridine) (P4VP) (Mw = 60 kDa), albumin from bovine serum (BSA) (Mw = 66 kDa), fluorescein isothiocyanate dextran (FITC-dextran) (Mw = 70 kDa and Mw = 4 kDa), methanol, ethanol, hydrofluoric acid (HF), ammoniumfluoride (NH<sub>4</sub>F), 4-(2-hydroxyethyl)piperazine-1-ethanesulphonic acid (HEPES), sodium borate, disodium hydrogen phosphate, hydrogen peroxide (H<sub>2</sub>O<sub>2</sub>) (30 %), ammonium hydroxide (NH<sub>4</sub>OH) (25 %), 3-(cyclohexylamino)-1-propanesulphonic acid (CAPS), 1-(3-dimethylaminopropyl)-3-ethylcarbodiimide hydrochloride (EDC), N-hydroxysulfosuccinimide sodium salt (sulfo-NHS), deuterium oxide (D<sub>2</sub>O) (99.9 atom% D), 3-aminophenylboronic acid hemisulfate salt, dithiodiglycolic acid, D-fructose, D-glucose, D-galactose, D-mannose, rhodamine B amine and tetramethylrhodamine isothiocyanate (TRITC) were purchased from Sigma-Aldrich (Taufkirchen, Germany).

Sodium hydroxide (NaOH), hydrochloric acid (HCl), sodium chloride (NaCl), sodium carbonate (Na<sub>2</sub>CO<sub>3</sub>), calcium chloride (CaCl<sub>2</sub>) and ethylenediaminetetraacetic acid disodium salt (EDTA) were obtained from Merck (Darmstadt, Germany).

Poly(acrylic acid) (PAA) (Mw = 50 kDa, 25 % solution) and poly(ethyleneimine) (PEI) (Mw = 70 kDa, branched, 30 % solution) were purchased from Polysciences Europe (Eppelheim, Germany).

Silicon oxide particles with mean diameters of 881 nm and  $4.48 \pm 0.26 \mu\text{m}$  were obtained from Microparticles GmbH (Berlin, Germany). Mucosol was obtained from Merz (Frankfurt, Germany).

ZnSe substrates for IR-measurements were purchased from Korth Kristalle GmbH (Kiel, Germany). Mica plates were purchased from Plano (Wetzlar, Germany) and QCM quartz crystals (Q-SENSE-QSX301, 5 MHz) were obtained from L.O.T.-Oriol GmbH (Darmstadt, Germany). Dialysis membranes with a molecular weight cut off of 12 - 14 kDa were obtained from Sigma-Aldrich (Taufkirchen, Germany).

All chemicals were used without further purification. All solutions were prepared with water from a three-stage Millipore Milli-Q Plus 185 purification system (Millipore, Bedford, USA) with a resistivity higher than 18.2 M $\Omega$ -cm. The structural formulas of the different polyelectrolytes and the carbohydrates used in this work are given in Figure 4.1 and Figure 4.2, respectively.

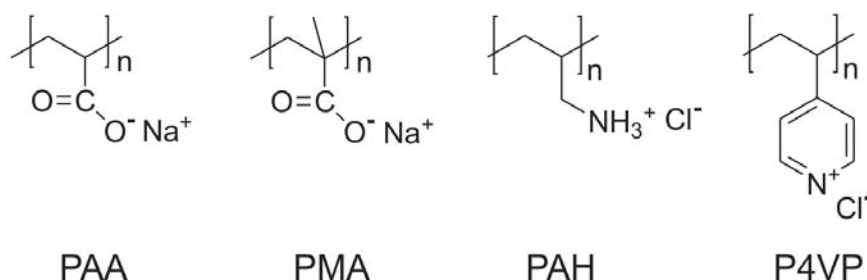


**Figure 4.1:** Structural formulas of the different polyelectrolytes used. All polyelectrolytes are shown in their charged forms.

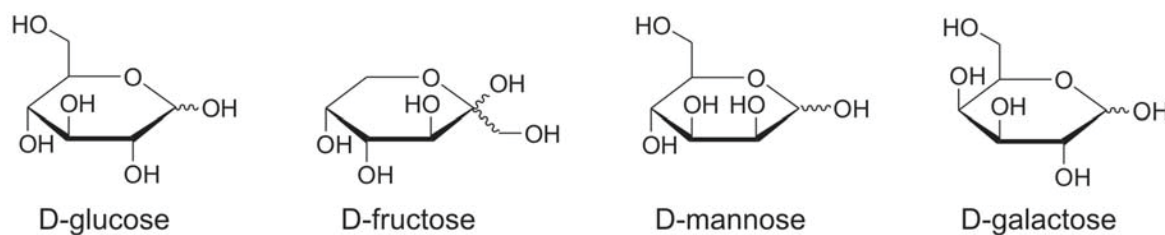


**Figure 4.2:** Chemical formulas of the different carbohydrates used in this study.

## 4.2 Syntheses

### 4.2.1 Labeling of PAH and BSA

Either 300 mg PAH (3.2 mmol of the amino function) or 300 mg BSA were dissolved in 60 mL sodium borate buffer (100 mM, pH 8.5) and mixed with a solution of 12 mg (0.03 mmol) TRITC in 60 mL of the same buffer. The reaction mixture was stirred for 12 h at room temperature. The labeled polymer was dialyzed for 1 week and lyophilized. The resulting yield of the labeling was determined by UV-VIS spectroscopy (see p. 39) to be 9 dye molecules per PAH (labeling degree of 1.27 %) and 12 dye molecules per BSA.

### 4.2.2 Labeling of PMA

100 mg PMA (0.93 mmol of the carboxylic function) were dissolved in 10 mL of HEPES buffer (50 mM) at pH 8.5 and mixed with a solution of 18.3 mg (0.04 mmol) rhodamine B

amine in 15 mL HEPES buffer (50 mM, pH 8.5). 0.9 mg (0.004 mmol) of sulfo-NHS were added and the solution was stirred for 5 minutes. After that 7.7 mg (0.04 mmol) EDC were added dropwise into the reaction mixture while stirring and the mixture was stirred for 12 h at room temperature. The labeled polymer was dialyzed in water for 1 week and lyophilized. The yield of the labeling was determined by UV-VIS spectroscopy (see p. 39) to be 4 dye molecules per PMA (labeling degree of 0.6 %).

### 4.2.3 Coupling of 3-aminophenylboronic acid to poly(acrylic acid)

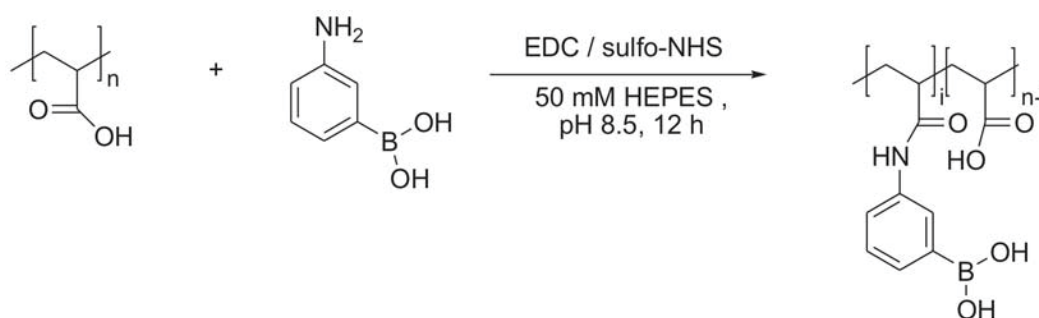


**Figure 4.3:** Scheme of the coupling of 3-aminophenylboronic acid to PAA.

A scheme of the reaction between 3-aminophenylboronic acid and PAA is given in Figure 4.3. 100 mg PAA (1.39 mmol of the carboxylic function) were dissolved in 10 mL HEPES buffer (50 mM) and the pH was adjusted to 8.5 with NaOH. A solution of 113.5 mg (0.61 mmol) 3-aminophenylboronic acid hemisulfate salt in 10 mL HEPES buffer (50 mM) at pH 8.5 was mixed with the PAA. 13.2 mg (0.061 mmol) sulfo-NHS in 2 mL HEPES buffer (50 mM, pH 8.5) were added dropwise into the solution and stirred for 5 minutes. 116.9 mg (0.61 mmol) EDC were dissolved in 2 mL HEPES buffer (50 mM, pH 8.5) and added to the reaction mixture, followed by stirring for 12 h at room temperature. The product was dialyzed for one week in order to remove all low molecular weight impurities, and the water was eliminated by freeze drying. The product was obtained as a white powder. The composition of the polymer was determined by elemental analysis (C/N ratio, see p. 37), showing a derivatisation of 15 % of the carboxylic acid moieties by phenylboronic acid. The reaction yield was 34 %.

The product will be named PAA-BOH from now on. <sup>1</sup>H-NMR (D<sub>2</sub>O, 200 MHz, see p. 38),  $\delta$  (ppm): 1.6 (CH<sub>2</sub>, s), 2.1 (CH, s), 6.9 - 7.6 (phenyl, m).

### 4.2.4 Coupling of dithiodiglycolic acid to 3-aminophenylboronic acid

The synthesis of a conjugate of dithiodiglycolic acid and 3-aminophenylboronic acid was performed according to the protocol described by [160] and a scheme of the reaction is



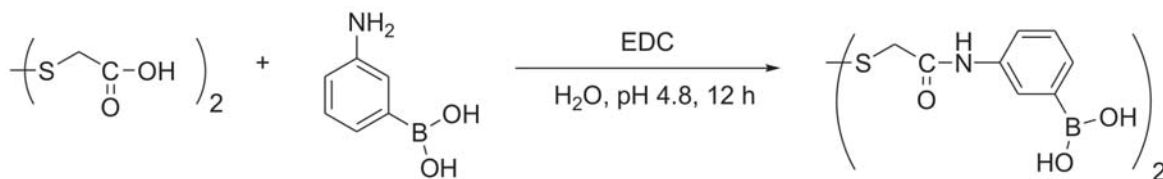


**Figure 4.4:** Scheme of the reaction between dithiodiglycolic acid and 3-aminophenylboronic acid.

given in Figure 4.4. 100 mg (0.55 mmol) dithiodiglycolic acid were dissolved in 5 mL H<sub>2</sub>O, followed by pH adjustment to 4.8 using NaOH (solution 1). 102.3 mg (0.55 mmol) 3-aminophenylboronic acid hemisulfate salt were dissolved in 15 mL H<sub>2</sub>O and the pH was adjusted to 4.8. After dissolution of the 3-aminophenylboronic acid, 134.2 mg (0.7 mmol) EDC were added (solution 2). Solution 1 was given dropwise to solution 2 in an ice bath and the reaction mixture was incubated for 1 h in ice, and afterwards overnight at 4 °C. A white precipitate appeared and was collected by centrifugation. The precipitate was dried in vacuo and purified by recrystallization from a methanol - water mixture. The product was obtained in a yield of 41 % (0.23 mmol, 96.6 mg).

The product will be named DTGA-PBA from now on. <sup>1</sup>H-NMR (D<sub>2</sub>O, 200 MHz, see p. 38): δ (ppm): 3.77 (-CH<sub>2</sub>-, 2H, s), 7.1 - 7.7 (phenyl, 4 H, m).

#### 4.2.5 Synthesis of CaCO<sub>3</sub> microparticles

Spherical CaCO<sub>3</sub> microparticles with an average diameter of  $4.4 \pm 0.5 \mu\text{m}$  were synthesized according to [142]. They were prepared by colloidal crystallization from supersaturated solution. The process was initiated by rapid mixing of equal volumes of CaCl<sub>2</sub> and Na<sub>2</sub>CO<sub>3</sub> solutions. A 0.33 M Na<sub>2</sub>CO<sub>3</sub> solution was rapidly poured into an equal volume of 0.33 M solution of CaCl<sub>2</sub> at room temperature. The solution was thoroughly agitated by a magnetic stirrer for 30 sec. After that, the agitation was stopped and the reaction mixture was left without stirring for 10 minutes, during which the primary precipitate of CaCO<sub>3</sub> transformed slowly into spherical microparticles. The precipitate was filtered, thoroughly washed with pure water and ethanol, and dried in air.

#### 4.2.6 Synthesis of BSA-CaCO<sub>3</sub> microparticles

CaCO<sub>3</sub> microparticles with encapsulated TRITC-BSA were synthesized according to a procedure reported by Petrov et al. [143]. The protocol was the same as for the synthesis of CaCO<sub>3</sub> particles, the only difference being that the 0.33 M Na<sub>2</sub>CO<sub>3</sub> solution was added to an equal volume of a 0.33 M solution of CaCl<sub>2</sub> containing 2 mg/mL TRITC-BSA. The average

diameter of the particles was  $4.7 \pm 0.6 \mu\text{m}$ . The amount of TRITC-BSA captured within the  $\text{CaCO}_3$  particles was  $70 \mu\text{g}/\text{mg CaCO}_3$ , as determined by UV-VIS spectroscopy (see p. 39).

## 4.3 Capsule preparation

### 4.3.1 LbL assembly on colloidal particles

Multilayers were assembled on the templates using the LbL technique. All polymer solutions were prepared with a concentration of 2 mg/mL of the polymer. The surface of  $\text{SiO}_2$  particles was treated with a mixture of 5:1:1  $\text{H}_2\text{O} : \text{NH}_4\text{OH} : \text{H}_2\text{O}_2$  for 20 min prior to the deposition of polyelectrolytes, followed by multiple water washing steps to yield neutral pH. This ensured a better attachment of the first polycation layer on the silica surface. For P4VP/PMA multilayers a solvent combination that contained 50 vol% methanol was chosen to provide solubility of P4VP at this pH [101]. The experimental details for the different solutions are given in Table 4.1. The pH values were adjusted with 0.1 mol/L HCl or 0.1 mol/L NaOH. The experimental conditions were chosen to ensure minimal aggregation of the templates during the assembly of the multilayers. In all cases the multilayers were assembled by successively immersing the particles into the respective polyelectrolyte solutions for 15 minutes, followed by centrifugation (1400 g, 1 min) and three washing cycles. For the different polymer combinations, the first layer was always the polycation or mannan, respectively.

**Table 4.1:** Experimental details for the different solutions used during the LbL assembly on colloidal templates. The pH was adjusted by the addition of HCl and NaOH.

polymers	core material	polymer solution	washing solution
PAH/PMA	$\text{CaCO}_3$	0.5 M NaCl, pH 6	$\text{H}_2\text{O}$ , pH 6
	$\text{SiO}_2$	0.2 M NaCl, pH 5	$\text{H}_2\text{O}$ , pH 5
P4VP/PMA	$\text{SiO}_2$	1:1 methanol : 0.2 M NaCl, pH 5	1:1 methanol: $\text{H}_2\text{O}$ , pH 5
mannan/ PAA-BOH	$\text{CaCO}_3$ / BSA- $\text{CaCO}_3$	0.5 M NaCl, 50 mM phosphate buffer, pH 11	0.5 M NaCl, 50 mM phosphate buffer, pH 11

### 4.3.2 Core dissolution

After the desired number of layers were deposited, the  $\text{CaCO}_3$  templates were dissolved by treatment with EDTA, followed by at least 5 washing steps at the same pH.  $\text{SiO}_2$  particles were dissolved with a buffer solution of 0.2 M  $\text{NH}_4\text{F}$  and HF (see in detail p. 49). To ensure a complete core removal, the buffer system was used five times for one hour. The resulting hollow polymeric capsules were washed five times with water at the same pH to remove HF,  $\text{H}_2\text{SiF}_6$  and  $\text{NH}_4\text{F}$ . In all experiments the centrifugation characteristics were 1400 g and 30 min. The experimental conditions for the core removal are given in Table 4.2.

**Table 4.2:** Experimental details for the different solutions used during the core removal. The pH was adjusted by the addition of HCl and NaOH.

core material	polymers	core dissolution	washing solution
$\text{SiO}_2$	PAH/PMA	0.2 M $\text{NH}_4\text{F}$ /HF, pH 4.5	$\text{H}_2\text{O}$ /HCl, pH 4.5
	P4VP/PMA	0.2 M $\text{NH}_4\text{F}$ /HF, pH 3.5	$\text{H}_2\text{O}$ /HCl, pH 3.5
$\text{CaCO}_3$	PAH/PMA	0.2 M EDTA, pH 7	$\text{H}_2\text{O}$
	mannan/PAA-BOH	0.1 M EDTA, pH 11	50 mM phosphate buffer, pH 11

### 4.3.3 Encapsulation of FITC-dextran

100  $\mu\text{L}$  of a 10 mg/mL FITC-dextran solution at pH 8 were added slowly to 100  $\mu\text{L}$  of a suspension of  $(\text{P4VP/PMA})_4$  capsules. After 15 min incubation, 15  $\mu\text{L}$  0.1 M HCl were added to reseal the capsule shells. The suspension was then centrifuged at 1400 g for 10 minutes and washed 5 times with water.

## 4.4 Measurement conditions

### 4.4.1 pH-measurements

The pH values of all capsule solutions were adjusted with 0.1 M HCl and 0.1 M NaOH. All measurements were performed with a digital pH-meter WTW pH 539 (WTW, Weilheim, Germany) using a combined glass / reference electrode, calibrated with standard buffer solutions of pH 4.0, 7.0 and 10.0.

### 4.4.2 Potentiometric titrations

The potentiometric titrations and data analysis were performed according to a procedure described by Petrov et al. [67]. PAH and PMA (Mw = 75.1 kDa) bulk solutions were prepared at a concentration of 0.5 mg/mL in water. The PAH/PMA stoichiometric complex was prepared directly in a 1:1 monomer unit molar ratio at 5.35 mM, leading to turbid solutions. The titration was performed after one day of complex incubation. The titrations of the weak polyelectrolytes as well as of the stoichiometric complex were performed from the alkaline region, after adjusting the pH with a concentrated NaOH solution to pH 11.6. The potentiometric titrations were performed with 0.2 M HCl, which was added in portions of 20  $\mu$ L to 15 mL of the polyelectrolyte solution. Each experiment included the blank titration of water under the same experimental conditions as the polyelectrolyte titration. Thus, the shift in the titration curve of the polyelectrolyte and the polyelectrolyte complex relative to the blank titration was only determined by the proton uptake of the polyelectrolytes. The ionization degree  $\alpha$  at a certain pH was obtained as the difference of the amount of H<sup>+</sup> added and that in the blank experiment. The pK<sub>app</sub> was determined at an ionization degree of 50 %.

### 4.4.3 Elemental analysis

The elemental analysis was conducted on a VarioEL CHNOS Elementaranalysator (Elementar Analysesystem GmbH, Hanau, Germany). The values for carbon, hydrogen and nitrogen were evaluated by gas-chromatography.

#### 4.4.4 Nuclear Magnetic Resonance

$^1\text{H}$ -Nuclear Magnetic Resonance (NMR) spectra were acquired with a NMR spectrometer DMX400 (Bruker, Karlsruhe, Germany). All spectra were measured in  $\text{D}_2\text{O}$  at room temperature. For the characterization of the signals the following abbreviations were used: s = singlet, d = doublet, t = triplet, q = quadruplet and m = multiplet.

#### 4.4.5 Confocal Laser Scanning Microscopy

Confocal micrographs of polyelectrolyte capsules were taken with a Leica TCS SP confocal laser scanning microscope from Leica (Bensheim, Germany) equipped with a 100x/1.4-0.7 oil immersion objective. Fluorescence labeling of PAH/PMA capsules was achieved by incorporating one layer of TRITC-PAH. For P4VP/PMA capsules one layer of fluorescently labeled PMA was incorporated during the capsule preparation. Mannan/PAA-BOH capsules were visualized by mixing the capsule suspension with a small volume of 1 mg/mL FITC-dextran ( $M_w = 4$  kDa) directly on the microscopic slide. The excitation wavelengths were 488 nm and 543 nm for fluorescein- and rhodamine-labeled samples, respectively. All experiments were conducted in a sealed chamber to ensure constant pH and ionic strength. For determination of the capsule diameter, fluorescence profiles of at least 20 capsules were analyzed with the Leica confocal software (LCS, Version: 2.5) and their diameters were averaged. The error bars correspond to the standard deviation of the averaging. All evaluated diameters represented an equilibrium state and did not change within several hours.

#### 4.4.6 Determination of the osmotic deformation

To determine the time dependence of the osmotic deformation of  $(\text{P4VP/PMA})_4$  capsules, in an initial set of experiments the osmotically induced buckling of labeled capsules with increasing glucose concentration was studied with a CLSM in order to define the critical concentration of the osmotic response. The critical concentration was determined as the concentration where 50 % of the capsules showed deformations of the shells. For the estimation of the critical permeation time, 100  $\mu\text{L}$  of a 0.2 M stock solution of glucose were added under gentle stirring to a 100  $\mu\text{L}$  capsule suspension at a certain pH, using a 100  $\mu\text{L}$  Hamilton syringe (Hamilton, Reno, USA). The final glucose concentration was 0.1 M. The flow rate of the stock solution was varied between 30  $\mu\text{L}/\text{min}$  and 3  $\mu\text{L}/\text{s}$ . The deformation of the capsules was observed by confocal microscopy. In each experiment at least 50 different capsules were investigated [131].

#### 4.4.7 Determination of the capsule concentration

The concentration of mannan/PAA-BOH capsules was calculated with a bright line counting chamber (Sigma-Aldrich, Taufkirchen, Germany), with a volume of 0.1  $\mu\text{L}$  per square. The capsule solution was diluted so that the amount of capsules in one of the squares was in the range of 10 - 20. The measurement was conducted after 15 minutes to ensure a sedimentation of all capsules. The sum of 4 different squares was taken for one measurement and a mean value of 3 measurements was determined.

#### 4.4.8 UV-VIS Spectroscopy

UV-VIS Spectroscopy was used to determine the coupling rate of TRITC and rhodamine B amine to the different polymers and for evaluating the amount of TRITC-BSA that was captured within  $\text{CaCO}_3$  particles. All UV-VIS spectra were recorded with the Cary 50 Conc. spectrophotometer (Varian GmbH, Darmstadt, Germany) in the range of 400 to 700 nm. The UV-VIS spectra were taken in double beam mode, including a blank sample consisting of the buffer solution.

#### 4.4.9 Fluorescence Spectroscopy

Steady state fluorescence measurements were performed with a Spex Fluorolog-2 (model FL-2T2) spectrofluorometer (HORIBA Jobin Yvon, München, Germany). Fluorescence was measured at  $90^\circ$  to the incident beam. The excitation wavelength used throughout the experiments was 556 nm and the excitation and emission slits were both adjusted to 0.8 nm. Emission spectra were recorded with steps of 1 nm and an integration time of 2 s.

#### 4.4.10 Infrared Spectroscopy

ZnSe slides were used as substrates for the capsule deposition. They were cleaned in a 2 % Mucosal solution for 30 min, followed by rinsing with water and ethanol. 10  $\mu\text{L}$  of capsule suspension at different pH were placed on the substrate and dried in air. Experiments were conducted on a Bruker Hyperion 2000 IR microscope (Bruker, Karlsruhe, Germany) with a frequency range from 400 - 4000  $\text{cm}^{-1}$ , which was equipped with a 15x IR-objective and a MCT-detector. Data were acquired in transmittance with a spectral resolution of 4  $\text{cm}^{-1}$  and 128 averaged scans. Each interferogram was divided by the corresponding background of the ZnSe substrate. Infrared microscopy was used, as it combines the advantages of infrared spectroscopy with the possibility to study small amounts of capsules.

#### 4.4.11 Single Particle Light Scattering

SPLS experiments were conducted on a home-built photometer equipped with a Nd:YVO<sub>4</sub> laser (Verdi V-2, Coherent). The light scattered by one particle at a given time was collected in the angular region of 5 - 10° in the forward direction. The intensity was recorded by a multichannel analyzer. Repetition of this process yielded a histogram of particle number vs. scattering intensity. From the maximum of the histogram, the thickness of the adsorbed multilayer was calculated with Mie-theory (analysis program: Coated Sphere by Dr. Bernhard Michel - Scientific Consulting, Feucht-Mosbach, Germany), using a refractive index of 1.47 for the polyelectrolyte layers [161].

#### 4.4.12 Measurement of the electrophoretic mobility

Electrophoretic mobilities of coated silica particles with a mean diameter of 881 nm were measured with a Malvern Zetasizer Nano-Z (Malvern Instruments, Worcestershire, UK). The electrophoretic mobility was converted into the  $\zeta$ -potential with the Smoluchowski relation, using an average mobility value based on 30 measurements. The pH was adjusted with addition of HCl and NaOH. Measurements were performed without additional electrolyte.

#### 4.4.13 Quartz Crystal Microbalance

A Q-Sense E4 apparatus from Q-Sense (Västra Frölunda, Sweden) was used in all experiments. All measurements were taken at 23 °C at the fundamental frequency as well as at the 3rd, 5th and 7th harmonic including the frequency shift and the dissipation. In Chapter 6 only the results of the frequency changes of the 3rd harmonic (15 MHz) are shown. The resonance frequencies of the crystal were measured with a precision of 1 Hz. QCM crystals with a fundamental frequency of 5 MHz were used in all experiments. It is possible to extract the viscoelastic properties of the deposited film by modeling the frequency and dissipation data obtained during the measurement, but this was beyond the scope of this thesis. In the experiments presented here, the QCM was used in a qualitative manner to verify the construction and destruction of multilayer films.

The crystals were cleaned by immersing them into a solution of 5:1:1 H<sub>2</sub>O : H<sub>2</sub>O<sub>2</sub> : NH<sub>4</sub>OH at 78 °C for 5 minutes followed by thorough rinsing with water. The measurement cell was cleaned with a solution of 2 % Mucosal for half an hour at room temperature. Afterwards it was rinsed with water and dried with nitrogen. Prior to the multilayer deposition, the gold surface of the crystal was modified with DTGA-PBA. For this, the crystal was incubated for 12 h in a solution of 1 mg/mL DTGA-PBA in 0.1 M NaOH, thoroughly washed with water and dried with nitrogen. The polymer solutions were injected

into the system with a peristaltic pump during 15 minutes with a velocity of 0.5 mL/min and rinsed during 5 minutes with the buffer solution. At each step the variation in the frequency as well as the dissipation were continuously registered. The polymer solutions were used in a concentration of 2 mg/mL. All assembly and washing solutions contained 0.5 M NaCl and 50 mM buffer. Phosphate buffer was used over the whole pH range studied. For the investigation of the influence of buffer on the layering, different buffers were used in a concentration of 50 mM: HEPES at pH 8, sodium borate at pH 9 and CAPS at pH 11. The sensitivity of assembled multilayers to different carbohydrates was studied in solutions containing 50 mM phosphate buffer.

#### **4.4.14 Atomic Force Microscopy**

AFM measurements were performed in air at room temperature using a Nanoscope III Multimode AFM (Veeco Instruments Inc., Woodbury, USA) operating in tapping mode. Silicon tips with a resonance-frequency of 285 kHz and a force constant of 42 N/m were obtained from NanoWorld AG (Neuchatel, Switzerland). The measurement as well as the following image editing (first order flattening) were conducted with the Nanoscope 5.12r3 software. The samples were prepared by placing a drop of the sample solution onto a freshly cleaved mica substrate and drying it at room temperature. To ensure a better attachment of the negatively charged capsules on the surface, the mica was precoated with poly(ethyleneimine). The single wall thickness of a capsule was determined as half of the height of the collapsed flat region of a dried shell. At least 20 profiles of different capsules were analyzed, and the mean thickness differences between the mica surface and the lowest region of the shells were averaged [162].

#### **4.4.15 Scanning Electron Microscopy**

SEM measurements were conducted with a Gemini Leo 1550 instrument (Zeiss, Oberkochen, Germany) at an operation voltage of 3 keV. A drop of the sample solution was placed onto a glass slide, dried in air and sputtered with gold.

#### **4.4.16 Energy-Dispersive-X-ray analysis**

Energy-Dispersive-X-ray (EDX) analysis was used to determine the elements that were present within a sample. For this, the sample was analyzed in a SEM with a X-ray detector. EDX analysis of capsules templated on SiO<sub>2</sub> particles was performed with a Zeiss DSM 940 scanning electron microscope (Zeiss, Oberkochen, Germany).



# 5 Weak polyelectrolyte capsules

## 5.1 Introduction

Capsules composed of weak polyelectrolytes are an interesting example of stimuli-sensitive microstructures, which exhibit a distinct and reversible change of properties in response to pH and ionic strength. The pH-sensitivity of these systems arises from the pH-responsive functional groups of the weak polyelectrolytes. As the linear charge density along the polymer backbone is a function of pH, the electrostatic interactions within the multilayer can easily be tuned, resulting in pH-dependent changes in morphology, size and permeability.

In the following, two different pH-sensitive polyelectrolyte combinations that vary considerably in their hydrophobic interactions will be investigated, namely capsules composed of PAH and PMA and capsules composed of P4VP and PMA.

The applied experimental conditions were always chosen in a way that maintained the colloidal stability of the particles during the adsorption steps and allowed for the subsequent core removal without destroying the capsule shells. Weak polyelectrolyte shells are not stable in extreme conditions, so that the choice of a suitable core material and the dissolution protocol are crucial steps in the formation of capsules composed of such polymers.

The aim set in this work was to obtain quantitative control of structural changes of capsule walls, which is mandatory for practical applications. In Section 2.4.2 it was shown that organic core materials, like MF and PS, can interfere with the multilayers and change the properties as well as the stability of the resulting polyelectrolyte capsules. Therefore, only inorganic core materials were considered as templates, which have the advantage of a complete core removal and of the absence of osmotic stress during dissolution. In addition, no buffer systems were used to allow a separate investigation of the effect of pH and ionic strength on the pH-response of weak polyelectrolyte capsules.

## 5.2 PAH/PMA capsules templated on $\text{CaCO}_3$

### 5.2.1 Titration experiments

The most important property of weak polyelectrolyte capsules is the pH-dependent charge density along the polymeric chains. To gain insight into the electrostatic interactions between weak polyelectrolytes in different pH domains, the acid-base equilibria of PAH and PMA bulk solutions and of the stoichiometric PAH/PMA interpolyelectrolyte complex were studied. In weak polyelectrolytes, each functional group is influenced by all other groups of the polymer, so that their dissociation behavior in solution is commonly described by an apparent dissociation constant ( $\text{pK}_{\text{app}}$ ), reflecting the overall acid dissociation equilibrium of the polyelectrolyte (see Section 2.1.2).

Figure 5.1 shows the titration curves of PAH and PMA bulk solutions and of the PAH/PMA stoichiometric complex. The degree of ionization  $\alpha$  is given as a function of the pH value of the solution. The  $\text{pK}_{\text{app}}$  values of PAH and PMA in bulk solution are 8.6 and 6.8, respectively. Both values are in good agreement with literature data [67, 100]. The titration curve of the PAH/PMA complex is divided into two regions in the alkaline and the acidic pH ranges. The branch in the alkaline domain corresponds to the ionization of the amino groups of PAH with a  $\text{pK}_{\text{app}}$  of 10.8, and the branch in the acidic domain corresponds to the ionization of the carboxylic groups of PMA with a  $\text{pK}_{\text{app}}$  of 3.9. In the complex the  $\text{pK}_{\text{app}}$  values of PAH and PMA are shifted by approximately 2-3 units to the alkaline (PAH) or to the acidic (PMA) region, respectively. The  $\text{pK}_{\text{app}}$  of the dissociable group of the polyanion is increased

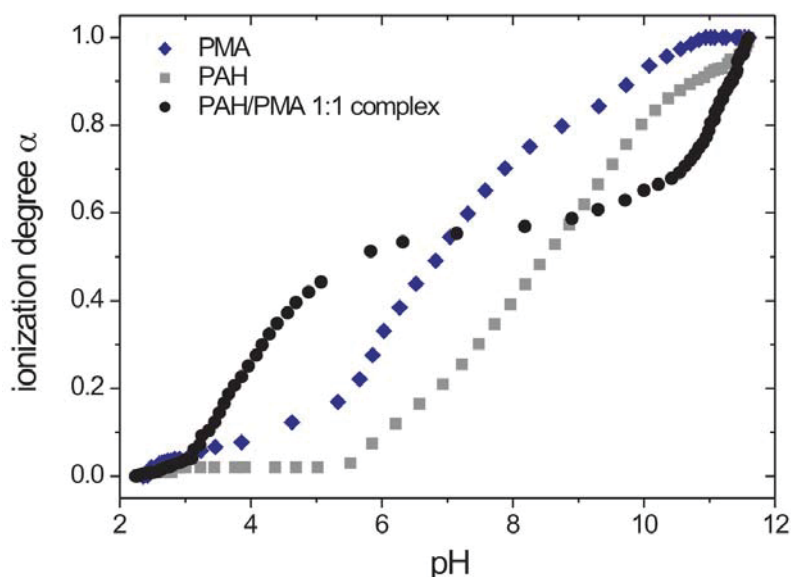


**Figure 5.1:** Potentiometric titration of PAH, PMA, and the stoichiometric PAH/PMA complex. The degree of ionization  $\alpha$  is plotted versus the pH value.

compared to that of the isolated group because the neighboring charges create an attractive potential for the proton. This effect may be reduced or even reversed by complexing with a polycation. This explains the  $pK_{app}$  shift to lower pH values (pH 3.9). Likewise one can understand the shift of the  $pK_{app}$  for the polycation in the complex to pH 10.8 [65, 71, 81].

### 5.2.2 Capsule preparation

Porous  $\text{CaCO}_3$  particles with an average diameter of  $4.4 \pm 0.5 \mu\text{m}$  were used as templates, because carbonate particles can easily be dissolved in neutral pH with EDTA, and the ions formed during dissolution do not interact with the polyelectrolyte multilayer. A maximum of 4 layers was adsorbed onto the  $\text{CaCO}_3$ -particles, as additional layers led to irreversible aggregation during the adsorption. After the multilayer adsorption, the core material was dissolved in 0.2 M EDTA. The morphology of the resulting capsules was monitored in dried state by AFM. Pictures of a typical  $(\text{PAH/PMA})_2$  capsule and of the capsule surface are given in Figure 5.2. Using AFM, the thickness of a PAH/PMA bilayer can be estimated to be  $13.36 \pm 4.6 \text{ nm}$ . As can be seen in Figure 5.2 b, the capsule surface is very rough. The roughness as well as the huge amount of polymeric material adsorbed per bilayer can be explained by properties of the template [39, 45].  $\text{CaCO}_3$ -particles have a very porous structure with a huge inner surface, as shown in the SEM pictures in Figure 2.5. BET analysis revealed a surface area of  $7.72 \cdot 10^{-10} \text{ m}^2$  per particle, compared to a surface area of  $7.11 \cdot 10^{-11} \text{ m}^2$  for a nonporous particle of the same size [141]. The pore size was in the range of 20 to 60 nm [142]. Therefore, polyelectrolytes cannot only adsorb onto the outer surface but also occupy space within the pores, resulting in an increased amount of polymer adsorbed onto these particles. The huge inner surface of the template material results in capsules that are not hollow but have a polymer matrix in the interior of the capsule [45].

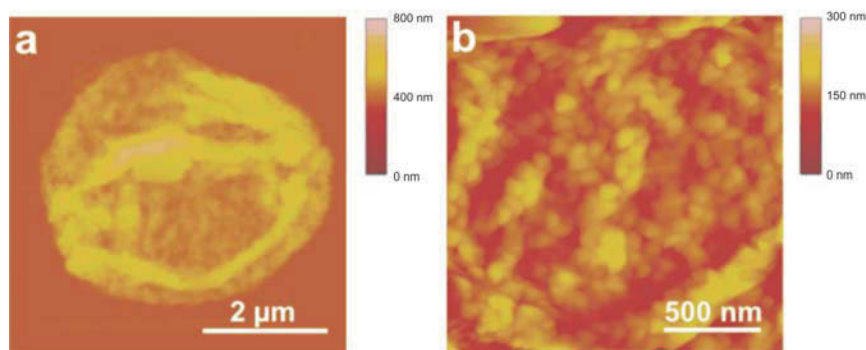


**Figure 5.2:** AFM images of  $(\text{PAH/PMA})_2$  capsules templated on  $\text{CaCO}_3$  particles. (a) Image of a dried capsule, (b) enlarged image of the capsule surface.

### 5.2.3 pH-dependent stability of (PAH/PMA)<sub>2</sub> capsules

The stability of (PAH/PMA)<sub>2</sub> microcapsules with varying pH was investigated, because these capsules are composed of two weak polyelectrolytes and the ionization degree of the bulk complex of these polymers is pH-sensitive. The capsules were prepared at pH 6 and exhibited a diameter of  $3.7 \pm 0.5 \mu\text{m}$ . Figure 5.3 shows the diameter of the polyelectrolyte shells as a function of pH. Two CLSM images illustrate the size of different capsules at pH 6 and pH 2.5, respectively. At pH values above 11.5 and below 2.5 capsule dissolution was observed. However, in the pH range between 2.5 and 11.5 these weak polyelectrolyte shells showed great stability. No significant changes in capsule diameter were seen at pH levels above 2.7, whereas at pH values below 2.7, a twofold increase in capsule diameter to  $8.1 \pm 1.3 \mu\text{m}$  was determined. The swollen multilayer shells were stable for several days. When the pH was decreased further, the capsules dissolved. In alkaline pH the stability of the capsules was different. When the pH was increased above 11.5 a swelling and immediate dissolution of the capsules occurred. It was not possible to stabilize the capsules in their swollen state in basic conditions.

The stability of (PAH/PMA)<sub>2</sub> capsules in the different pH regimes can be explained when taking into account the electrostatic interactions present within the layers. A schematic sketch of these interactions is given in Figure 5.4. At pH 6 both polyelectrolytes are highly charged, as the respective  $\text{pK}_{\text{app}}$  values in the multilayer complex are 3.9 (PMA) and 10.8 (PAH). Hence, there is a global compensation of charges between the polycation and the polyanion. By decreasing the pH, more and more carboxylic groups of PMA are pro-

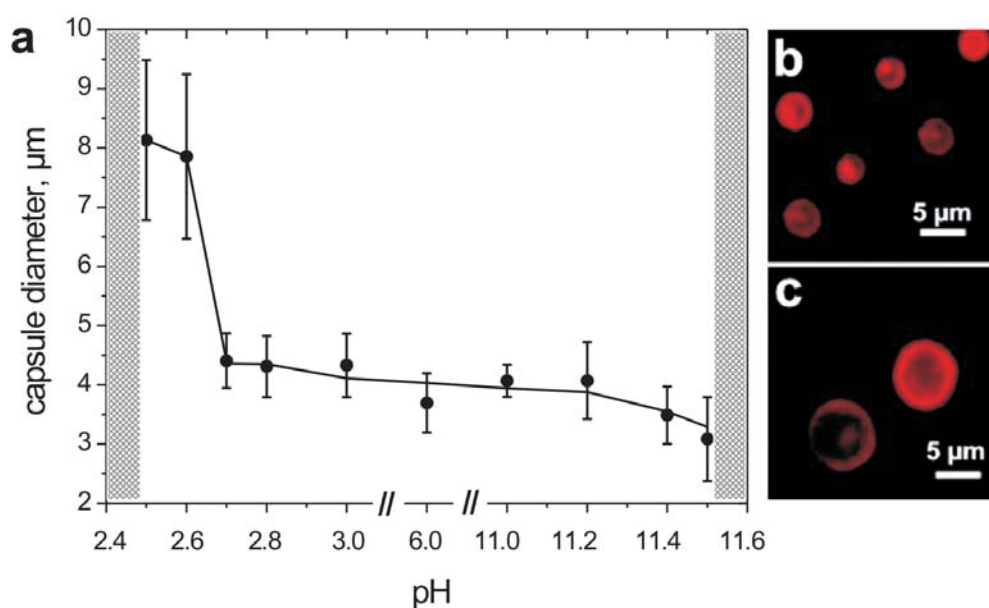


**Figure 5.3:** Diameter of (PAH/PMA)<sub>2</sub> capsules as a function of pH (a). The shaded areas indicate the regions in which the capsules dissolved. CLSM images of different capsules at pH 6 (b) and pH 2.5 (c).

tonated, and only a few ionic pairs between PAH and PMA are maintained, leaving PAH with uncompensated positive ammonium groups. When the pH is increased, the carboxylic groups stay in their ionized form, whereas the ammonium groups of PAH gradually are deprotonated, resulting in a lower degree of electrostatic interactions within the multilayer and uncompensated negative charges. The positive or negative excess charges lead to electrostatic repulsion. In addition, counterions are attracted to ensure local electroneutrality. The higher concentration of counterions compared to the bulk can increase the local osmotic pressure and lead to a swelling effect. The swelling is further promoted by the lack of electrostatic interactions between the polymers to stabilize the capsules [38, 163].

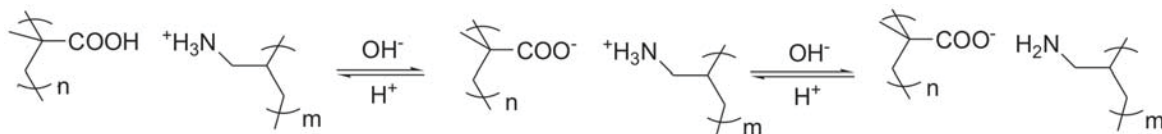


**Figure 5.4:** Scheme of the interactions within PAH/PMA multilayers at different pH.

Comparing the degree of protonation of PMA in a multilayer (see Section 5.1) with the pH value at which the swelling is observed, it is obvious that an ionization degree of less than 10 % of the carboxylic groups is required to observe swelling. It is possible to compare the titration behavior of stoichiometric polyelectrolyte complexes and of multilayered capsules made of the same polyelectrolyte pair, as they show the same proton binding pattern [67]. Similar results have been reported for the disintegration of other weak polyelectrolyte systems on flat substrates [66, 73].

If the only acting force is electrostatic repulsion, the swelling results in an immediate dissolution of the polyelectrolyte multilayers, because the remaining electrostatic interactions are not strong enough to maintain the integrity of the shells. This effect can be observed in basic conditions. However, in the acidic pH domain another interaction plays a role in stabilizing the PAH/PMA shells. At low pH, the uncharged carboxylic groups of PMA are known to interact by hydrogen-bonding [98], resulting in an additional stabilization of the multilayer. Furthermore, PMA in solution exhibits conformational changes at low pH, which are related to hydrophobic associations of the polymeric backbone [14, 164]. Both interactions are assumed to prevent the swollen capsules from dissolution at low pH, and thereby act as a counterforce to the electrostatic destabilization.

The interplay between stabilizing and destabilizing forces is an important condition for stimuli-responsive properties. As it was possible to stabilize swollen capsules at low pH, the reversibility of the size change was investigated. The capsules were alternately exposed to solutions of pH 6 and pH 2.5. Three washing steps at pH 6 ensured a constant ionic strength in different cycles. The results of these experiments are presented in Figure 5.5.

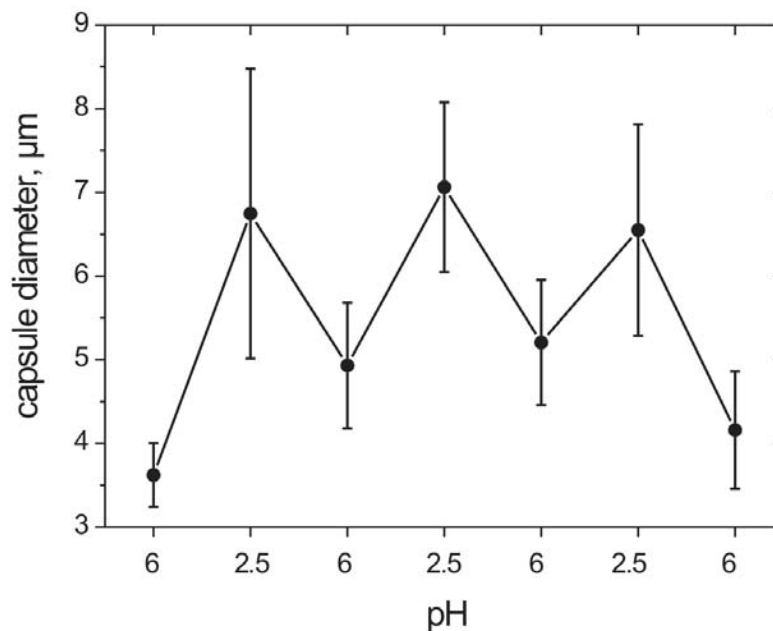


**Figure 5.5:** Diameter of  $(\text{PAH/PMA})_2$  capsules as a function of an alternately changed pH value.

The diameter of the capsules is shown in dependence of the pH of the medium. The swelling was reversible and repeatable when the capsules were cyclically exposed to pH 6 and pH 2.5. The mean capsule diameters were 3.5 - 5  $\mu\text{m}$  at pH 6 and 6.5 - 7.5  $\mu\text{m}$  at pH 2.5, respectively. The first swelling induced the largest differences in the size of the capsules. This can be explained by the porosity of the  $\text{CaCO}_3$  core, which leads to the formation of a polyelectrolyte matrix inside the capsules. When the whole structure is swollen, these polymers are partially incorporated into the shell, leading to differences between individual capsules because the degree of porosity is different for each core. A repetition of the swelling reduces this effect, as the matrix is only partially rebuilt when the diameter of the capsule is decreased. The observed reversibility offers the potential for a wide range of applications, as it is possible to change periodically between two different states of the system by simply changing the pH of the surrounding medium.

However,  $\text{CaCO}_3$  templates are polydisperse and have a porous structure that favors the formation of a polymeric matrix in the capsule interior. This can be a disadvantage, particularly for studying the permeability of the shells.

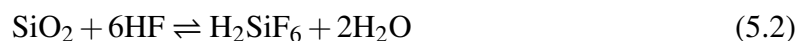
## 5.3 PAH/PMA capsules templated on SiO<sub>2</sub>

### 5.3.1 Dissolution of SiO<sub>2</sub> with HF

An alternative inorganic core material to CaCO<sub>3</sub> is silicon oxide, but formerly the acidic conditions for the dissolution with hydrofluoric acid (HF) only allowed its usage as a template for strong polyelectrolyte capsules [40–42] or for hydrogen bonded multilayers that are stable in acidic conditions [43,44]. Schütz and Caruso assembled weak polyelectrolyte multilayers on SiO<sub>2</sub> cores, but only after the polyelectrolytes were covalently crosslinked, the core material was removed with 1 M HF [84].

Silica particles are commonly dissolved with diluted aqueous solutions of hydrofluoric acid. As HF is a weak acid with a pK<sub>a</sub> of 3.2 at 25 °C [165], the pH of its aqueous solution is a function of the HF concentration. When SiO<sub>2</sub> particles were used as templates for the fabrication of hollow microshells, the dissolution process was accomplished in rather acidic conditions, which are not suitable for weak polyelectrolytes. Itoh and coworkers used 46 % HF for the dissolution step [41], Schütz et al. dissolved the cores with 1 M HF [84] and Adalsteinsson et al. worked with a concentration of 0.5 M HF [40]. The lowest HF concentration for the template dissolution reported by Köhler et al. was 0.1 M [42], resulting in a solution pH of 2.1. At this pH the electrostatic interactions within the multilayers of weak polyelectrolytes are too reduced to keep the integrity of the shells. Thus, the pH of the medium has to be increased.

Theoretically it is possible to work with a reduced HF concentration, but this would result in 0.4 L aqueous HF solution for the dissolution of 10 mg SiO<sub>2</sub> at pH 3. A better choice is to use a buffer system prepared of HF and NH<sub>4</sub>F. According to the Henderson-Hasselbach equation, the pH of the buffer system is only related to the pK<sub>a</sub> of the acid and the relative concentrations of HF and NH<sub>4</sub>F [148]. Hence, it is possible to work in mild pH conditions with an increased HF concentration. The chemical equations (5.1) and (5.2) illustrate the interplay of the creation of HF in the buffer equilibrium and the consumption of HF during the dissolution of SiO<sub>2</sub>.



The combination of the two reactions insures a constant amount of hydrofluoric acid and a constant pH of the solution which is critical for both multilayer and colloidal stability during the core dissolution process.

AFM images of dried PAH/PMA capsules after core removal using a 0.2 M NH<sub>4</sub>F solution at different pH values are displayed in Figure 5.6. At pH 4 and below, no stable capsules could

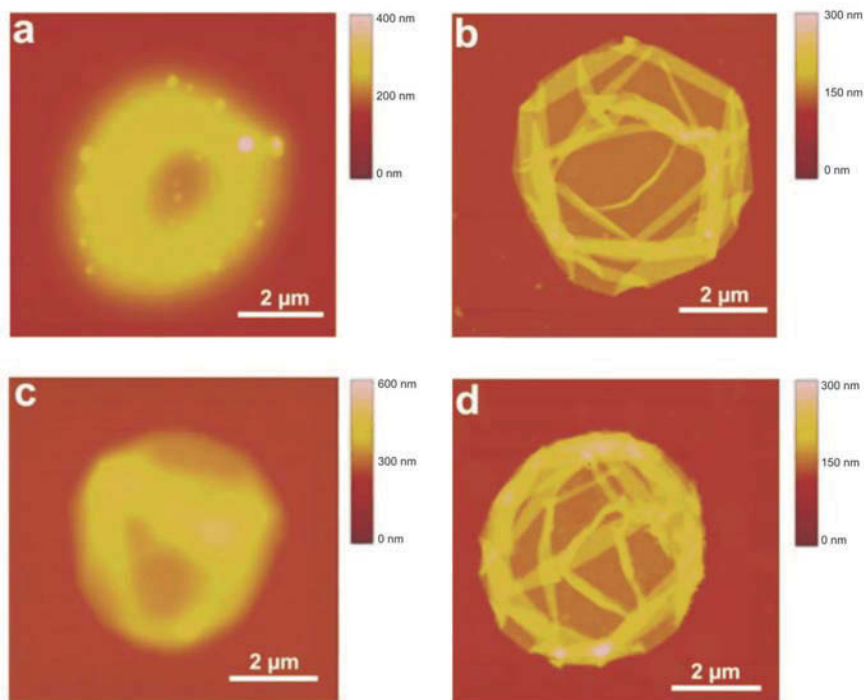


**Figure 5.6:** AFM images of dried capsules templated on  $\text{SiO}_2$ . (PAH/PMA<sub>75kDa</sub>)<sub>4</sub>, dissolution with 0.2 M  $\text{NH}_4\text{F}$  at pH 5 (a). (PAH/PMA<sub>75kDa</sub>)<sub>4</sub>, dissolution with 0.2 M  $\text{NH}_4\text{F}$  at pH 4.5 (b). (PAH/PMA<sub>75kDa</sub>)<sub>8</sub>, dissolution with 0.2 M  $\text{NH}_4\text{F}$  at pH 4.5 (c), (PAH/PMA<sub>790kDa</sub>)<sub>4</sub>, dissolution with 0.2 M  $\text{NH}_4\text{F}$  at pH 4.5 (d).

be obtained, as the electrostatic interactions between the polymers are too low to provide the integrity of the shells during the dissolution step. In Figure 5.6 a the dissolution of the core at pH 5 for capsules made of 8 polymer layers is shown. The shell structure is fuzzy and the mean height of more than 100 nm also suggests that there was still silica gel trapped inside the capsules. An example of a (PAH/PMA)<sub>4</sub> capsule with the core dissolution at pH 4.5 is given in Figure 5.6 b. Dissolving the template at a pH of 4.5 led to smooth and thin hollow capsules until a maximum of 14 layers. If more than 14 polymer layers were adsorbed onto the silicon oxide, complete core removal could not be achieved under the above mentioned conditions. An AFM image of PAH/PMA capsules made of 16 layers is shown in Figure 5.6 c. The blurred structure of the shell and the increased height profile suggest that some silica was still present in the capsules, probably because the shells were too thick or too dense to allow the core material to penetrate. Increasing the molecular weight of PMA to 790 kDa on the other hand did not have any influence on the dissolution process and an AFM image of stable capsules of 8 layers of PAH and high molecular weight PMA is displayed in Figure 5.6 d. For the capsules shown in Figure 5.6 b and 5.6 d, no silicon could be detected in EDX-measurements, ensuring the complete dissolution of the core.

AFM measurements were performed on dried capsules to estimate the thickness of their walls. The results are shown in Figure 5.7. For capsules made of low molecular weight



PMA the thickness increased linearly from 8 to 14 layers with a resulting bilayer thickness of  $3.0 \pm 0.2$  nm. The thickness of capsules prepared with high molecular weight PMA was  $3.4 \pm 0.3$  nm per bilayer. The small differences in the thickness of the shells could be due to a larger entanglement of the polymers when the molecular weight is increased, leading to an increased thickness of each layer. These thickness values are lower than the reported 5 - 5.5 nm per bilayer found for most of the strong polyelectrolyte systems that were adsorbed with an ionic strength of 0.5 [42].

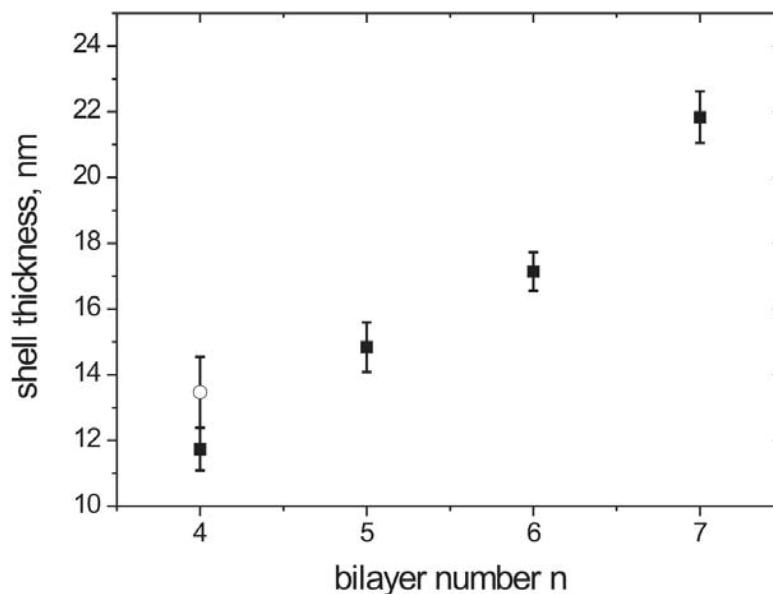


**Figure 5.7:** Thickness of the capsule wall as measured by AFM for  $(\text{PAH}/\text{PMA}_{75\text{kDa}})_n$  (closed symbols) and  $(\text{PAH}/\text{PMA}_{790\text{kDa}})_4$  (open symbol).

The reduced shell thickness can be explained by the differences of the salt concentration used during the adsorption steps. For the assembly of PAH/PMA multilayers a salt concentration of 0.2 M was used, which is less than the sodium chloride concentration of 0.5 M that is normally reported for the assembly of strong polyelectrolyte layers. The reduced ionic strength leads to the formation of thinner multilayers (see Section 2.5.1). Another influencing variable is the pH-dependent thickness behavior of weak polyelectrolyte systems that was studied in detail by Shiratori et al. [71]. For PAH the apparent  $\text{pK}$  is shifted from 8.6 in solution to 10.8 in a complex with PMA. For PMA the  $\text{pK}_{\text{app}}$  is shifted from 6.8 in water to 3.9 in a complex with PAH (see p. 44). As both polymers were adsorbed at pH values below (PAH) and above (PMA) their respective  $\text{pK}_{\text{app}}$  in a multilayer, they yield thin films like strong polyelectrolytes.

### 5.3.2 pH-dependent stability of (PAH/PMA<sub>75kDa</sub>)<sub>4</sub> capsules

Weak polyelectrolyte capsules templated on SiO<sub>2</sub> were stable over a broad pH range, but dissolved at extremely high or low pH. The stability of the capsules as a function of pH as well as CLSM images of the dissolution process are shown in Figure 5.8. Shells made of 8 layers of PAH and low molecular weight PMA were stable within the pH range from 2.3 to 11. In this pH range the size of the capsules was nearly constant with a mean diameter of  $4.4 \pm 0.3 \mu\text{m}$ , corresponding to the size of the silicon oxide templates. If the pH was increased or decreased to extreme values the shells swelled and dissolved within seconds. The dissolution at low pH is shown in Figure 5.8 b - d. As described for (PAH/PMA)<sub>2</sub> capsules templated on CaCO<sub>3</sub> particles (see Section 5.2), the stability in the intermediate pH range can be explained by a global compensation of charges between the ammonium groups of PAH and the carboxylic groups of PMA. At low and at high pH the excess positive and negative charges, respectively, destabilize the multilayer structure (see Figure 5.4). At a critical pH the electrostatic attraction between positive and negative groups is not strong enough to

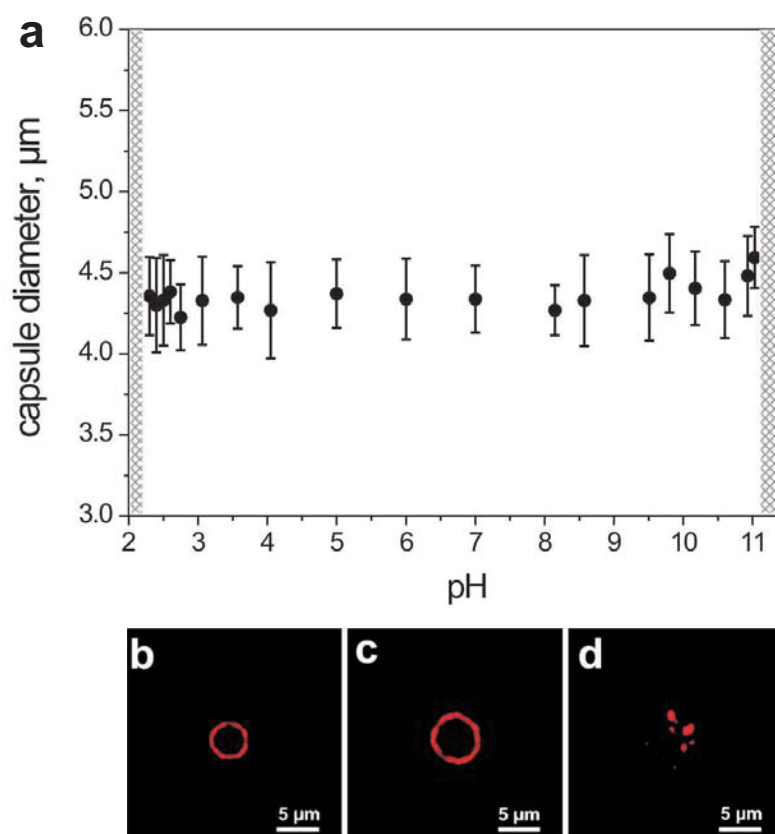


**Figure 5.8:** Diameter of (PAH/PMA<sub>75kDa</sub>)<sub>4</sub> capsules templated on SiO<sub>2</sub> as a function of pH. The shaded areas indicate regions in which the capsules dissolved (a). CLSM images of the dissolution process at low pH. Addition of 0.1 M HCl (pH < 2) (b), swelling of the capsules was observed within 1 s (c), dissolution of the capsules was observed after 2 s (d).

keep the multilayers stable, and the capsules swell and dissolve. Similar effects have also been reported at high pH for the dissolution of PAH/PSS capsules templated on  $\text{CaCO}_3$  or  $\text{MnCO}_3$  [38].

In contrast to the stable swollen capsules observed at low pH for PAH/PMA<sub>75kDa</sub> capsules prepared on  $\text{CaCO}_3$  (see Section 5.2), it was not possible to stabilize swollen capsules templated on  $\text{SiO}_2$  at low pH, regardless of the number of deposited layers. The differences in stability could be a result of the different nature of the core material. The large cavities in the  $\text{CaCO}_3$  particles result in a much higher amount of adsorbed polymer material, leading to the formation of a polymeric matrix. For the adsorption on  $\text{CaCO}_3$  particles a bilayer thickness of  $13.36 \pm 4.6$  nm was observed, compared to the bilayer thickness of  $3.0 \pm 0.2$  nm for the deposition on  $\text{SiO}_2$  particles. These differences in the amount of adsorbed polymer could explain the different stability of swollen capsules at low pH.

### 5.3.3 pH-dependent stability of (PAH/PMA<sub>790kDa</sub>)<sub>4</sub> capsules

(PAH/PMA)<sub>4</sub> capsules prepared of high molecular weight PMA showed a different pH-dependent stability at the edges of the stability range than capsules prepared with low molecular weight PMA. The capsule size as a function of pH is depicted in Figure 5.9. The capsules were stable within the pH range from 2.3 to 11.1 and dissolved in extreme conditions. From pH 2.4 to 10.4 the mean diameter was nearly constant with  $4.4 \pm 0.3$   $\mu\text{m}$ . Below pH 2.4 the capsules swelled by 20 % to a mean diameter of  $5.5 \pm 0.6$   $\mu\text{m}$ . In the pH range from 10.4

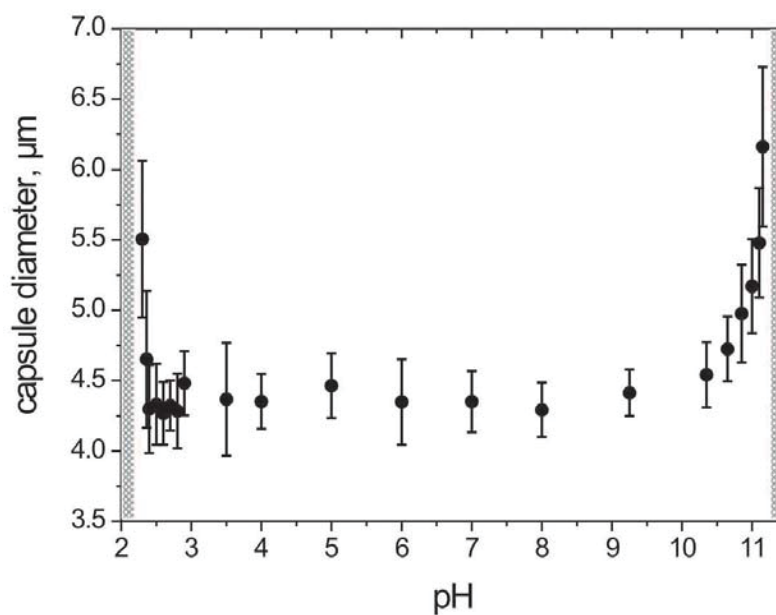


**Figure 5.9:** Diameter of (PAH/PMA<sub>790kDa</sub>)<sub>4</sub> capsules as a function of pH. The shaded areas indicate regions in which the capsules dissolved.

to 11.1 they swelled by 35 % to a diameter of  $6.2 \pm 0.6 \mu\text{m}$ . Both swollen structures were stable for several days. At low pH the swelling occurred over only 0.1 pH unit, whereas at high pH the increase in size was a more continuous transition over 0.7 pH units.

One parameter influencing the stable swollen state at low pH can be attributed to intermolecular hydrophobic stabilization of uncharged PMA that is accompanied by a conformational change of the polymer backbone from coil to globule of PMA in aqueous solution [14, 164]. In addition, uncharged polycarboxylic acids are stabilized by hydrogen bonds, that can stabilize polyelectrolyte multilayers in acidic media [98] (see p. 46). Furthermore, one also has to consider the polymeric entanglement as an important factor in the stabilization process, as capsules prepared of low molecular weight PMA do not show any stabilization of the swollen state. At high pH, the entanglement of polymers seems to be the only stabilization, as no other efficient forces counteracting the electrostatic repulsion are known for uncharged polyallylamine. Déjournat et al. found a similar stabilizing effect of the swollen state at high pH of PAH/PSS capsules and they attributed the modified pH response to a rigidification of the structure by increasing either the number of layers or the molecular weight of the assembled polyelectrolyte [38].

The reversibility of the swelling as a function of pH is displayed in Figure 5.10. Swollen capsules at pH 2.3 and 11.1 were washed with water at pH 4 and 6, respectively, and the capsule diameter was determined after one hour. The diameter of capsules that were previously swollen at low pH decreased to  $4.5 \pm 0.2 \mu\text{m}$ , whereas capsules that were first exposed to a solution of pH 11.1 only showed a decrease in size to  $5.2 \pm 0.3 \mu\text{m}$ .

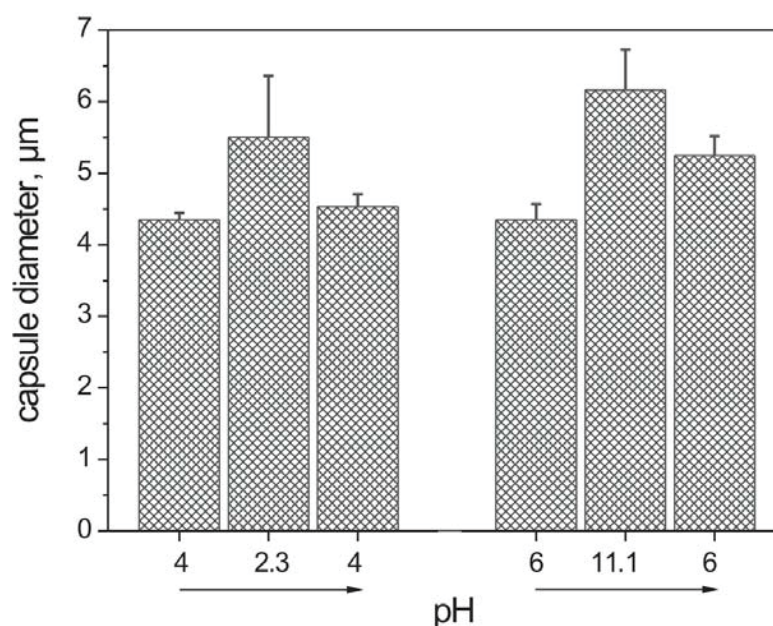


**Figure 5.10:** Reversibility of the swelling of  $(\text{PAH}/\text{PMA}_{790\text{kDa}})_4$  capsules at low and at high pH.

A possible explanation for the differences in the reversibility of the swelling could be the different polymer conformations at low and at high pH. When the pH is changed after the capsules are swollen, the repulsion between neighboring functional groups is reduced and the electrostatic attraction between the different layers is increased. A change in entanglement of the layers can counteract the shrinking of the shell, resulting in a size that is larger than that of the original capsules.

### 5.3.4 Influence of ionic strength on (PAH/PMA<sub>790kDa</sub>)<sub>4</sub> capsules

When swollen (PAH/PMA<sub>790kDa</sub>)<sub>4</sub> capsules at low and at high pH were exposed to solutions of increased ionic strength, they dissolved within seconds. When the pH-dependent stability with increased ionic strength was investigated, the stability of the capsules as well as the swelling behavior were altered. The results are shown in Figure 5.11.

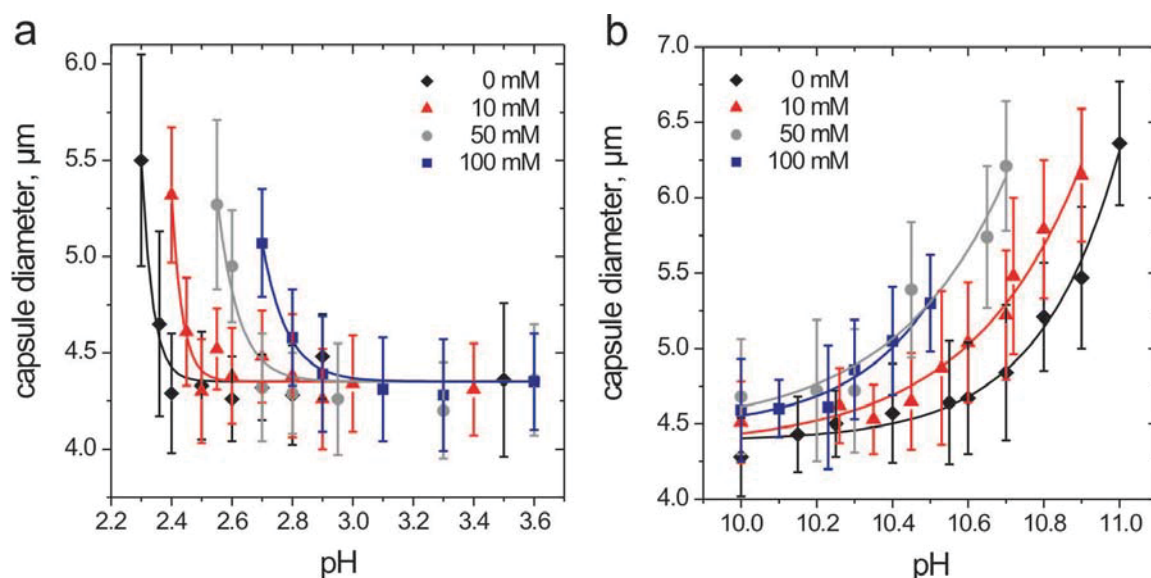


**Figure 5.11:** Influence of the addition of NaCl on the pH-dependent stability of (PAH/PMA<sub>790kDa</sub>)<sub>4</sub> capsules. Low pH region (a), high pH region (b). The lines serve as visual guides.

The increase of the ionic strength led to less stable capsules in the pH regions of 2 - 3 and 10 - 11. The stability range was decreased compared to the situation without added salt. At low pH the swelling set in at a slightly increased pH value, whereas in basic pH the swelling set in at a decreased pH value. Additionally, at a given pH, the capsule diameter was increased when the ionic strength was increased.

Figure 5.11 a describes the swelling at low pH with the addition of 10 - 100 mM NaCl. For all salt concentrations investigated at low pH, the maximal stable swelling was slightly reduced in size compared to the swelling without added salt, but the observed effect was still within the range of the error bar. All swollen capsules dissolved when the pH was lowered

further. Figure 5.11 b shows the stability of capsules that were exposed to solutions containing 10 - 100 mM NaCl in the pH range from 10 to 11. Here it was also observed that swollen capsules dissolved, once the pH was increased further. The general expectation would be to observe a decrease in capsule swelling with increasing ionic strength at a given pH, due to a reduction of the difference in ion concentration between the multilayer surface and the bulk. However, the experimental results showed an increased swelling with increasing ionic strength at a given pH.

These results can be understood when one considers the local charge distribution near the polymeric shells. In the low pH region there is an excess of positive charges of ammonium groups of PAH present within the multilayer. If there were no counterions in the solution, protonation of the amino groups would be hindered due to the electroneutrality condition. The addition of salt (NaCl) to such a system favors the protonation of the ammonium groups, as the positive charges can be compensated by  $\text{Cl}^-$ . This results in an increase of the ionization degree of the polymer chains. As a consequence, the onset of swelling of weak polyelectrolyte capsules in acidic solutions is shifted to higher pH values, and the swelling at a given pH is increased when the ionic strength of the solution is increased.

This shift in the protonation / deprotonation equilibrium was also found in the pH range from 10 - 11, at which an increased ionic strength induced the onset of swelling at a decreased pH. Such a behavior is similar to the osmotic brush regime that is well known for polyelectrolyte brushes composed of weak polyacids or polybases [166–169]. The observed effects of an increase in the ionic strength reported here occurred at much lower salt concentrations than the smoothing and shrinking of capsules composed of PAH/PSS. In that case the shrinking was attributed to a rearrangement of polyelectrolyte chains resulting in an energetically more stable shrunk state [57,58].

### 5.3.5 Investigation of the role of calcium-ions on the multilayer stability

The functional groups of weak polyelectrolytes are protonated or deprotonated depending on the pH of the solution, therefore they either participate in the electrostatic interactions with the other polymer or are available for selective reactions at the uncomplexed moieties. The potential of such reactions was studied by the addition of  $\text{Ca}^{2+}$  to the shells at different pH values. Calcium ions are known to bind to  $-\text{COO}^-$  groups [135, 170], leading to the formation of complexes that can precipitate in solution. The effect of  $\text{Ca}^{2+}$ -binding at low pH is demonstrated in Table 5.1. The increase of the calcium concentration led to a decrease in the capsule stability at low pH and the onset of swelling at a slightly higher pH. This allowed for a selective tuning of the stability of the multilayers as a function of the amount of added calcium and pH.

**Table 5.1:** Stability and swelling of (PAH/PMA<sub>790kDa</sub>)<sub>4</sub> capsules at low pH as a function of the concentration of calcium ions in the solution.

CaCl <sub>2</sub> concentration, mmol/L	pH of the onset of capsule swelling
0	2.3
1	2.4
5	2.6
10	2.7
20	2.9

The reduced stability could be influenced by the competitive binding of Ca<sup>2+</sup>, ammonium groups of PAH and H<sup>+</sup> to the carboxylic groups, thereby reducing the electrostatic interactions between PAH and PMA which stabilize the multilayers. Furthermore, an increase in the ionic strength could lead to a reduction of the stability of capsules at low pH, as it was observed for the addition of NaCl. Most probably a combination of these factors destabilized the shells at low pH.

The effect of calcium in the basic pH range is illustrated in Figure 5.12. The exposure of capsules to a solution of 10 mM CaCl<sub>2</sub> increased the aggregation between the shells, as the outermost layer is negatively charged (-COO<sup>-</sup> groups of PMA) and a bridging of Ca<sup>2+</sup> be-

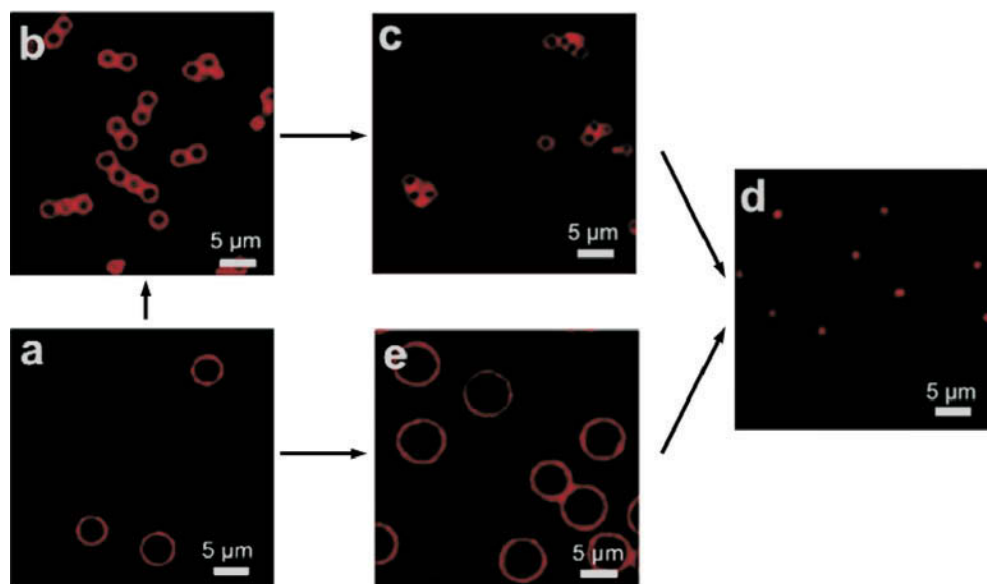


**Figure 5.12:** CLSM images of the effect of calcium ions on (PAH/PMA<sub>790kDa</sub>)<sub>4</sub> in the basic pH range. Capsules in water at pH 7 (a) and at pH 11.1 (e). Capsules in 10 mM CaCl<sub>2</sub> at pH 7 (b), at pH 10 (c) and in 10<sup>-4</sup> M CaCl<sub>2</sub> at pH 11.1 (d). Experimentally the process has been proceeded from either a-b-c-d or a-e-d.

tween different capsules is favored. Furthermore, the capsule size decreased with increasing pH, leading to shrunk particles at a pH of 11.1 (Figure 5.12 a-b-c-d). If calcium chloride in a concentration of  $10^{-4}$  M was added to swollen capsules at pH 11.1 a shrinking of the structures to small particles was induced (Figure 5.12 a-e-d). The addition of HCl or EDTA to the shrunk particles could not restore the original size.

A mechanism for the calcium-binding is proposed in Scheme 5.13. The ammonium groups of PAH are deprotonated in basic medium, resulting in carboxylic groups that are not taking part in electrostatic interactions. As calcium ions are present in the solution, they bind to the carboxylic groups and form a complex. Since there are only few electrostatic interactions between the polymers left at pH 11.1, a small amount of calcium is sufficient to form a precipitate. The addition of EDTA or HCl reduces either the amount of  $\text{Ca}^{2+}$  by complexation or the available binding sites for calcium, but there is no shape memory in the system that would restore the original size.

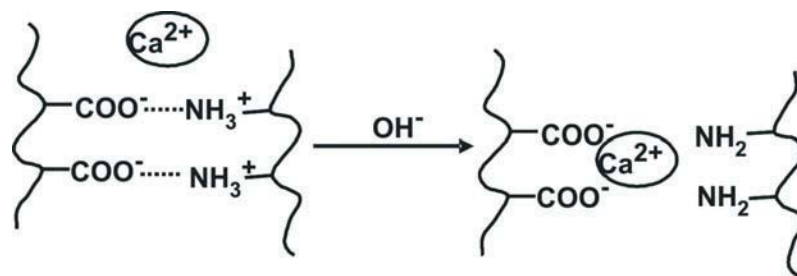


**Figure 5.13:** Mechanism of the binding of calcium ions to carboxylic groups in basic medium.

Uncompensated carboxylate and ammonium groups within multilayers of weak polyelectrolytes were also used as anchoring points for the synthesis of nanoparticles by Rubner and coworkers as well as by Schütz and Caruso [77–79]. In these studies, the charge excess was created during the LbL assembly. In contrast, the results above clearly indicate that post-assembly pH changes result in uncomplexed moieties within the film, that can be used for reactions that are restricted to free functional groups within the multilayer.



## 5.4 P4VP/PMA capsules

### 5.4.1 Formation of P4VP/PMA multilayers on silica templates

A second weak polyelectrolyte system was investigated, namely capsules composed of P4VP and PMA. Both polyelectrolytes used for the multilayer assembly are known for their hydrophobic interactions, P4VP is insoluble in water in its uncharged form [171] and PMA exhibits H-bonding stabilization [98] and hydrophobic interactions at low pH [14, 164]. Thus, capsules prepared with this polymer combination should be stabilized by attractive forces that counteract the electrostatic repulsion.

P4VP and PMA were alternately adsorbed onto silicon oxide particles with a mean diameter of 881 nm at pH 5. The adsorption process can be monitored by microelectrophoresis (Figure 5.14). Bare SiO<sub>2</sub> particles at pH 5 displayed a  $\zeta$ -potential of -56 mV. Regular alternation of the  $\zeta$ -potential between ca.+35 mV and ca.-47 mV for the P4VP and PMA layers, respectively, was found, suggesting successful deposition of P4VP and PMA. The first P4VP layer displayed a higher  $\zeta$ -potential of +63 mV in comparison to the following odd layers.

The higher potential can be understood if one takes into account that the weak polybase can adjust its charge depending on the local environment to maximize the charge compensation (see Section 2.6.2). The alternation in the sign of the  $\zeta$ -potential and therefore of the surface charge of the covered templates occurred with each additional layer, indicating the existence of electrostatic interactions for the assembly of the multilayers.

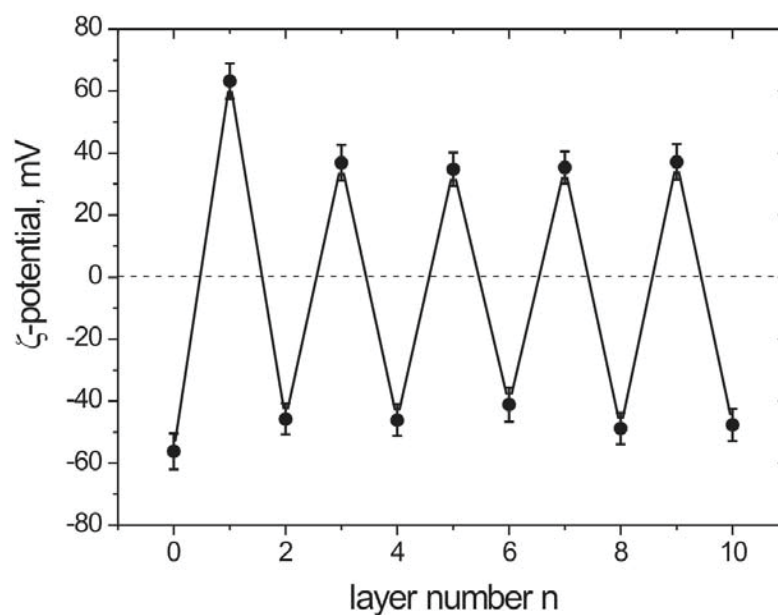


**Figure 5.14:**  $\zeta$ -potential of P4VP/PMA coated silica particles with a diameter of 881 nm as a function of the number of deposited layers. Odd layer numbers correspond to the deposition of P4VP, even layer numbers represent the deposition of PMA. All measurements were performed in deionized water at pH 5.

Notably the change in the sign of the  $\zeta$ -potential does not indicate whether adsorption or desorption has occurred with each polyelectrolyte cycle. A clear indication of the adsorption process of the polyelectrolytes can be given by Single Particle Light Scattering of the covered colloids. Figure 5.15 describes the thickness of the multilayer as a function of the layer number  $n$ , for the adsorption of 16 layers of P4VP and PMA onto silica particles with a mean diameter of 881 nm. The adsorption process followed in a linear manner. Using a refractive index of 1.47 [161], an average thickness of  $6.1 \pm 0.8$  nm per bilayer was found.

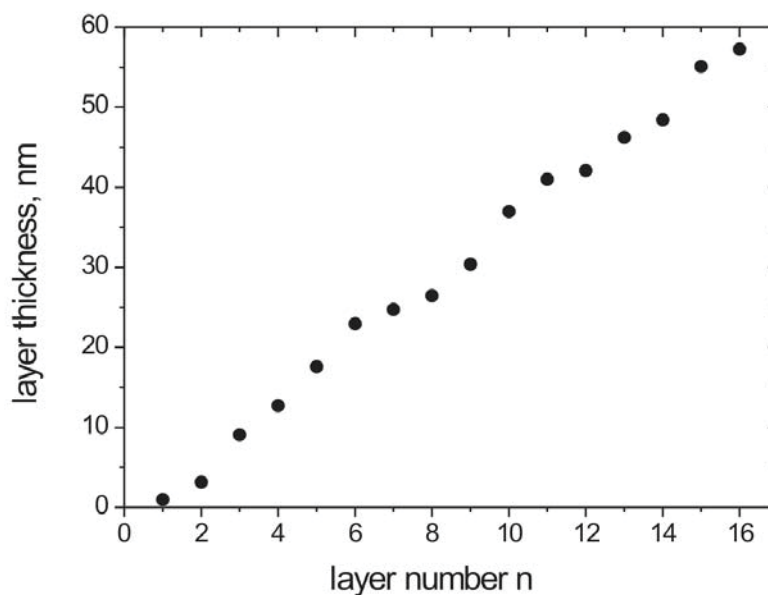


**Figure 5.15:** P4VP/PMA multilayer film thickness on SiO<sub>2</sub> particles with a diameter of 881 nm, as monitored by SPLS.

As the multilayer is composed of two polyelectrolytes with weak acid or base groups, the charge density along the polymer backbone and the density of the individual charges within the multilayers should be a function of pH. The surface charge of colloidal particles can be studied with microelectrophoresis, from which the  $\zeta$ -potential can be calculated. The electrophoretic mobility of silicon oxide particles (diameter: 881 nm) coated with (P4VP/PMA)<sub>4</sub> and with (P4VP/PMA)<sub>4</sub>P4VP layers as a function of pH of the dispersing medium was investigated. Particles coated with eight layers resulted in an outermost layer consisting of the polyanion PMA while particles coated with nine layers led to a multilayer that was terminated by the polycation P4VP. The results are shown in Figure 5.16.

Irrespective of the outermost layer the  $\zeta$ -potential could be reversed from negative to positive values by increasing the acidity of the solution. As it is well established that polyelectrolyte multilayers comprise networks of interpenetrated polymer chains (see Section 2.4.1), the surface charge is not only determined by the last adsorbed layer but the underlying polyanion or polycation layer also has an influence on the surface charge, explaining the observed reversal

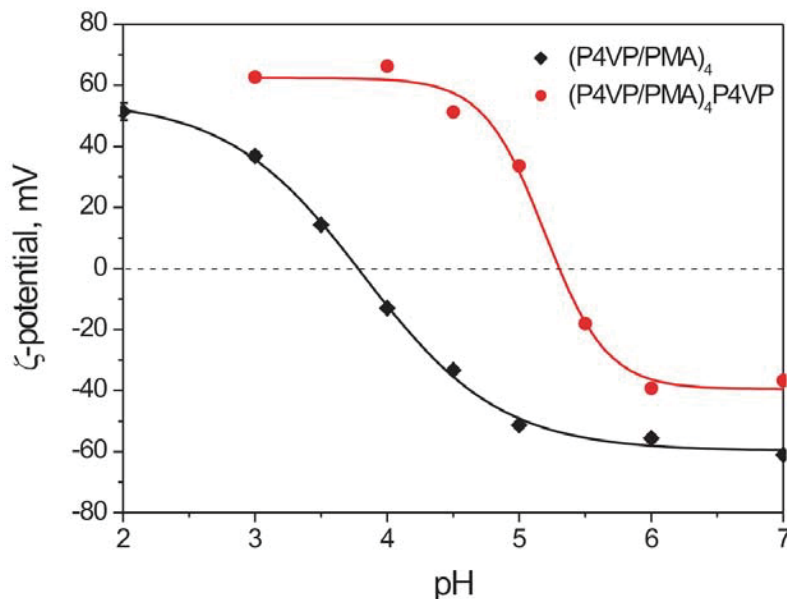


**Figure 5.16:**  $\zeta$ -potential titration curves of silica particles with a diameter of 881 nm coated with  $(P4VP/PMA)_4$  and  $(P4VP/PMA)_4P4VP$  layers. The solid lines serve as visual guides.

of the  $\zeta$ -potential. The graphs in Figure 5.16 represent titration curves and can therefore be used to determine the apparent dissociation constants of the acid and base functional groups on the surface [81]. This is particularly useful, as aqueous solutions containing P4VP can not be titrated over the complete range of  $\alpha$ , because P4VP is only water-soluble at low pH and precipitates in the range of higher pH. The apparent dissociation constant is given by the pH at the inflection point of the  $\zeta$ -potential titration curves [172]. This resulted in  $pK_{app}$  values of 3.8 and 5.3 for PMA and for protonated P4VP adsorbed onto a multilayer, respectively. The acid-base equilibria in multilayers deviate from the solution behavior of the corresponding polymers, as they do not only depend on the external pH and ionic strength, but also on the local microenvironment including the charge density of an oppositely charged self-assembled polyelectrolyte and the charge of the polymer included in the top layer (see Section 2.6.2).

The electrostatic interaction between polyacid and polybase increases the dissociation in both polymers. The increase in base strength of P4VP from dilute solution ( $pK_{app} = 4.3$  [171]) to the adsorbed state may be attributed to the influence of negatively charged carboxylic groups of the underlying PMA layer in promoting the protonation of the pyridine groups, which is bigger than the resistance to protonation because of electrostatic repulsion of neighboring groups. The same argument can be used for the increased acidity of PMA in the multilayers compared to the solution behavior, as in this case the charge density of the PMA chains decreases with decreasing pH, but at the same time the protonation degree of the P4VP chains from the previously adsorbed layer is increased. The protonated P4VP strongly promotes

the dissociation of the  $-\text{COOH}$  groups to neutralize the high residual positive charge obtained with decreasing pH, leading to a decrease in the  $\text{pK}_{\text{app}}$  of the PMA terminated surface in comparison to the solution  $\text{pK}_{\text{app}}$  of 6.8 (see p. 43).

### 5.4.2 Formation of capsules

Silicon oxide particles with a mean diameter of  $4.48 \mu\text{m}$  were used as templates for the deposition of polyelectrolyte multilayers. After the core dissolution with a buffer system composed of ammonium fluoride and hydrofluoric acid, hollow capsules could be obtained. SEM and AFM pictures of dried capsules composed of 10 layers are shown in Figure 5.17. The mean thickness per bilayer as determined by AFM was  $3.6 \pm 0.4 \text{ nm}$ . This value was much lower than the obtained bilayer thickness of  $6.1 \pm 0.8 \text{ nm}$  determined by SPLS. One possible explanation for the observed differences can be the water content of the multilayers, as AFM data were collected on dried capsules whereas SPLS experiments were conducted in wet state. Differences in layer thickness appear with drying and loss of water within the multilayers [173].

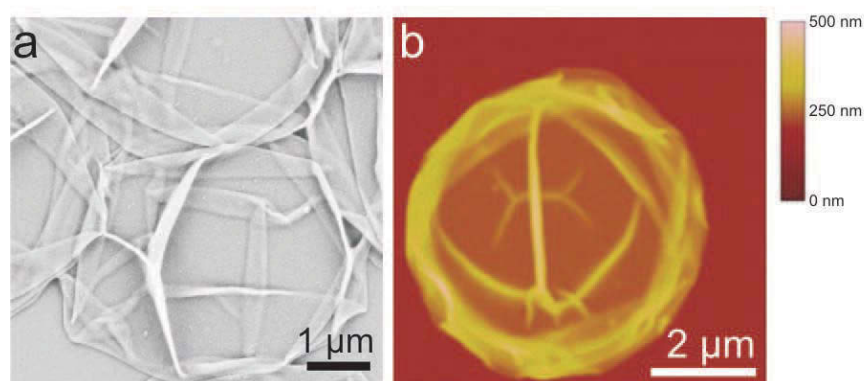


**Figure 5.17:** SEM (a) and AFM (b) pictures of dried hollow  $(\text{P4VP/PMA})_5$  capsules.

$\zeta$ -potential measurements of multilayers adsorbed onto silica particles investigate the surface charge and therefore the ionization degree of a polycation or polyanion adsorbed on top of a multilayer. But this technique does not give any information about the dissociation behavior in the interior of the film. To gain more insight into the interactions present within the layers at different pH and therefore into the stability of the shells, infrared spectra of polyelectrolyte capsules were measured. Infrared spectroscopy measurements were made on capsules dried from suspensions of different pH, and differences in the IR-bands of  $-\text{COO}^-$  and  $-\text{COOH}$  of PMA and of pyridine and pyridinium groups of P4VP were investigated.

The drying process can have an influence on the exact pH value, but nevertheless the evaluation of IR bands of multilayered shells provides an indication of the interactions present within the layers [68]. The IR spectra of capsules as a function of pH are shown in Figure 5.18. The individual spectra are overlaid for clarity. The absorption band at  $1560\text{ cm}^{-1}$  is attributed to the carboxylate ( $-\text{COO}^-$ ) asymmetric stretch, whereas the band at  $1716\text{ cm}^{-1}$  originates from  $\text{C}=\text{O}$  of the carboxylic groups ( $-\text{COOH}$ ). The peak centered at  $1638\text{ cm}^{-1}$  is associated with the in plane stretch of the charged pyridinium ring and the peak centered at  $1604\text{ cm}^{-1}$  stems from the neutral ring [66, 174].

Pure PMA exhibits a strong absorption band at  $1701\text{ cm}^{-1}$  which is due to the stretching of the uncharged dimerized or associated form of carboxylic groups. The shift to higher frequencies compared with pure PMA is an indication that hydrogen bonds among the carboxylic groups of PMA are partly detached and intermolecular hydrogen bonds are formed with P4VP [43]. The relative ratios of  $-\text{COOH}$  and  $-\text{COO}^-$  and of unprotonated and protonated P4VP in the capsules were not investigated quantitatively because of the overlap with bands associated with the in-plane vibration of pyridine groups in the region of  $1518 - 1573\text{ cm}^{-1}$  [66, 101]. The peak at  $1716\text{ cm}^{-1}$  that is assigned to the uncharged carboxylic groups was present over most of the pH range investigated and it only vanished in the pH

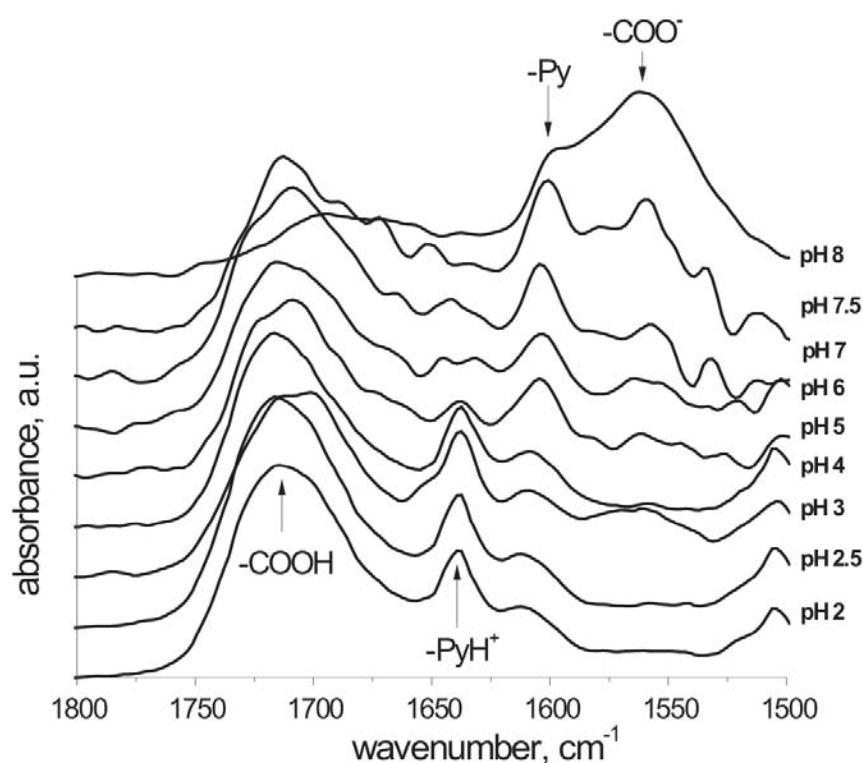


**Figure 5.18:** Infrared-spectra of  $(\text{P4VP/PMA})_5$  capsules as a function of pH. The spectra are overlaid with an arbitrary offset for clarity.

range from 7.5 to 8. At pH values higher than 6 the intensity of the peak at  $1560\text{ cm}^{-1}$  increased. The absorption associated with the protonated pyridinium groups existed until a pH of 5, whereas in the range from pH 5 - 8 the intensity of the peak centered at  $1604\text{ cm}^{-1}$  increased. In the intermediate pH region pyridine as well as pyridinium groups coexist within the multilayer while only a small fraction of the carboxylic groups is deprotonated. A summary of the different interactions within the film as a function of pH is shown in Figure 5.19.

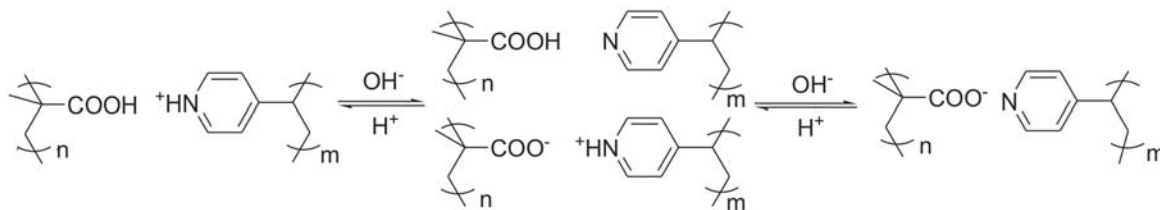


**Figure 5.19:** Summary of the interactions within P4VP/PMA multilayers at different pH.

In the intermediate pH range the stabilization between the layers seems to be due to a combination of hydrogen-bonding and electrostatic interactions. Multilayer films composed of P4VP and PAA that are assembled in pure methanol are stabilized only by hydrogen-bonding interactions [93, 175]. Pure H-bonding interactions were also observed, when PAA was deposited from acidic aqueous solutions and P4VP from ethanol [60]. On the other hand, Abe et al. only considered electrostatic interactions between the polyelectrolytes when they discussed the stability of a polyelectrolyte complex of PMA and P4VP in different water : methanol mixtures [176]. Cho et al. regarded multilayers formed of P4VP and PAA prepared in a water : methanol mixture at pH 3.5 to be mainly stabilized by hydrogen-bonding but also considered electrostatic interactions to be present within the layers [101]. Sukhishvili and coworkers studied the ionization and pH-dependent stability of flat multilayers with PMA and QP4VP with different alkylation degrees ranging from 12 to 98 %. They found that film growth at pH 5 was primarily controlled by electrostatic interactions [66]. Whereas in the intermediate pH range the multilayers are stabilized both by hydrogen-bonding and electrostatic interactions, higher and lower pH values lead to an excess of negative and positive charges within the film, respectively. Whenever there is an increase of the concentration of one charged group in combination with a decrease of the attractive (electrostatic or H-bond) interactions between different layers, the multilayers are destabilized. A comparison of the  $\zeta$ -potential data with the IR-spectra shows a different charge regulation of the functional groups on the surface and within the multilayers. The data suggest that the interactions within the layers are stabilized against pH changes. A similar stabilization of the degree of ionization within a PAH/PSS multilayer was reported by Itano et al. [86].

### 5.4.3 pH-dependent behavior of P4VP/PMA capsules

Capsules composed of 10 layers of P4VP and PMA exhibited a pH-dependent stability. In Figure 5.20 the capsule diameter is shown as a function of pH, and confocal micrographs of individual capsules at different pH are given.

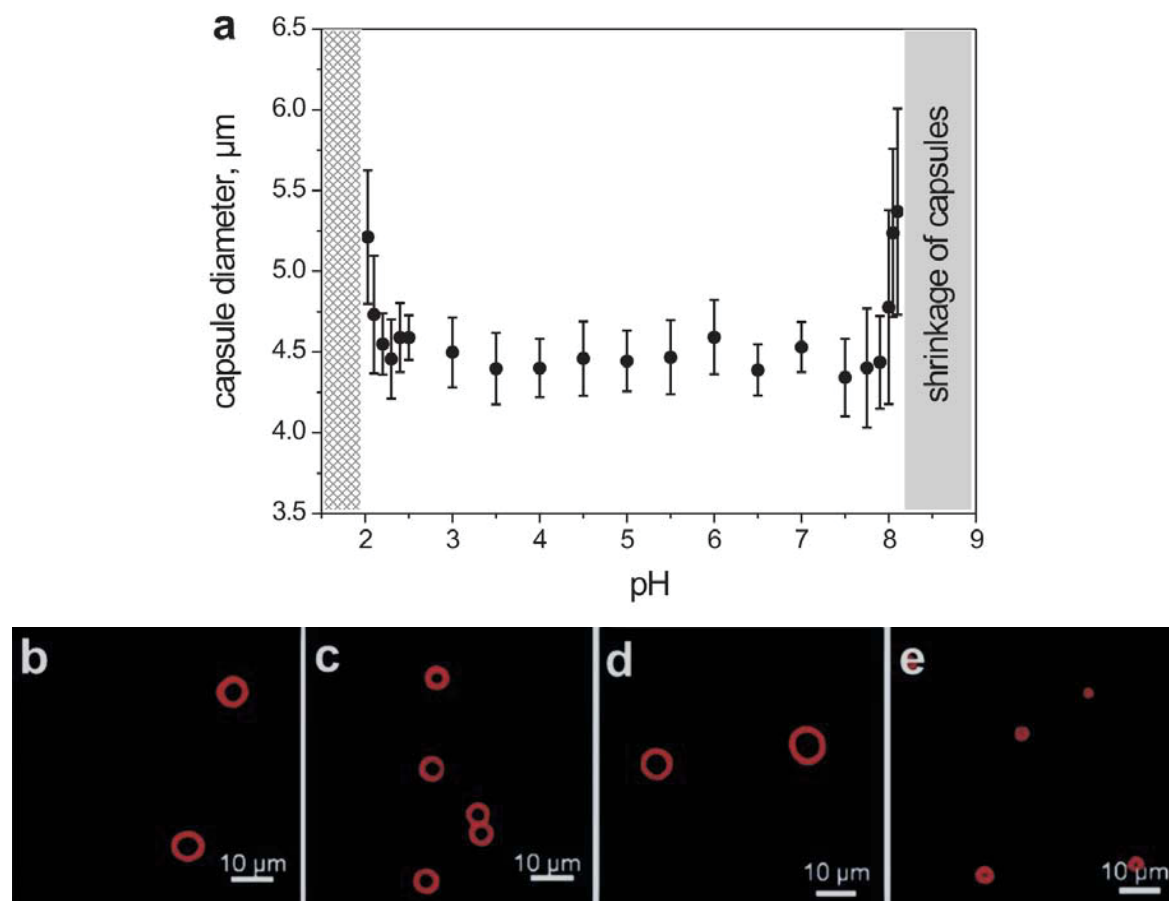


**Figure 5.20:** Diameter of  $(\text{P4VP/PMA})_5$  capsules as a function of pH (a). The shaded area indicates the region in which the capsules dissolved ( $\text{pH} < 2$ ). At  $\text{pH} > 8.1$  the capsules shrunk to particle-like structures. CLSM images of individual capsules at different pH are shown in panels b - e: swollen state at pH 2 (b), initial state at pH 5 (c), swollen state at pH 8.1 (d), collapsed state at pH 9 (e).

In the intermediate pH range from 2.2 - 7.9 the capsules were stable with a diameter of  $4.5 \pm 0.3 \mu\text{m}$  as measured by CLSM, which was determined by the diameter of the template. When the pH was reduced to pH 2 the capsules swelled by 16 % to a diameter of  $5.3 \pm 0.4 \mu\text{m}$  and with further reduction of the pH the multilayers decomposed and dissolved. At a pH of 8 a similar phenomenon was observed, the systems swelled to a diameter of  $5.4 \pm 0.6 \mu\text{m}$ , which corresponds to a swelling of 20 %. When the pH was further increased the capsules shrunk, until they reached a globular state with diameters below  $2 \mu\text{m}$ . This complicated pH-dependent behavior can be rationalized by the electrostatic interactions

within the multilayers in combination with hydrophobic interactions. As can be inferred from the IR-data (see Figure 5.18) the interactions within the multilayers are stable over a broad pH range, due to charge regulation. At low pH, positive pyridinium groups occur within the layers that are not compensated by negatively charged carboxylic groups. Therefore, they reduce the possible electrostatic and hydrogen-bonding interactions between PMA and P4VP and destabilize the capsules. Furthermore, the excess of positive groups induces electrostatic repulsion between them. To ensure the overall electroneutrality of the system, counterions are accumulated in the vicinity of the shells and / or within the layers. The higher ion concentration as compared to the bulk exerts an osmotic pressure that tends to swell the capsules. The swollen states are stabilized by hydrophobic interactions within the layers, as both PMA and P4VP show hydrophobic stabilization. For PMA in solution, e.g. there is a drastic change of dissociation at low pH, that is due to the conformational change of PMA from a compact structure to a random coil one [14, 164]. Furthermore, uncharged carboxylic acid groups can stabilize the system by intramolecular hydrogen-bonds that can occur within the same layer as well as between different layers of PMA [98].

At pH 8 a similar situation occurs. From the infrared data as well as from the  $\zeta$ -potential it can be inferred that the P4VP is not charged at that pH, whereas the PMA remains in its fully charged state. Therefore, interactions between different layers are reduced and the excess of negative carboxylic groups in the multilayers leads to a destabilization of the capsule shells. This electrostatic destabilization is counteracted by hydrophobic interactions of the uncharged P4VP [93]. P4VP is a hydrophobic polymer that is water insoluble when the degree of ionization is less than 35 % [171], thus it stabilizes the swollen multilayers. When the pH is increased further, the hydrophobic attraction and surface tension are the most prominent forces leading to shrinkage and an irreversible collapse of the capsules, resulting in particle-like structures, which do not possess the characteristics of capsules anymore.

The presence of hydrophobic stabilization in water is further evidenced in conditions where this hydrophobic stabilization is decreased. In a mixture of 1:1 methanol and water both polymers are soluble over a broad pH range, so that uncharged P4VP does not precipitate, and hydrophobic stabilization of PMA at low pH is reduced. Therefore, the hydrophobic interaction becomes inoperative [171, 176]. When examining the stability of capsules in a solution of 1:1 methanol and water at different pH, stable capsules were observed over the same pH range between pH 2 and 8, but no stable swollen state could be found and neither any shrinkage of the systems when the pH was increased above 8. At the edges of stability the capsules swelled and dissolved within a second. The large stability range of the capsules correlates with the charge regulation within the multilayers that was observed in the IR-spectra.



The pH, at which the capsules swelled and dissolved were different from the solution  $pK_{app}$  values of the component polyelectrolytes, the one in the alkaline region was higher than the  $pK_{app}$  of PMA and the one in the acidic region was lower than the  $pK_{app}$  of P4VP. This suggests, as well as the IR data, that interactions within multilayers are stabilized against pH change. The association of hydrophobic elements of a polymer chain can increase the local density of weak functional groups and / or decrease the local dielectric constant experienced by weak functional groups. In both cases it is more difficult to ionize the weak groups due to an unfavorable electric potential. In other words, cooperative interactions stabilize the polyelectrolyte layers, and this can also explain the drastic onset of swelling within 0.1 pH unit.

Abe et al. observed plateaus in the potentiometric titration curves of P4VP/PMA complexes in solution in the acidic and basic pH ranges that correspond well to the edges of stability found for (P4VP/PMA)<sub>5</sub> capsules. They also detected dissociation of the complex into the component polyelectrolytes at such pH values [176]. The stability range is similar to that reported for flat multilayers of 10 layers of P4VP and PAA by Caruso and co-workers, where the films were stable up to  $pH \sim 7$ , after which the desorbed amounts increased in the range from pH 7.5 to 9 [101]. Sukhishvili et al. studied the ionization and pH-dependent stability of flat multilayers with PMA and QP4VP with different alkylation degrees. They observed dissolution of the multilayers below pH 2, due to protonation of carboxylic groups and disruption of polymer / polymer ionic contacts. The stability of the multilayer in acidic conditions was dependent on the alkylation degree of QP4VP [66]. They attributed the destruction of the multilayers to the protonation of a small (< 5%) residual fraction of carboxylic groups that was included into polymer / polymer ionic pairs and suggested that a cooperative effect in the formation of polymer / polymer ionic pairs might play an additional role in film stability.

The detected stability of P4VP/PMA capsules at neutral pH was much higher than usually found for purely hydrogen-bond stabilized multilayers. For such systems the dissolution occurs at pH 6.9 (PVPON/PMA), pH 4.6 (PEO/PMA) and pH 3.6 (PEO/PAA) [88, 89]. The increased stability of the P4VP/PMA system in slightly basic medium may be influenced by electrostatic interactions between PMA and P4VP, which are not present in multilayers that are only stabilized by H-bond interactions [101].

With the adsorption of more polyelectrolyte layers the amount of polymer adsorbed is increased. This results in a higher swelling degree both at low and at high pH. The results are shown in Figure 5.21. The increase in swelling degree at pH 8.1 as a function of layer number was much more prominent than at pH 2. For 16 layers the capsules swelled by 70 % in basic medium compared to 23 % at pH 2.

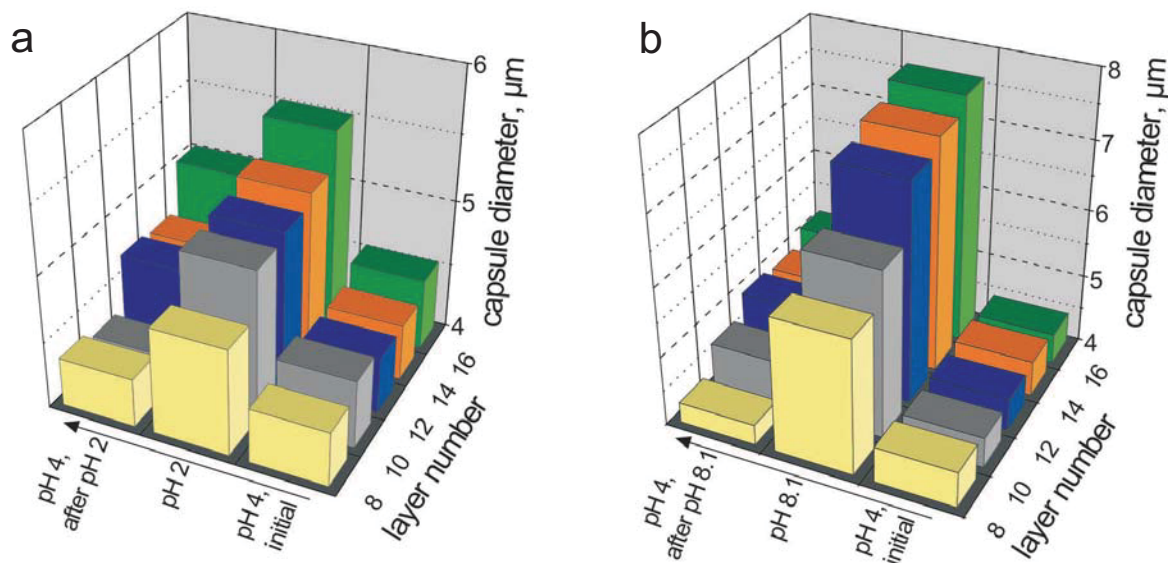


**Figure 5.21:** Swelling degree and reversibility as a function of layer number. Swelling at pH 2 (a), swelling at pH 8.1 (b).

An increase in the swelling can be explained, as more polymeric material leads to an increase in the osmotic pressure induced by the counterions. In addition, the capsules, which were swollen to a higher extent, were still stable because of increased entanglement and hydrophobic interactions with additional layers. When capsules in their swollen state at low and at high pH were washed with water at pH 4, and the diameter was determined after one hour, the swelling was reduced irrespective of the number of adsorbed layers. For capsules swollen at pH 2 real reversibility was achieved for 8 and 10 layers. Capsules composed of 12 to 16 layers only showed a reduction in size to a diameter of 4.7 - 5  $\mu\text{m}$ . Capsules swollen at pH 8.1 could be shrunk back to their original size in the whole range from 8 to 16 layers. This reversibility is an important prerequisite for any application involving weak polyelectrolyte capsules, as it opens the possibility for the system to reversibly exist in two different states, a swollen and a shrunk one.

#### 5.4.4 Influence of ionic strength on the pH-dependent stability

The addition of sodium chloride to the swollen capsules led to a destruction of the multilayers. At pH 2 capsules dissolved within seconds, whereas at pH 8.1 capsules shrunk to particles. When the pH-dependent behavior with increased ionic strength was investigated, the stability of the capsules as well as the swelling behavior were altered. The results are shown in Figure 5.22.

The increase of the ionic strength led to less stable capsules in the pH regions of 2 - 3 and 7 - 8. The stability range was decreased compared to the situation without added salt. At

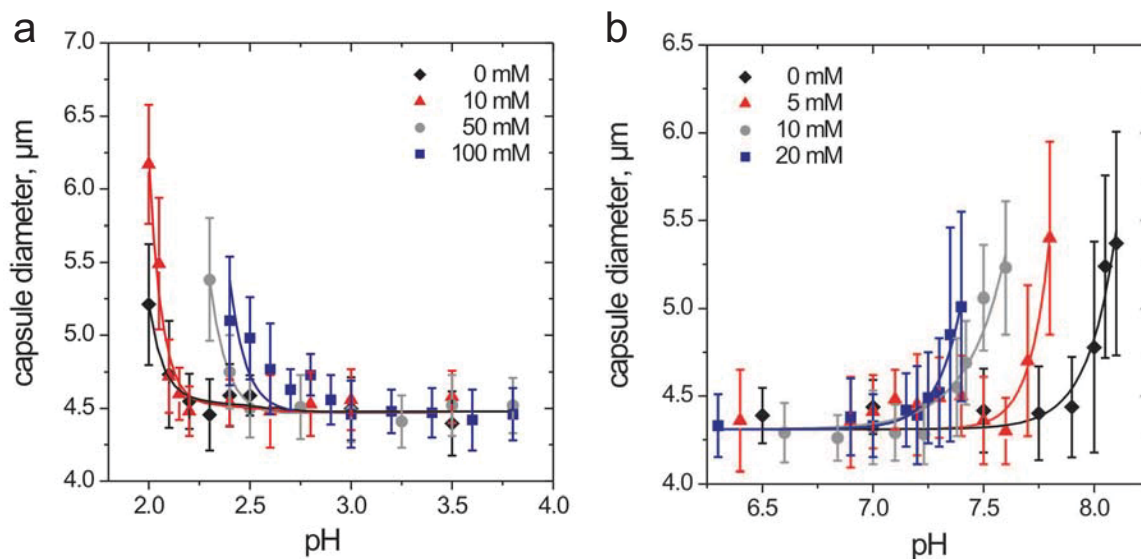


**Figure 5.22:** Influence of added NaCl on the pH-dependent stability of (P4VP/PMA)<sub>5</sub> capsules in the low pH region (a) and in the neutral pH region (b). The solid lines serve as visual guides.

low pH the swelling set in at a slightly increased pH value, whereas in basic pH the swelling started at a decreased pH value. Additionally, at a given pH, the capsule diameter was increased when the ionic strength was increased.

Figure 5.22 a describes the swelling at low pH with the addition of 10 - 100 mM NaCl. The swelling without added NaCl and with 10 mM NaCl set in at the same pH, but the capsules swelled more when 10 mM NaCl was added. This finding can be explained, when taking into account that the ionic strength of a HCl solution at pH 2 is already 10 mM, therefore the addition of 10 mM NaCl only increases the ionic strength by a factor of 2. For all other salt concentrations investigated at low pH the maximal stable swelling was reduced in size compared to the swelling without added salt. All swollen capsules dissolved when the pH was lowered further.

Figure 5.22 b shows the stability of capsules that were exposed to solutions containing 5 - 20 mM NaCl in the pH range from 6 to 8. Swollen capsules shrunk once the pH was increased further. Data for the shrunk states are not shown, as the capsule size during the shrinking process was time dependent and the final particle-like state was mainly due to precipitated P4VP. In contrast to the shrinking process, the sizes of swollen capsules were stable at least for several hours.

The degree of dissociation of the P4VP and PMA within the multilayered capsules increased with increasing salt concentration and the observed changes in the pH-response were similar to those obtained for PAH/PMA<sub>790kDa</sub> capsules (see Section 5.3.4).

The differences in the salt concentrations that were needed to induce a change at neutral / basic pH can be explained by the different pH ranges at which the swelling set in.

The interpretation of the salt induced changes in swelling behavior follows the same line as in the case of PAH/PMA capsules (see Section 5.3.4). At neutral pH, the self-regulating mechanism of the association / dissociation equilibrium of the weak polyacid strongly reduces the charges along the chain at low salt concentration. The local concentration of protons near the weak polyelectrolytes with no external salt present is governed by the requirement of charge neutrality. However, when the ambient solvent contains ions other than protons some of these cations can be exchanged with the protons without violating the charge neutrality. As a consequence the degree of dissociation increases. The reduced capsule stability found in the pH range from 2 - 3 can be understood likewise.

#### **5.4.5 Permeability of (P4VP/PMA)<sub>4</sub> capsules for low molecular weight compounds**

Polyelectrolyte capsules show different permeability for macromolecules and low molecular weight compounds like water, salt and fluorescent dyes. Depending on the polymers in the capsule wall and the type of template used, the capsules are permeable for small molecules, but impermeable for polymers (see Section 2.7). Permeability for low molecular weight compounds like fluorescent dyes through the capsule shell is commonly investigated by Confocal Laser Scanning Microscopy studies, using fluorescence recovery after photobleaching (FRAP). Fluorescein-containing substances are normally used as probe molecules, because they are easily bleachable. In the case of P4VP/PMA capsules FRAP studies could not be used to determine the permeability because of several reasons: I) Fluorescein-containing fluorescent dyes have pH-responsive properties, resulting in a significant decrease of the fluorescence intensity at low pH, which would not allow for any investigation of the capsules' permeability at low pH. II) The shell of P4VP/PMA capsules was dense, independent of the number of layers adsorbed, therefore the permeation time for small dye molecules like fluorescein was in the range of 15 to 30 min, whereas FRAP measurements are normally conducted within seconds to a few minutes. III) In the swollen state, due to the fast permeation, it was not possible to record any kinetics of the fluorescence recovery, because of the resolution of the scan.

Therefore, the permeability of (P4VP/PMA)<sub>4</sub> capsules for glucose was derived from the time dependence of osmotic response experiments, detected by CLSM. Glucose was chosen as an osmotically active low molecular weight substance, which is not expected to interact with the capsule wall, and thus to change the pH-dependent stability of the capsules as in the case of NaCl. When polyelectrolyte capsules are exposed to a sudden osmotic pressure gradient they shrink and show a pronounced inward buckling phenomenon [177, 178]. The osmotic

pressure is due to a difference in concentrations between the bulk solution and the capsule interior, so that quantitative information concerning the permeation of molecules can be drawn from the kinetic aspects of the buckling phenomena [123, 131]. The critical concentration ( $c_{\text{crit}}$ ) of glucose to induce buckling was established in an initial set of experiments conducted at pH 4. Various amounts of glucose were added at once to the capsule suspension to establish the concentration at which 50 % of the capsules showed a deformation of the shells. The percentage of deformed capsules as a function of the glucose concentration is given in Figure 5.23. A critical glucose concentration of 25 mmol/L could be determined.

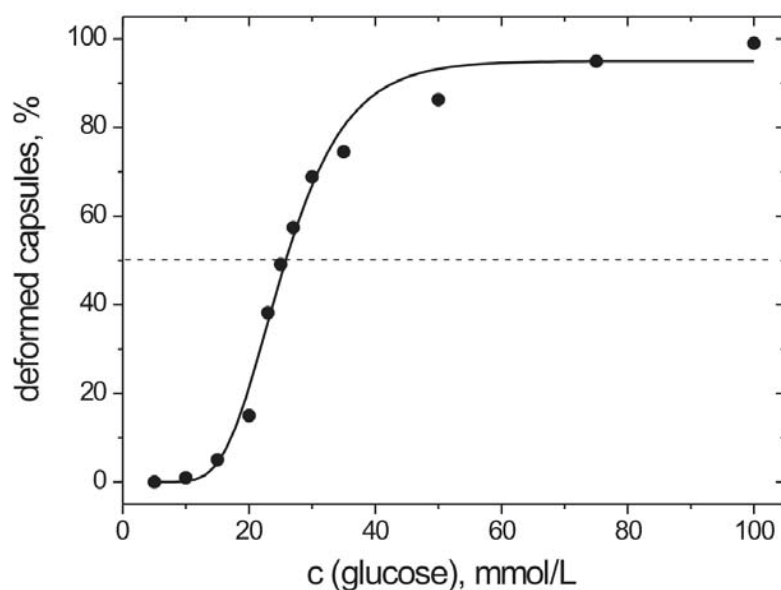


**Figure 5.23:** Percentage of deformed (P4VP/PMA)<sub>4</sub> capsules as a function of the concentration of glucose at pH 4. The solid line serves as a visual guide.

Below this concentration, the osmotic pressure caused by the concentration gradient between the interior of the capsule and the bulk solution was not high enough to induce a significant degree of buckling. The kinetic response of the osmotic deformation was observed by adding 100  $\mu\text{L}$  of a 0.2 mol/L stock solution of glucose to 100  $\mu\text{L}$  of a capsule suspension with flow rates ranging from 46  $\mu\text{L}/\text{min}$  to 125  $\mu\text{L}/\text{min}$ , corresponding to concentration changes from 1.05 mM/s to 1.85 mM/s. The occurring deformations could be related to the time necessary to reach the critical glucose concentration.

When glucose equilibrated faster or with the same time constant between the capsule interior and the bulk, the induced pressure difference was not high enough to cause buckling effects. Figure 5.24 shows the increase of glucose concentration with time, depending on the flow rate, together with some typical CLSM images of the different buckling regimes at pH 4. In all cases the final glucose concentration of 0.1 M was well above the critical concentration of 25 mM. For flow rates of less than 50  $\mu\text{L}/\text{min}$  nearly no changes in capsule shape were visi-

ble. A noticeable osmotic response was found if the addition of glucose was conducted with a flow rate of about  $51 \mu\text{L}/\text{min}$ . If the addition of glucose was even faster, buckling was observed for nearly all capsules. If a flow rate of  $51 \mu\text{L}/\text{min}$  was applied about 50 % of the capsules showed shape changes. With a threshold concentration of  $25 \text{ mmol}/\text{L}$  this resulted in a time of  $17.5 \text{ s}$  to reach this particular concentration.

If the addition of glucose occurs more slowly, the concentrations inside and outside partially equilibrate and consequently deformations are largely absent, as observed for a flow rate of  $46 \mu\text{L}/\text{min}$ . If the concentration increase is considerably faster, the water flux from the capsule interior is much faster than the equilibration of the glucose concentration, resulting in a complete collapse of the shells. When  $17.5 \text{ s}$  are assumed as a lower limit for the critical

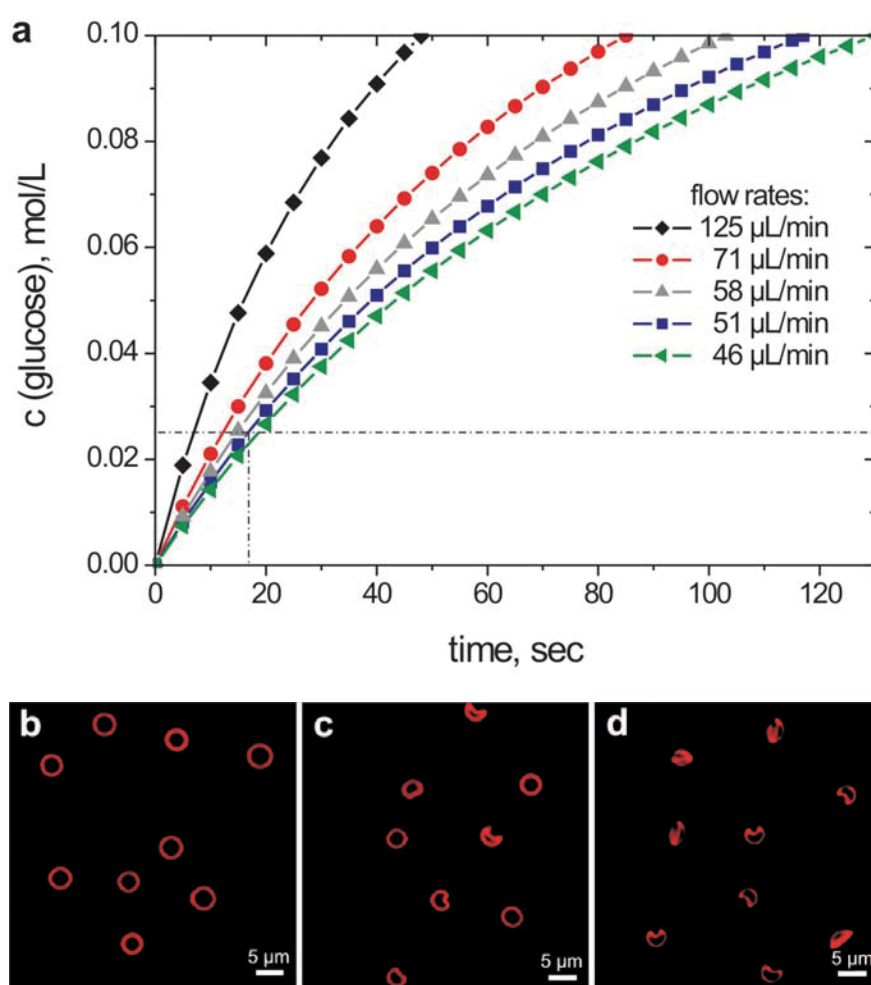


**Figure 5.24:** Variation of the concentration slope and osmotic deformation of  $(\text{P4VP}/\text{PMA})_4$  capsules. Glucose concentration as a function of time. The final concentration was reached with different flow rates of a  $0.2 \text{ mol}/\text{L}$  stock solution of glucose. The dashed lines show the critical glucose concentration as well as the critical time to reach it (a). CLSM images of corresponding capsules with a flow rate of  $46 \mu\text{L}/\text{min}$  (b),  $51 \mu\text{L}/\text{min}$  (c) and  $58 \mu\text{L}/\text{min}$  (d).

time of glucose permeation, it is possible to calculate an upper limit for the permeability  $P$  of the capsule wall [131],

$$P = \frac{V}{At_{\text{crit}}} \ln 2 = \frac{r}{3t_{\text{crit}}} \ln 2 \quad (5.3)$$

with the capsule volume  $V$ , the capsule surface area  $A$ , the capsule radius  $r$  and the critical time for permeation  $t_{\text{crit}}$ . If a possible uncertainty in the determination of the critical time is taken into account, the permeability of (P4VP/PMA)<sub>4</sub> capsules for glucose is in the range of  $2.8 - 3.2 \cdot 10^{-8}$  m/s.

In Section 5.4.3 it was shown that for P4VP/PMA capsules the electrostatic interactions and the stability of the shells vary with pH. Therefore, it was interesting to investigate the influence of pH on the permeability of these capsules for glucose. The results for the permeability as well as for  $c_{\text{crit}}$  and  $t_{\text{crit}}$  are given in Table 5.2 and 5.3 for the acidic and the neutral pH range, respectively.

**Table 5.2:** Determination of the permeability of (P4VP/PMA)<sub>4</sub> capsules for glucose at low pH. The permeability was calculated with the capsule diameters given in Section 5.4.3.

pH	$c_{\text{crit}}$ , mmol/L	$t_{\text{crit}}$ , s	permeability, m/s
4	$25 \pm 2$	$17.5 \pm 1.2$	$2.8 - 3.2 \cdot 10^{-8}$
2.5	$21 \pm 2$	$14 \pm 2$	$3.2 - 4.3 \cdot 10^{-8}$
2.3	$22 \pm 2$	$19.7 \pm 2$	$2.4 - 2.9 \cdot 10^{-8}$
2.1	$29 \pm 2$	$15.6 \pm 2$	$3.1 - 3.7 \cdot 10^{-8}$
2	> 1000	< 1	$> 6.2 \cdot 10^{-7}$
$2 \Rightarrow 4$	$46 \pm 2$	$9.8 \pm 2.3$	$4.3 - 6.9 \cdot 10^{-8}$

**Table 5.3:** Determination of the permeability of (P4VP/PMA)<sub>4</sub> capsules for glucose at neutral pH. The permeability was calculated with the capsule diameters given in Section 5.4.3.

pH	$c_{\text{crit}}$ , mmol/L	$t_{\text{crit}}$ , s	permeability, m/s
7	$28 \pm 2$	$15.6 \pm 1.2$	$3.1 - 3.6 \cdot 10^{-8}$
7.5	$26 \pm 2$	$17.3 \pm 1.5$	$2.8 - 3.4 \cdot 10^{-8}$
7.7	$28 \pm 2$	$19.6 \pm 1.8$	$2.4 - 2.9 \cdot 10^{-8}$
7.9	$25 \pm 2$	$12.8 \pm 2$	$3.5 - 4.8 \cdot 10^{-8}$
8	> 1000	< 1	$> 5.5 \cdot 10^{-7}$
$8 \Rightarrow 4$	$47 \pm 2$	$10.3 \pm 2.1$	$4.2 - 6.3 \cdot 10^{-8}$

Over a wide range of pH values from 2.1 to 7.9 the permeability of the capsules was nearly unchanged, ranging from about  $2 \cdot 10^{-8}$  m/s to about  $4 \cdot 10^{-8}$  m/s. Only at the edges of the stability range there was a huge increase of the permeability of more than one order of magnitude to values higher than  $5.5 \cdot 10^{-7}$  m/s. For swollen capsules it was not possible to determine the permeation time for glucose, as in these cases the capsules did not show any buckling effects even in the presence of 1 mol/L glucose. Therefore, the given permeabilities at pH 2 and 8 represent a lower limit, which was assumed with a critical permeation time of 1 sec. In the swollen state glucose is free to permeate through the capsule wall and equilibrates very quickly the internal and external concentrations. The resulting osmotic pressure difference is too small to induce buckling. When capsules were incubated at pH 2 and 8, respectively, for 1 h and were immersed in a solution of pH 4 for 1 h to equilibrate the shell structure, the established permeability for glucose showed a slightly increased value in the range of  $4 \cdot 10^{-8} - 7 \cdot 10^{-8}$  m/s. This could be due to changes in the arrangement within the capsule wall when the electrostatic interactions are changed as well as due to the swelling / shrinking cycle.

The permeability can be related to the diffusion coefficient  $D$  inside a membrane of thickness  $h$ ,

$$D = hP \quad . \quad (5.4)$$

For the unperturbed capsule size this would result in  $D \approx 3 \cdot 10^{-16} - 6 \cdot 10^{-16}$  m<sup>2</sup>/s, with a thickness of 3.6 nm per polyelectrolyte bilayer. When the capsules are swollen, only a lower limit for the diffusion coefficient can be obtained, as only a lower limit for the permeability is known. In this case the thickness can be calculated if one assumes that the volume of the capsule shell is not changed during the swelling. Thus a decreased shell thickness of the swollen capsules is obtained, according to

$$V = 4\pi r^2 h \quad h_2 = \frac{r_1^2 h_1}{r_2^2} \quad . \quad (5.5)$$

At pH 2 this would result in a wall thickness of 10 nm, and at pH 8 of 12.7 nm. The corresponding diffusion coefficients are  $D > 6.2 \cdot 10^{-15}$  m<sup>2</sup>/s at pH 2 and  $D > 7 \cdot 10^{-15}$  m<sup>2</sup>/s at pH 8. The shrinking of capsules that were immersed at pH 2 and pH 8, respectively, yields a diffusion coefficient of around  $6 \cdot 10^{-16} - 1 \cdot 10^{-15}$  m<sup>2</sup>/s.

The diffusion coefficients obtained for unswollen P4VP/PMA capsules are much lower than the ones found by Ibarz et al. for PAH/PSS capsules templated on MF, which were in the range of  $\sim 10^{-14}$  m<sup>2</sup>/s [125]. On the other hand, they are close to the diffusion coefficients of  $1.7 \cdot 10^{-16} - 1 \cdot 10^{-16}$  m<sup>2</sup>/s obtained by Antipov et al. when studying the diffusion of fluorescein through PAH/PSS multilayers [128]. The higher permeability in the case of MF particles could be due to the formation of pores during the core dissolution step (see



Section 2.7). In contrast, the system investigated by Antipov et al. did not involve a core dissolution step prior to the permeability studies, as the multilayers were directly assembled onto precipitated fluorescein particles. The fact that the diffusion coefficients observed for P4VP/PMA capsules templated on SiO<sub>2</sub> are in the same range as the ones reported by Antipov et al. provides evidence that the core dissolution protocol used here is gentle enough to maintain the integrity of the capsule shell.

#### 5.4.6 Permeability of (P4VP/PMA)<sub>4</sub> capsules for polymers at pH 8

The pH-dependent permeability changes of P4VP/PMA capsules provides an opportunity for the loading and release of macromolecules. Several attempts have been made for controlled uptake and release of polymers by a change in pH or ionic strength (see Section 2.7). Neither of these approaches is particularly suitable in physiological conditions. However, the reversible swelling and corresponding permeability changes of P4VP/PMA capsules in neutral pH conditions at pH 8 would be favorable for the encapsulation and release of biomolecules, e.g. enzymes or proteins that are not stable at reduced or increased pH or at higher ionic strength.

The permeability of P4VP/PMA capsules was studied using FITC-dextran with a molecular weight of 70 kDa. Dextran is a polysaccharide that consists of glucose monomers and is charge-neutral, thus the onset of the permeability changes for dextran should be similar to the ones observed for glucose. The permeability of (P4VP/PMA)<sub>4</sub> capsules for FITC-dextran at pH 6 and pH 8 is shown with CLSM images in Figure 5.25.

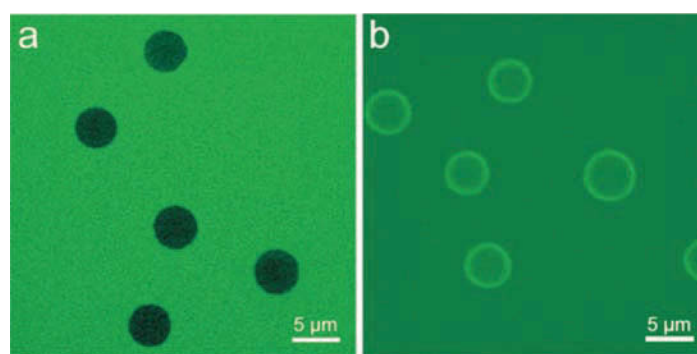


**Figure 5.25:** CLSM images showing hollow capsules in a FITC-dextran solution at pH 6 (a) and pH 8 (b).

At pH 6 the capsule interior remained dark and no FITC-dextran could permeate through the shell within 12 h. At pH 8, however, the polymer was equally distributed within the capsule interior and the bulk solution within less than one minute. The reversibility of the swelling and the concomitant changes in permeability provided the possibility to enclose the

polymeric material in the interior of the capsules by a reduction of the solution pH. Following washing steps removed the excess of FITC-dextran from the bulk solution, only leaving behind the entrapped dextran within the capsules. A CLSM image of P4VP/PMA capsules filled with FITC-dextran is displayed in Figure 5.26 a. A fluorescence profile of one of the filled capsules is shown in Figure 5.26 b.

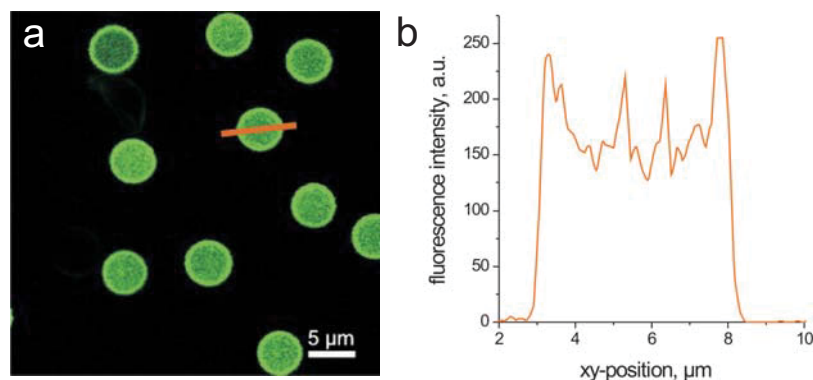


**Figure 5.26:** CLSM image of (P4VP/PMA)<sub>4</sub> capsules that are filled with FITC-dextran (a). The fluorescence profile of one filled capsule is given in (b).

The fluorescence intensity at the capsule wall was slightly increased in comparison to the capsule interior, which could result from the entanglement of dextran within the multilayer or from nonspecific interactions with the polyelectrolytes. In addition to confocal microscopy, the encapsulation of FITC-dextran was also studied with AFM. Figure 5.27 displays AFM images of empty and filled (P4VP/PMA)<sub>4</sub> capsules together with the corresponding height profiles. Empty shells exhibited the typical folds and creases that arise from the evaporation of the aqueous content leading to a collapse of the film. The height of the flat regions of 30 nm corresponds to two capsule walls on top of each other. If the same capsules were filled with FITC-dextran from a bulk solution of 5 mg/mL, the shells did not collapse with folds but rather showed a uniform appearance with increased thickness at the edges. The average height of the dried capsules increased to 54 nm, of which only 30 nm are attributed to the capsule wall material. The additional 24 nm correspond to dried FITC-dextran. From these numbers and the capsule diameter the amount of encapsulated polymer can be estimated. For the individual capsule shown it was approximately 140 % of that expected for an equal distribution of FITC-dextran in bulk and in the capsule interior. The slightly increased amount of polymeric material can be explained by the reduction in capsule size during shrinkage, at which the polymers are already captured inside. Additionally, accumulation of the polymer per capsule may also be enhanced by adsorption onto the shell due to nonspecific interactions between the multilayer and FITC-dextran.

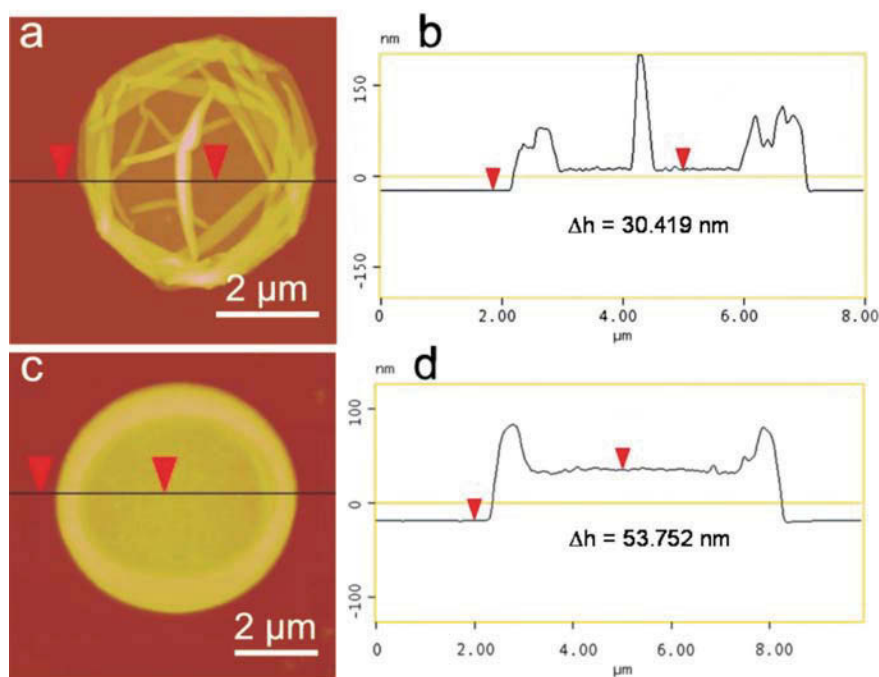


**Figure 5.27:** AFM images of empty (P4VP/PMA)<sub>4</sub> capsules (a) and capsules filled with FITC-dextran (c), with the corresponding height profiles (b,d).

## 5.5 Theoretical model for pH-dependent capsule swelling

### 5.5.1 Development of the theoretical model

The above results concerning the pH-dependent swelling as well as the influence of ionic strength on weak polyelectrolyte capsules can be theoretically described by the combination of two opposing forces. An expansive force, due to ion entropy that is balanced by an elastic contractive force. In that case, the equilibrium size of the capsules can be derived from the balance of forces. The proposed theoretical model describes the swelling of weak polyelectrolyte capsules as a function of material properties, like shell thickness, Young's modulus and pK-values, as well as of external parameters like pH and ionic strength.

As the capsules swell to an equilibrium size (swelling stops after a certain thermodynamically most favorable size has been reached, at least on a time-scale of several hours to days), a theoretical approach was used, in which the capsule size is explained by a balance of forces at equilibrium. A similar approach was used by Vinogradova and coworkers to describe the swelling of capsules that is caused by an osmotic pressure difference across the shell because of encapsulated polyelectrolytes. In that study a contractive force that counteracts the osmotic pressure was described as an elastic force [87]. In the system studied here, the osmotic force is not due to enclosed polyelectrolyte but arises from small ions, that compensate for the charge excess of the weak polyelectrolyte multilayers at low and at high pH. At an

intermediate pH there exists a global compensation of charges and no additional ions are required for the charge balance. In this pH region the expansive force is zero and the capsule possesses its unperturbed size. At lower and higher pH values an increase in the capsule size would be expected because of the development of a charge excess. The experimental results, however, show a broad pH plateau in which the capsule diameter is constant. These findings are introduced into the theoretical model by taking into account that the ionization degree of a weak polyelectrolyte does not depend on the solution pH, but on the local pH within the multilayer. Over a broad pH range it is energetically more favorable for the system to change the electrostatic potential within the multilayer to keep the charge balance within the shell, than to accept a charge excess that results in an expansion of the shell, and therefore in an increase of the elastic energy. Above or below a critical pH it becomes more favorable for the system to increase the elastic energy than to change the electrostatic potential even more and the capsule starts to expand.

The excess charge of the polymer leads to an increased ion concentration next to and within the shell, which results in an osmotic expansive force to reduce the ion concentration within and next to the shell, resulting in a favorable decrease of free energy. The decrease in ion concentration can occur in two different ways, either the shell polymer density is reduced or the shells outer surface area is increased, thus creating more space for the diffuse layer of small ions on each side of the multilayer.

An accurate description of the pH-dependent swelling of capsules would have to include both elements. Thus, one would have to consider the polymer density profiles within the multilayers in detail, calculate the electrostatic potential profile inside and outside the shell [179], and determine the free energy associated with each shell thickness and polymer density.

Additionally, it would be necessary to include how the elasticity modulus depends on shell polymer density, pH and ionic strength, and finally one would have to assume that the expansion of the polymeric chains is isotropic. The total free energy could then be minimized to determine the equilibrium shell thickness and capsule size.

In order to circumvent many of these unknown aspects, and to derive a relatively simple model for capsule swelling, it is assumed that the electrostatic potential within the multilayer structure is rather constant and close to zero (no excess of ions), with only a sharp peak in the potential (and therefore an ion concentration increase) near the edges [179]. This approach is also experimentally supported by von Klitzing et al., who showed that the electrostatic potential rapidly decays to zero when moving from the solution-film interface into the polyelectrolyte multilayer film [64].

For the development of the theoretical model it is assumed that the electrostatic potential within the multilayer is constant, and charge excess due to ions within the shell is neglected.

Instead, only the ions in the two diffuse layers on each side of the shell are considered. With respect to the elasticity modulus it is initially assumed that it does not depend on pH or ionic strength. This is justified, as experimental measurements of the elasticity modulus for other systems did not show a notable dependence on the ionic strength below 1 M [58, 180], while Schlenoff and coworkers found a decrease of only 10 % in the elasticity modulus upon addition of 100 mM salt [181]. Later on, an empirical dependence of the elasticity on the ionic strength is used to improve the fit of the model to the experimental data.

For ideal Hookean behavior the elastic energy per capsule  $U_{el}$  is given by [87]

$$U_{el} = \frac{4\pi E h_0}{1 - \nu} \Delta R^2 \quad (5.6)$$

with the elasticity (Young's modulus)  $E$ , the unperturbed wall thickness  $h_0$ , the Poisson's ratio  $\nu$  ( $\nu = 0.5$  for incompressible materials such as most rubbers) and the difference between the capsule radius  $R$  and the unperturbed radius  $R_0$ ,  $\Delta R$ .

Electrostatically, the multilayer shell is described as a quasi-Donnan phase, *Donnan* because it is assumed to have a common electrostatic potential, *quasi* because it is not charge-neutral in itself, but only in combination with the diffuse layers of small ions on both sides. As both the shell thickness  $h_0$  and the Debye length  $\kappa^{-1}$  are small in comparison to the capsule radius  $R$  a planar geometry can be assumed. Thus, the electroneutrality is given by [182]

$$Z_a = \frac{\kappa}{\pi l_B} \sinh \frac{y}{2} + 2h_0(1 - \phi)c_\infty \sinh y \quad (5.7)$$

with the net polymer charge per unit surface area  $Z_a$ , the Bjerrum length  $l_B$ , the polymer volume density  $\phi$ , the ionic strength  $c_\infty$  and the dimensionless electrostatic potential  $y$ . The right-hand side of the equation represents the sum of the charge of the two diffuse layers of small ions and the charge of the ions within the shell, which are considered to be point charges. In the following, the contribution of the ions within the shell will be neglected, resulting in

$$y = 2 \operatorname{arcsinh} \frac{Z_a \pi l_B}{\kappa} \quad (5.8)$$

Assuming a low-potential Debye-Hückel (DH) limit, equation 5.8 can be simplified to

$$y = 2 \frac{Z_a \pi l_B}{\kappa} \quad (5.9)$$

In the DH-limit the electrostatic free energy (of a capsule of a fixed charge  $Z$ ) is given by

$$F_{el} = \frac{1}{2} Z y \quad (5.10)$$

with the total polymer charge per capsules  $Z = Z_a A$  ( $A = 4\pi R^2$  is the capsule surface area). When the capsules swell,  $Z$  is constant, but  $Z_a$  varies.

Combining equations 5.6, 5.9, 5.10 and taking into account the definitions of  $l_B$  and  $\kappa^{-1}$  results in

$$F_{tot} = \frac{\kappa Z^2}{8c_\infty A} + \frac{4\pi E h_0}{1-\nu} \Delta R^2, \quad (5.11)$$

which can be differentiated with respect to  $R$  to obtain in equilibrium

$$-\frac{1}{8\pi} \frac{dF_{tot}}{dR} = 0 = \frac{\kappa Z^2}{8c_\infty A^2} R - \frac{E h_0}{1-\nu} \Delta R. \quad (5.12)$$

Assuming that  $R \approx R_0$  (and therefore  $A \approx A_0$ , with 0 referring to the unperturbed state), this equation simplifies to

$$\frac{\Delta R}{R_0} = \pi l_B (1-\nu) \frac{Z^2}{E h_0 A_0^2 \kappa}. \quad (5.13)$$

Equation 5.13 shows that the relative change in Radius  $\Delta R/R_0$  scales with the square of the polymer charge excess  $Z$ , with the ionic strength to the power  $-1/2$ , and the Young's modulus  $E$  and the initial thickness  $h_0$  to the power  $-1$ .

When considering polymers consisting of ionizable segments instead of having a fixed charge, as was assumed in the equations above, the final expression for the energy and the resulting diameter given by equations 5.12 and 5.13 should not change, as the expansive electrostatic force on the capsule shell depends on the capsule polymer charge  $Z$ , but not on the mechanism by which the charge is established. Hence, it does not depend on whether the polymers are ionizable or have a fixed charge. Equation 5.13 is also valid for ionizable polymers, but then the charge  $Z$  is related to  $y$  by

$$Z = n \sum_{A,B} z_i \beta_i \alpha_i \quad (5.14)$$

with the total number of ionizable monomers per capsule  $n$  and the fraction of monomers that are either cationic or anionic  $\beta_i$ .  $A$  stands for the polyanions,  $B$  for the polycations,  $z_i$  is the sign of the charge ( $+1$  for a polycation segment  $B$ ,  $-1$  for a polyanion segment  $A$ ), and  $\alpha_i$  is the ionization degree, which is obtained from [183]

$$\alpha_i = (1 + 10^{z_i(\text{pH} - \text{pK}_i)} e^{z_i y})^{-1} \quad (5.15)$$

with the intrinsic pK-value  $\text{pK}_i$  and the solution pH. With the help of this model it is possible to calculate the electrostatic potentials  $y$  within the capsule wall and to obtain the ionization degrees  $\alpha_i$  of the two polyelectrolytes in the shell.  $\alpha_A$  and  $\alpha_B$  can be calculated from equations 5.14 and 5.15 together with 5.8 and  $Z_a = Z/A_0$ , resulting in an increase in the diameter of the capsules according to equation 5.13.

### 5.5.2 Modeling the experimental data

In the following, theoretical and experimental results for  $(\text{PAH}/\text{PMA}_{790\text{kDa}})_4$  and  $(\text{P4VP}/\text{PMA})_5$  capsules templated on  $\text{SiO}_2$  are compared. It is assumed that there are as many ionizable anionic as cationic polymer segments, resulting in  $\beta_i = 0.5$ . Small variations of  $\beta$  between  $0.4 < \beta_i < 0.5$  do not influence notably on the predicted size. The Young's modulus is assumed to be  $E = 30$  MPa, which is in the range of  $E$ -values from literature [181, 184, 185]. For the wall thickness, experimentally determined thicknesses of dried shells are used, namely  $h_0 = 13.5$  nm for  $(\text{PAH}/\text{PMA})_4$  capsules and  $h_0 = 19.5$  nm for  $(\text{P4VP}/\text{PMA})_5$  capsules. The intrinsic pK values are taken from literature [14, 171, 186]. For PMA  $\text{pK}_A = 4.5$ , for PAH  $\text{pK}_B = 8.5$  and for P4VP  $\text{pK}_B = 5$ . Based on data in [84] and [33] it is derived that there are  $\sim 4 \cdot 10^8$  segments of each polymer per bilayer in a  $4.5$   $\mu\text{m}$  diameter shell, resulting in a total number of polyelectrolyte segments of  $n \sim 3.2 \cdot 10^9$  for  $(\text{PAH}/\text{PMA})_4$  capsules and of  $n \sim 4 \cdot 10^9$  for  $(\text{P4VP}/\text{PMA})_5$ , which are the numbers that are used in the calculation.

The electrostatic force depends on the ionic strength  $c_\infty$  (resulting in  $\kappa$ ), which is induced by the added salt as well as by the ionic strength due to the addition of acid / base to adjust pH; the effect of the addition of base or acid is described by  $(10^{-\text{pH}} + 10^{\text{pH}-14})$  in M).

The experimental data for  $(\text{PAH}/\text{PMA})_4$  and  $(\text{P4VP}/\text{PMA})_5$  capsules can be described well by the theoretical model and the results are shown in Figure 5.28.

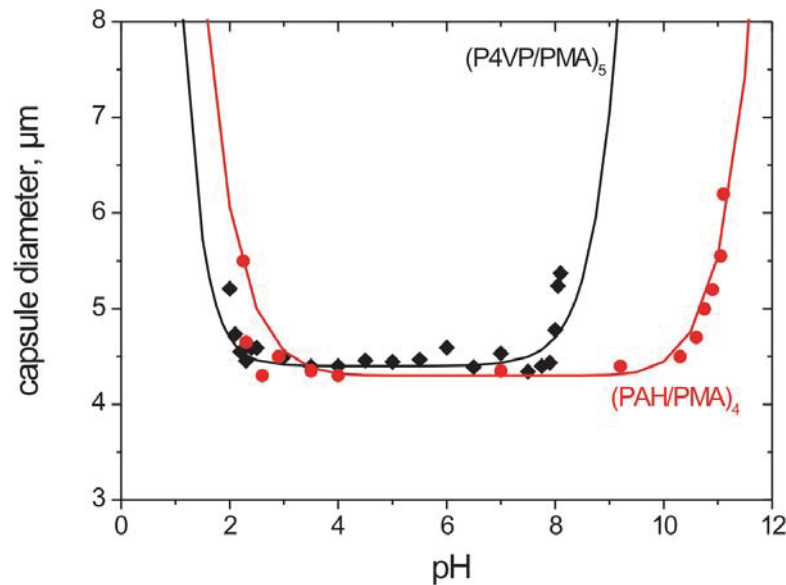


**Figure 5.28:** Capsule diameter as a function of pH, data points represent the experimental values and the lines the theoretical fits ( $E = 30$  MPa,  $\nu = 0.5$ ,  $\beta = 0.5$ ,  $\text{pK}_A = 4.5$ .  $(\text{PAH}/\text{PMA})_4$  capsules:  $h_0 = 13.5$  nm,  $n = 3.2 \cdot 10^9$ ,  $\text{pK}_B = 8.5$ ,  $2R_0 = 4.3$   $\mu\text{m}$ , 0 mM NaCl added;  $(\text{P4VP}/\text{PMA})_5$  capsules:  $h_0 = 19.5$  nm,  $n = 4.0 \cdot 10^9$ ,  $\text{pK}_B = 5$ ,  $2R_0 = 4.4$   $\mu\text{m}$ , 1 mM NaCl).

The capsule diameter ( $2R$ ) is given as a function of pH without additional salt in the system. Error bars are omitted for clarity. To describe the swelling of  $(\text{P4VP/PMA})_5$  capsules well with the model it was necessary to include 1 mM of additional salt. This could possibly still be present in the solution due to the dissolution protocol of these capsules at pH 3.5.

The influence of increased ionic strength on the swelling behavior of  $(\text{PAH/PMA})_4$  and  $(\text{P4VP/PMA})_5$  capsules both at low and at high pH is shown in Figure 5.29. The given ionic strength is a consequence of the added salt. Additionally, the ionic strength is increased because of the pH adjustment. The pH- and ionic strength dependent swelling is best described for  $(\text{PAH/PMA})_4$  capsules at high pH, but for both systems in acidic and basic conditions the

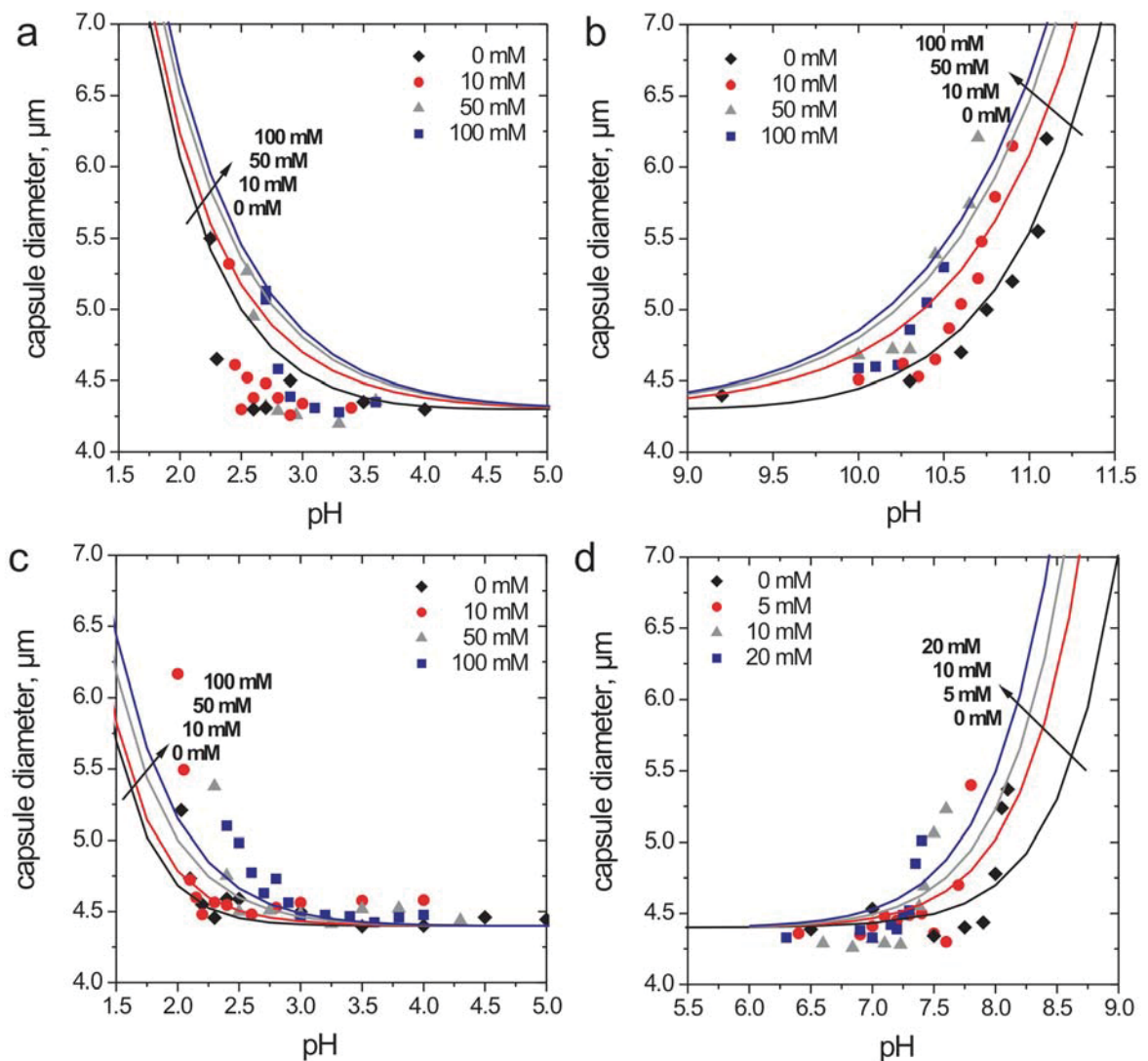


**Figure 5.29:** Influence of pH and the addition of NaCl on the diameter of  $(\text{PAH/PMA})_4$  and  $(\text{P4VP/PMA})_5$  capsules. The data points represent the experimental values and the theoretical model is given by the solid lines.  $\text{PAH/PMA}$  capsules at low (a) and at high pH (b) ( $E = 30 \text{ MPa}$ ,  $\nu = 0.5$ ,  $\text{pK}_A = 4.5$ ,  $\text{pK}_B = 8.5$ ,  $\beta = 0.5$ ,  $h_0 = 13.5 \text{ nm}$ ,  $n = 3.2 \cdot 10^9$ ,  $2R_0 = 4.3 \mu\text{m}$ ).  $\text{P4VP/PMA}$  capsules at low (c) and at high pH (d) ( $E = 30 \text{ MPa}$ ,  $\text{pK}_A = 4.5$ ,  $\nu = 0.5$ ,  $\beta = 0.5$ ,  $h_0 = 19.5 \text{ nm}$ ,  $n = 4.0 \cdot 10^9$ ,  $\text{pK}_B = 5$ ,  $2R_0 = 4.4 \mu\text{m}$ ).



experimental observation of an increased capsule diameter with increasing ionic strength at a given pH value is reproduced quite well, even though the theoretical curves do not match the experimental data exactly. In agreement with the experimental data for P4VP/PMA capsules at low pH there is only a small difference in the capsule diameters for 0 and 10 mM added NaCl.

This observation of a polyelectrolyte structure swelling with increased ionic strength is in general quite uncommon and only observed for weakly-charged systems at low ionic strength, such as for ionizable polyelectrolyte brushes, where it is called the osmotic brush regime [166–169]. If the polyelectrolytes had a fixed charge,  $Z$  would be independent of ionic strength and thus equation 5.13 would predict that with increasing ionic strength the capsule diameter should swell less. In that case, the increased ionic strength would decrease the osmotic pressure difference, and the elastic forces would contract the polyelectrolyte shell. For ionizable segments, however, at very low ionic strength the ionization degree of the polymer segments is low because of the high electrostatic potentials. When the ionic strength is increased, the electrostatic potentials are reduced and the ionization degree increases, resulting in an increase of the capsule size.

In Figure 5.30 a the experimental data and a theoretical prediction of the influence of ionic strength on the diameter of P4VP/PMA capsules at pH 2.3 are shown. The red curve is based on a constant value for  $E$ , which is independent of ionic strength. If the elasticity is

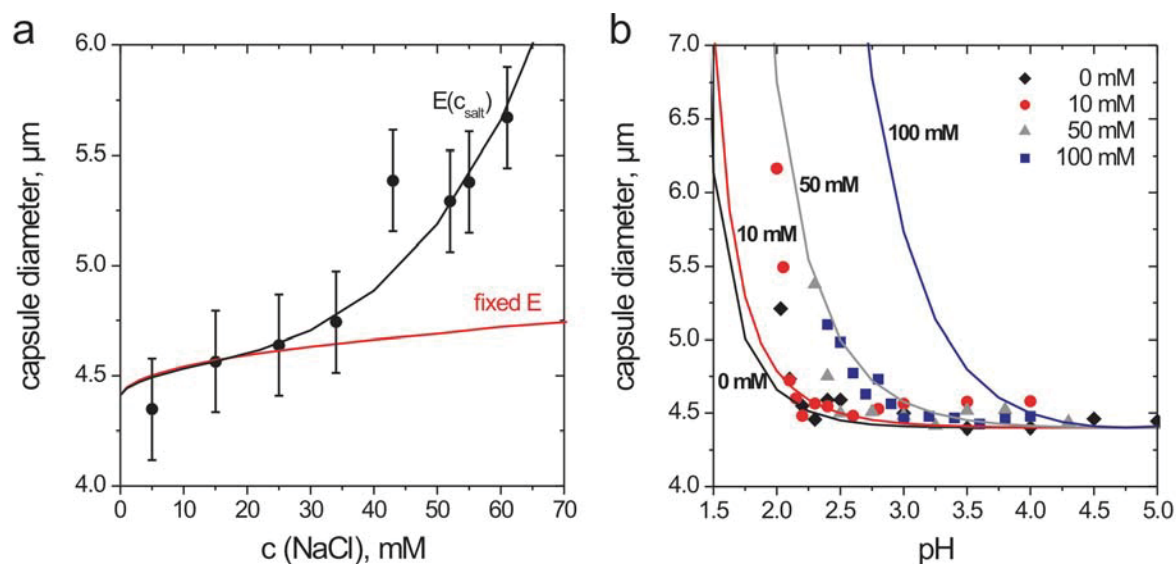


**Figure 5.30:** (a) Diameter of  $(\text{P4VP/PMA})_5$  capsules at pH 2.3.  $c_{\text{salt}}$  is the total salt concentration. The data points represent the experimental values and the theoretical model is given by the solid lines. The red curve is based on a fixed value for the elasticity modulus  $E$ , whereas the black curve is based on  $E$  decreasing with  $c_{\text{salt}}$  to the power 3. (b) Data and theory of the swelling of P4VP/PMA capsules with NaCl at low pH, including the empirical  $E$ - $c_{\text{salt}}$  relation from (a).

independent of the ionic strength, the theoretical model predicts that the diameter increase levels off, whereas the experimental observation was that the diameter steadily increased with ionic strength. An explanation for the observed difference could be that with increasing ionic strength the elasticity modulus gradually decreases [181]. To test this hypothesis, Figure 5.30 also shows the results of a calculation in which the elasticity modulus decreases as a function of the ionic strength, according to  $E = 30/(A + B \cdot c_{\text{salt}}^3)$  (in MPa) with the empirical parameters  $A = 0.9$  and  $B = 1.4 \cdot 10^{-5}$  with  $c_{\text{salt}}$  in mM. With this expression of  $E$  the black curve is obtained.  $E$  remains independent of ionic strength up to 15 mM in agreement with the observation that there was no pronounced difference in swelling for 0 and 10 mM added NaCl and increases at higher ionic strength. Using this simple empirical function it is possible to obtain a good fit of the model to the experimental data. However, this expression for the decrease of  $E$  with ionic strength is empirical and without a physical basis.

The empirical relation between  $E$  and the ionic strength of the solution was further used to repeat the calculation of the P4VP/PMA capsules' swelling with increased ionic strength at low pH (Figure 5.29 c). The results of this calculation are given in Figure 5.30 b. As in Figure 5.29 c the predictions for 0 and 10 mM added salt remain close to one another, which is in agreement with the experimental data. In Figure 5.29 c the swelling with ionic strength above 10 mM was underestimated. If a dependence of the elasticity modulus on the ionic strength is included according to the above mentioned empirical relation, the swelling with increased salt concentration is too pronounced and overestimates the actual dependence. However, the experimentally observed strong increase in diameter over a short pH range is much better described by taking into account a salt dependence of the elasticity modulus.

# 6 Carbohydrate-sensitive multilayers

## 6.1 Introduction

Phenylboronic acids are known to form covalent bonds with diol compounds such as carbohydrates (see Section 2.6.3). Thus, it should be possible to assemble multilayers, which are not stabilized by electrostatic interactions, but instead rely on the formation of ester-bonds between a phenylboronic acid moiety and a polysaccharide. The stability of the resulting multilayers should depend on the stability of the ester-bond. Although covalent bonds are formed, the reaction is reversible and makes this interaction ideal for the development of a stimuli-sensitive system. The ester-bond formation depends on pH and on the competition between polysaccharides and low molecular weight carbohydrates. Therefore, these parameters should have an influence on the assembly and on the destruction of the resulting multilayers.

## 6.2 Polymers used in the multilayer assembly

A phenylboronic acid moiety was coupled to PAA by amide-bond formation between the carboxylic groups of PAA and aminophenylboronic acid hemisulfate, see Section 4.2.3. The substitution degree was 15 % with respect to the phenylboronic acid groups. The resulting polymer was soluble in aqueous solutions with pH values higher than 5. In the following this polymer is named PAA-BOH.

The multilayers were assembled by ester-bond formation between PAA-BOH and the uncharged polysaccharide mannan. Mannan is a structural part of the cell walls of yeast cells and is composed of mannose monomers. This polymer has a highly branched structure with  $\alpha$ -1,2- and  $\alpha$ -1,3-linked side chains attached to an  $\alpha$ -1,6-linked backbone. No simple repeating unit in mannan has been evidenced [187, 188]. The molecular weight of the polysaccharide is between 40 and 60 kDa.

## 6.3 Sugar-sensitive multilayers on flat substrates

### 6.3.1 Formation of multilayers as a function of pH

The formation of multilayers of mannan and PAA-BOH was monitored by QCM-D in the pH range from 7 to 11. Prior to the multilayer assembly, the gold surface on the quartz crystal was modified with DTGA-PBA to yield a surface that could bind mannan. The experimental details for the synthesis of DTGA-PBA and for the surface coating are described in Section 4.2.4 and 4.4.13. The deposition of 7 bilayers of mannan/PAA-BOH on the modified crystal surface was monitored. During each step adsorption was allowed for 15 minutes, followed by a 5 minutes washing step in buffer solution at the same pH. The results for the pH-dependent multilayer formation are shown in Figure 6.1 a. The evolution of  $-\Delta F/\nu$  at 15 MHz (3rd harmonic) during the assembly of the multilayer is shown. As the reduced frequency of a QCM crystal is proportional to an increase of the deposited mass on the crystal surface, all frequency changes are described as  $-\Delta F/\nu$ . For thin and rigid films  $\Delta F/\nu$  can be converted into the deposited mass with the Sauerbrey relation (see p. 28). For hydrated multilayer films this equation may not be valid due to viscous dissipation in the film and was therefore not used to deduce quantitative data [155]. When discussing the frequency shifts in a QCM-D experiment one always has to keep in mind that the changes in frequency do not only account for the adsorbed polymeric material but also for the water that is present within the film [156].

At pH 7 and 8 no multilayer could be assembled. At pH 7, the first adsorbed layer of mannan resulted in a decrease of the resonance frequency of 40 Hz, but no further polymer adsorption was obtained. At pH 8, the first three layers of mannan and PAA-BOH could be assembled successfully, but each following PAA-BOH layer stripped off the previously adsorbed mannan layer so that there was a small alteration in the frequency change but no increase in the deposited mass. The resulting decrease of the resonance frequency was in the order of 60 Hz. At pH 9, a huge increase in the deposited amount was observed with each additional layer, resulting in a final frequency change of more than 1.5 kHz. No saturated deposition after 15 minutes was observed. At pH 10 and 11, the adsorption process followed a linear manner, and the adsorbed amount was less than at pH 9. The frequency changes after the adsorption of 14 layers were 470 Hz and 266 Hz for multilayers assembled at pH 10 and 11, respectively. In both cases the saturated deposition of the next layer was accomplished in less than five minutes.

To be able to compare the layer adsorption at different pH, 50 mM phosphate buffer was used to adjust the pH values, as this buffer covers the whole range of pH values studied in the experiments. The effect of different buffer systems is shown in Figure 6.1 b.

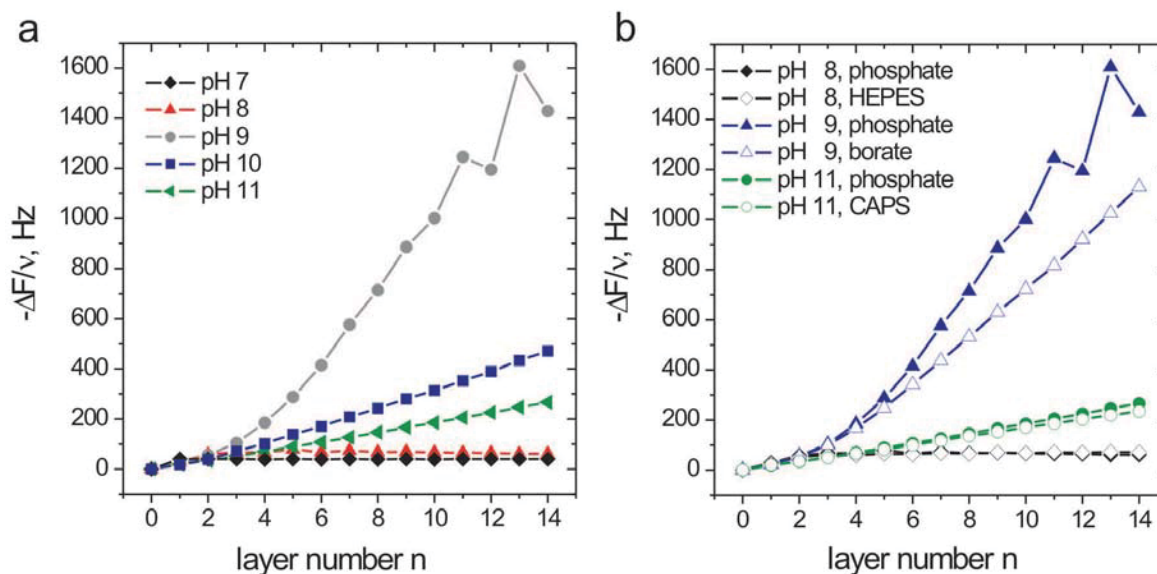


**Figure 6.1:** pH-dependent assembly of mannan/PAA-BOH multilayers as monitored by QCM-D (15 MHz). All pH values were adjusted with 50 mM phosphate buffer (a). Comparison between the assembly with a phosphate buffer (50 mM) and HEPES buffer (50 mM) at pH 8, 50 mM sodium borate buffer at pH 9 and CAPS buffer (50 mM) at pH 11 (b).

At pH 8, no multilayer formation could be observed, irrespective of using a phosphate or a HEPES buffer to adjust the pH. At pH 11, both phosphate and CAPS buffer allowed for a stable multilayer formation and the choice of the buffer did not show any effect on the adsorbed amount. At pH 9, much material was adsorbed onto the quartz crystal, no matter if a phosphate or a borate buffer was used for the assembly of the multilayers. When a borate buffer was used, regular film growth was observed for more than 10 layers, whereas for the phosphate buffer the deposition of PAA-BOH during the 12th and 14th layer resulted in a removal of material from the film.

The pH-dependent multilayer formation can be understood if one takes into account the stability of the ester formed between the phenylboronic acid moiety and the diols of mannan. The ester formation is pH-sensitive, because only the tetrahedral form of the phenylboronic acid is able to form stable esters with diols (see Section 2.6.3). For phenylboronic acid a  $pK_a$  between 8 and 9 is generally reported [110, 111]. This can explain why it is not possible to form multilayers of PAA-BOH and mannan at pH values lower than 9. In addition, the stability of the complex increases with increasing pH. At pH 9, the polymers are weakly bound, resulting in a loopy conformation and large amounts of polymer adsorbed. It could be possible that the films are very hydrated or that adsorbed polymers can diffuse within the layers. This could also explain why no saturation of the deposition was observed after 15 minutes. Furthermore, the weak bond formation can be the reason for the desorption of polymer from the film for 12 and 14 layers. At pH 10 and 11, the ester formation is favored,

resulting in thinner films, due to increased interactions between the layers. Another aspect that has to be considered is the increased negative charge of the PAA-BOH with increasing pH, both because of the tetrahedral boronate and the negatively charged carboxylic groups. The electrostatic repulsion between the negative charges results in an adsorption of this polymer in a more stretched conformation. This can lead to the adsorption of less material.

When no multilayer assembly or stable film growth were observed, the choice of the buffer system did not show any effect on the stability of the layers. Only at pH 9, the adsorbed amount and the stability of the layers were sensitive to the used buffer system, which could be due to a loopy and little stabilized multilayer structure. To compare the data obtained at different pH, in the following only phosphate buffers are used to adjust pH. The above results show that it is possible to assemble multilayers of mannan and PAA-BOH at pH values of 9 and higher without electrostatic stabilization between the polymers.

In addition, the pH-dependent stability of (mannan/PAA-BOH)<sub>7</sub> multilayers is reversible. Films that were prepared at pH 11 and were subsequently exposed to solutions of lower pH at the same ionic strength were stable until pH 9. When they were immersed to a solution of pH 8 the film decomposed within less than 1 minute.

A scheme of the formation of multilayers of mannan and PAA-BOH on modified gold-surfaces is given in Figure 6.2.

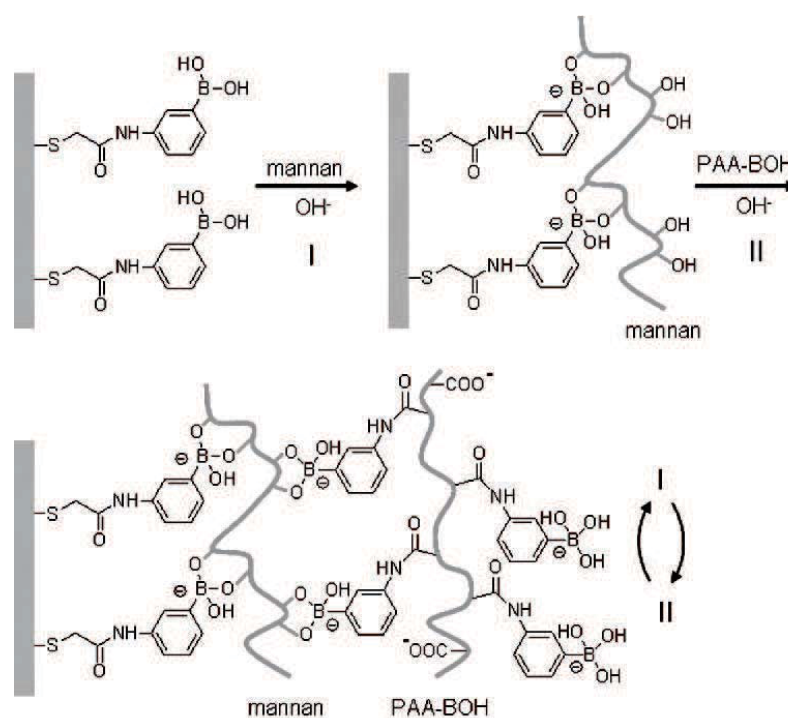


**Figure 6.2:** Scheme of the multilayer formation between mannan and PAA-BOH at high pH.

### 6.3.2 Stability of multilayers with increasing sugar concentration

(Mannan/PAA-BOH)<sub>7</sub> multilayers assembled on modified Au-coated quartz crystals at pH 11 were immersed into sugar solutions with increasing concentrations at pH 11. The films were incubated in each concentration for 15 minutes. The frequency changes of the third harmonic with increasing concentrations of fructose, mannose, galactose and glucose are shown in Figure 6.3.

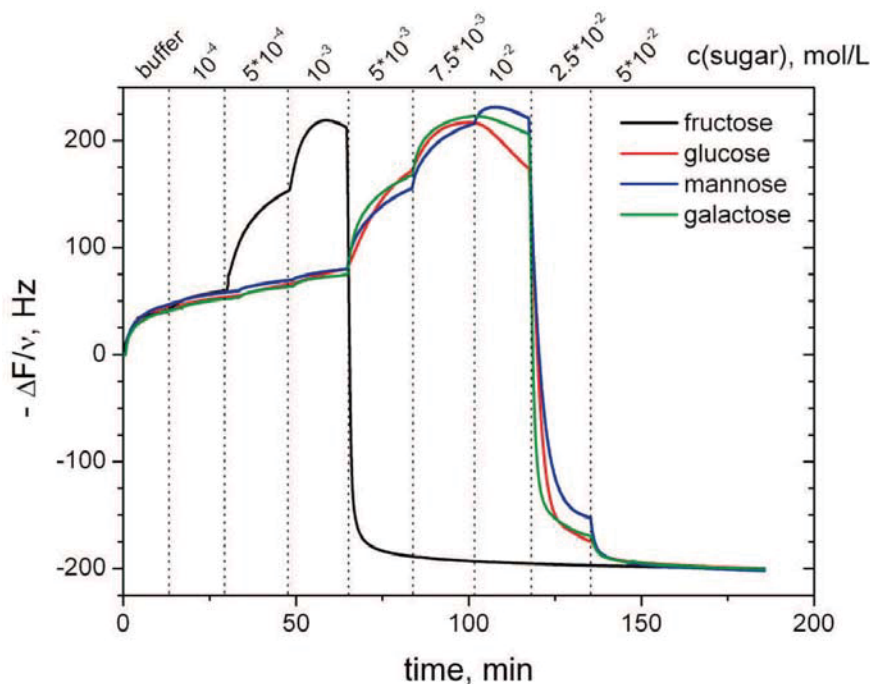


**Figure 6.3:** Effect of increasing concentrations of fructose, glucose, mannose, and galactose at pH 11 on (mannan/PAA-BOH)<sub>7</sub> multilayers as monitored by QCM-D (15 MHz).

During the first 15 minutes the multilayers were exposed to a 50 mM phosphate buffer solution at pH 11. This exposure was accompanied by a reduced frequency of around 40 Hz. The frequency shift can be attributed to the incorporation of more water within the layers, as the layer assembly was accomplished in a solution of 0.5 M NaCl and 50 mM phosphate buffer. The reduced ionic strength can lead to the formation of an osmotic pressure difference that is accompanied by the accumulation of water within the layers.

When fructose was added, the deposited mass was increased until a concentration of  $1 \cdot 10^{-3}$  M fructose was reached, which can be attributed to additional binding of fructose to PAA-BOH on boronic acid moieties that were not incorporated in the ester-bond formation with mannan. At a concentration of  $1 \cdot 10^{-3}$  M fructose the adsorbed mass reached a maximum and then slowly decreased. When the fructose concentration was increased to  $5 \cdot 10^{-3}$  M, the film was destroyed in less than 2 minutes. The destruction of the multilayer can be explained by competitive adsorption of monomeric fructose and polymeric

mannan to the phenylboronic acid binding sites. When glucose, galactose and mannose were added in increasing concentrations, a small decrease in frequency was observed until a concentration of  $5 \cdot 10^{-3}$  M was reached. For sugar concentrations between  $5 \cdot 10^{-3}$  and  $1 \cdot 10^{-2}$  M the frequency decreased substantially and was finally twice the value of the original multilayer film. For all three carbohydrates the adsorbed mass passed through a maximum at  $1 \cdot 10^{-2}$  M. Irrespective of the carbohydrate, the multilayer decomposed within less than 5 minutes when it was exposed to a sugar concentration of  $2.5 \cdot 10^{-2}$  M. If the (mannan/PAA-BOH)<sub>7</sub> films were exposed to the carbohydrate concentration, at which the adsorbed amount passed through a maximum ( $1 \cdot 10^{-3}$  M for fructose,  $1 \cdot 10^{-2}$  M for galactose, fructose, mannose) the multilayer was slowly degraded until it was completely destroyed. Regarding fructose, this destruction was finished after 7 h, and the films were destructed after 12 - 14 h for glucose, galactose and mannose.

The ester-bond formation between a diol and a boronic acid moiety is covalent but reversible, thus it is possible to decompose (mannan/PAA-BOH)<sub>7</sub> multilayers by the addition of low molecular weight carbohydrates. In all investigated cases, the addition of carbohydrates in a low concentration first led to a decrease of the resonance frequency. The reduced frequency corresponded to an increased adsorbed mass that can be caused by a higher hydration of the multilayer and additional low molecular weight sugar within the layers, which can bind to free boronic acid moieties. Additionally there can be a competition between bound mannan and low molecular weight sugars for the binding to phenylboronic acid groups. At a critical concentration the adsorbed amount passed through a maximum. At this carbohydrate concentration a destruction of the multilayer over several hours was observed. In contrast, if the carbohydrate concentration was increased beyond the critical concentration the multilayer was destroyed within several minutes. At this concentration the amount of low molecular weight sugar seems to be sufficient to destroy the multilayer because of a competition reaction.

The sensitivity of (mannan/PAA-BOH)<sub>7</sub> films to fructose was about an order of magnitude higher than the one to glucose, galactose and mannose. In the concentration range investigated it was not possible to distinguish between glucose, galactose and mannose. This finding is in good agreement with literature data. James et al. and Springsteen and coworkers reported equilibrium constants for the binding of fructose to phenylboronic acid that were one order of magnitude higher than the ones for galactose, mannose and glucose [111, 116].



### 6.3.3 pH-dependent stability of multilayers with increasing fructose concentration

(Mannan/PAA-BOH)<sub>7</sub> films that were assembled at pH 9, 10 and 11 were exposed to fructose at the same pH with increasing concentrations. The results for pH 10 and 11 are shown in Figure 6.4.

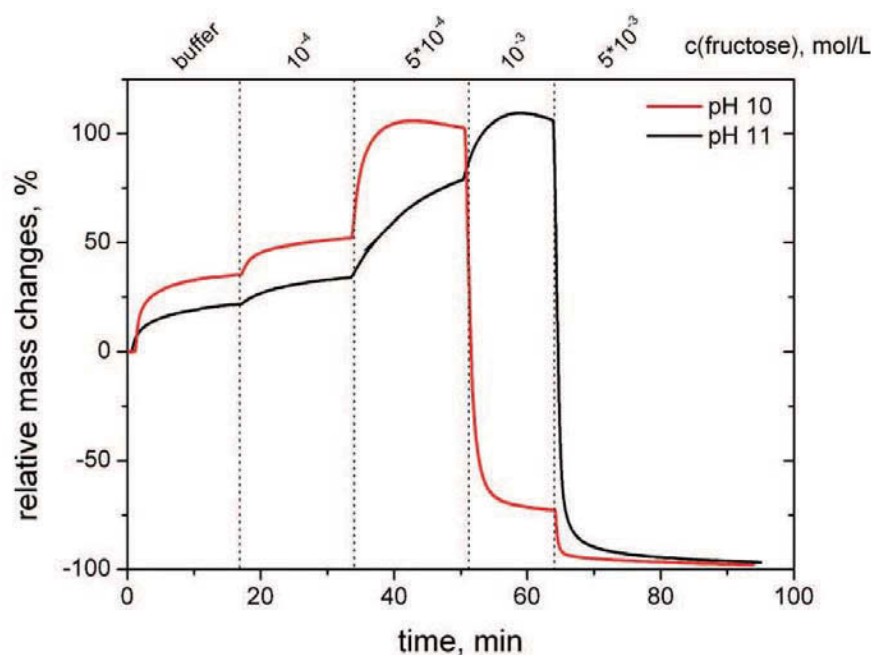


**Figure 6.4:** Stability of (mannan/PAA-BOH)<sub>7</sub> multilayers as a function of the fructose concentration at pH 10 and 11 as monitored by QCM-D (15 MHz).

Multilayers that were assembled at pH 9 (0.5 M NaCl, 50 mM phosphate buffer) decomposed within minutes, if they were immersed in a 50 mM phosphate buffer solution at the same pH. Thus, it was not possible to investigate the stability with increasing fructose concentrations at pH 9.

For better comparison, the frequency changes (QCM-D, 15 MHz) for multilayers assembled at pH 10 and 11 are shown as percentage values. With increasing fructose concentration the layers assembled at pH 10 and 11 both showed an increase in the mass of around 100 % before the decomposition of the film started. This huge increase in mass is probably caused by the uptake of water and fructose within the multilayer. At pH 10 the films decomposed at a fructose concentration of  $1 \cdot 10^{-3}$  M, whereas films assembled at pH 11 only started to decompose at a fructose concentration of  $5 \cdot 10^{-3}$  M.

The pH of the environment strongly affects the sensitivity of phenylboronic acid compounds for carbohydrates [111]. The sugar-sensitive properties of phenylboronic acid are greatly enhanced when the system is operated above the  $pK_a$  of the phenylboronic acid derivatives, which is often situated between 8 and 9. When the phenylboronic acid moiety is coupled to

poly(acrylic acid), the presence of the carboxylic groups has an influence on the  $pK_a$  of the phenylboronic acid, thus severely complicating the system. At pH 9, the multilayer assembly resulted in very thick and probably hydrated films. In addition, the multilayer decomposed if it was immersed into a solution with slightly decreased ionic strength. Both observations indicate that the formation of a stable multilayer is not yet possible at that pH. When the fructose concentration was increased, films assembled at pH 11 showed a higher stability than films assembled at pH 10, indicating that a more stable multilayer was formed at higher pH.

## 6.4 Sugar-sensitive capsules

### 6.4.1 Preparation of capsules

It was possible to assemble stable multilayers of PAA-BOH and mannan on flat substrates, so that this polymer combination was chosen for the preparation of microcapsules. As the assembly at pH 11 was the most stable one for flat multilayers, this pH was used for the preparation of mannan/PAA-BOH capsules.  $CaCO_3$  particles were used as templates, because they have two advantages. They can be dissolved over nearly the complete pH range and it is possible to incorporate various substances, in this case TRITC-BSA, within the core by coprecipitation. The coating of  $CaCO_3$  particles without coprecipitated TRITC-BSA at pH 11 was followed by  $\zeta$ -potential measurements after each adsorption step. The results are shown in Figure 6.5.

For the deposition of all layers the  $\zeta$ -potential was negative, clearly ruling out the influence of electrostatic stabilization of the multilayers. The  $\zeta$ -potential of the bare particles was -20 mV and changed regularly between ca. -40 and -48 mV upon adsorption of mannan and PAA-BOH, respectively. In contrast to electrostatic self-assembly, there was no surface charge reversal, and the negative charge of the surface could be maintained throughout the entire self-assembly process, thus preventing particle aggregation.

After the deposition of 7 bilayers of mannan/PAA-BOH the core material was removed with 0.1 M EDTA at pH 11 at which the multilayers were most stable. CLSM images of empty capsules and of capsules filled with TRITC-BSA are shown in Figure 6.6.

Transmission images are shown to prove the complete removal of the core material. For empty capsules the fluorescence labeling was achieved by the adsorption of FITC-dextran (4 kDa) onto the capsule shells. The fluorescence of filled capsules was caused by encapsulated TRITC-BSA. It should be noted that capsules composed of less than 14 polymer layers were not stable enough to keep encapsulated TRITC-BSA within the capsule interior. Most

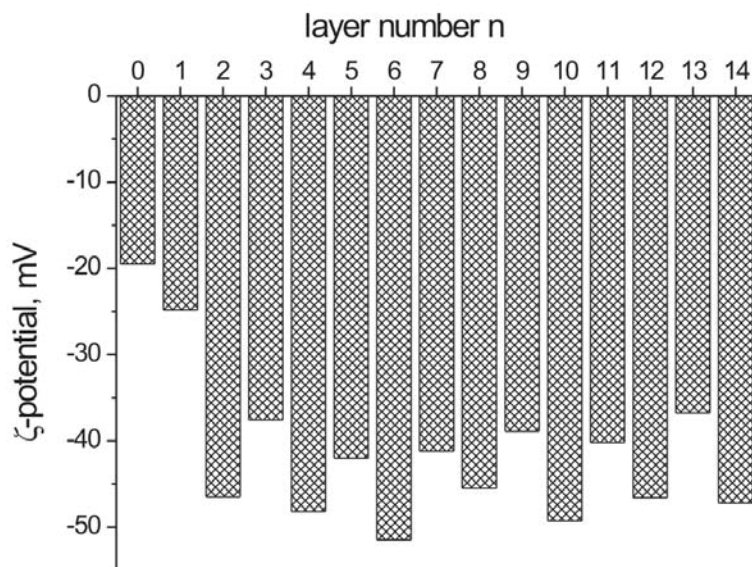


**Figure 6.5:**  $\zeta$ -potential of mannan/PAA-BOH coated  $\text{CaCO}_3$  particles as a function of the number of deposited layers. Odd layer numbers correspond to the deposition of mannan, even layer numbers represent the deposition of PAA-BOH. All measurements were performed at pH 11.

probably, the stability of the capsule wall depends on the amount of ester-bonds, which is increased when more polymer layers are added.

Dried (mannan/PAA-BOH)<sub>7</sub> capsules were investigated by AFM. Typical AFM images of empty and filled capsules are shown in Figure 6.7. Empty capsules (Figure 6.7 a) did not show the typical folds and creases observed for electrostatically assembled multilayer capsules. Upon drying the capsules collapsed on the substrate in a ringlike fashion. The thickness per bilayer was  $1.3 \pm 0.2$  nm, which is much lower than the thicknesses observed for electrostatically stabilized multilayers (refer to p. 50). On the other hand, capsules that were filled with TRITC-BSA showed a thickness of  $\sim 62$  nm, of which ca. 18 nm are attributed to the capsule wall.

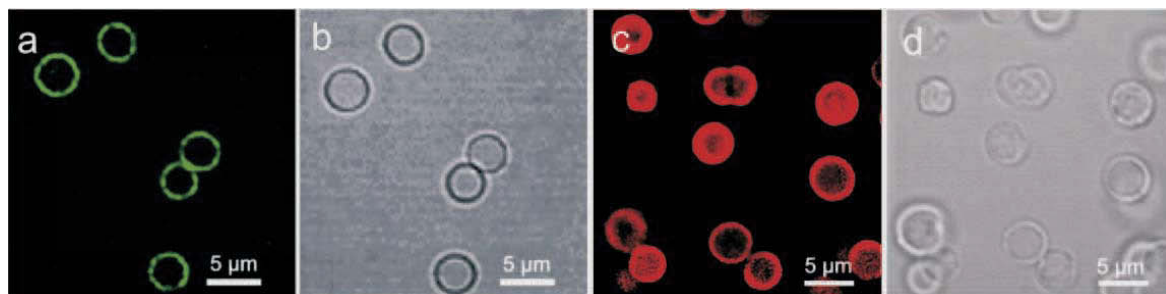


**Figure 6.6:** CLSM images of empty (mannan/PAA-BOH)<sub>7</sub> capsules in the fluorescence (a) and transmission mode (b), and of (mannan/PAA-BOH)<sub>7</sub> capsules filled with TRITC-BSA in the fluorescence (c) and transmission mode (d).

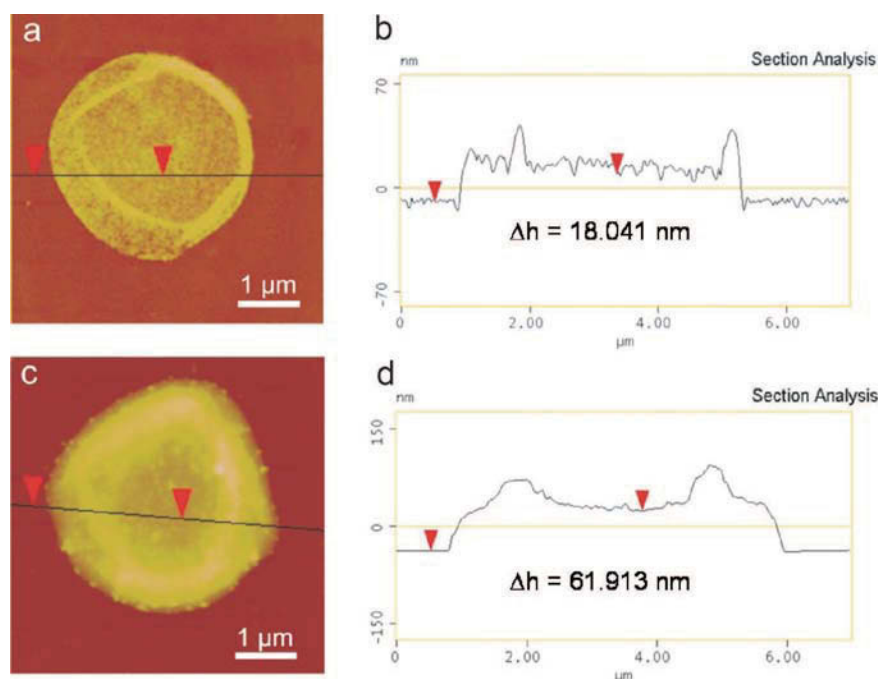


**Figure 6.7:** AFM images of empty (mannan/PAA-BOH)<sub>7</sub> capsules (a) and of TRITC-BSA filled capsules (c), with the corresponding height profiles (b,d).

#### 6.4.2 Stability of capsules with increasing sugar concentration

The stability of (mannan/PAA-BOH)<sub>7</sub> multilayer shells in increasing concentrations of glucose, mannose, galactose and fructose was investigated at pH 11 in a 50 mM phosphate buffer. For each experiment 2 mL of a suspension of TRITC-BSA filled capsules was used. The capsule concentration was  $3 \cdot 10^8$  capsules/L. The capsules were exposed to carbohydrates at different concentrations for 15 minutes, followed by centrifugation. The release of encapsulated TRITC-BSA was measured as the increase of the fluorescence intensity of the supernatant at  $\lambda = 580$  nm. The fluorescence intensity was recorded relative to the intensity corresponding to the complete release of TRITC-BSA. The capsule concentration was chosen to ensure that the fluorescence intensity was proportional to the concentration of TRITC-BSA. The results are summarized in Figure 6.8.

At all sugar concentrations a small amount of TRITC-BSA was detectable in the supernatant. A possible explanation can be found in the incorporation of low molecular weight carbohydrates into the multilayers, which already loosen the layer structure and enhance the permeation of BSA. When the capsules were destroyed, all encapsulated TRITC-BSA was released and detectable in the fluorescence of the supernatant. For fructose a sharp increase in the fluorescence intensity was detected in the concentration range from  $1 \cdot 10^{-3}$  to  $3 \cdot 10^{-3}$  M, and for glucose, mannose and galactose a sharp increase in the fluorescence intensity was found between  $1 \cdot 10^{-2}$  and  $3 \cdot 10^{-2}$  M. The concentration range in which the

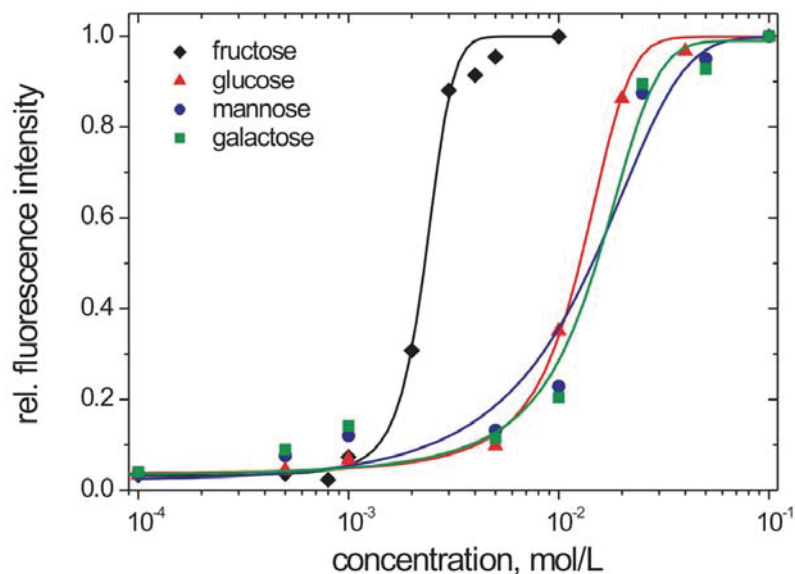


**Figure 6.8:** Relative fluorescence intensity (at  $\lambda = 580$  nm) of the supernatant of a capsule suspension with increasing sugar concentration. The lines serve as visual guides.

increase in the fluorescence of the supernatant was found is in good agreement with the one observed for (mannan/PAA-BOH)<sub>7</sub> on flat substrates. Furthermore, the sensitivity for glucose was in the same concentration range, as the one reported by De Geest et al. [109]. They used a different approach for the sensing of glucose by incorporating a phenylboronic acid compound into electrostatically stabilized multilayer capsules and monitoring the glucose-induced change in electrostatic interactions within the multilayers.

The response of the studied multilayer films to several carbohydrates could lead to the design of sugar-sensing devices. Particularly, the high selectivity for fructose compared to the other investigated carbohydrates could be used for the development of sugar-sensitive delivery systems with the capsule content as a chemical amplifier.

## 7 Summary and conclusion

The aim of this work was the development of stimuli-responsive microcapsules with the focus on pH-sensitivity and on carbohydrate-sensing. Two different combinations of weak polyelectrolytes were used for the preparation of pH-dependent microcapsules that vary considerably in their hydrophobicity.

The investigation of the pH-dependent properties of weak polyelectrolyte capsules was driven by the aim to obtain a quantitative control of structural changes of the capsule shell which is mandatory for practical applications. To achieve this goal it was necessary to use core materials that do not affect the integrity of the capsule wall. Thus, silica cores were used as templates for the deposition of weak polyelectrolyte multilayers and a new approach for the dissolution of these particles in mild pH conditions was reported. The application of a buffer system allowed a high concentration of hydrofluoric acid in combination with an increased pH that ensured the stability of the weak polyelectrolyte multilayers during the core dissolution.

The first investigated pH-responsive system consisted of microcapsules composed of two weak polyelectrolytes, poly(allylamine hydrochloride) (PAH) and poly(methacrylic acid) (PMA), that were assembled either on  $\text{CaCO}_3$  or on  $\text{SiO}_2$  particles. These capsules were stable over a wide pH range from 2.5 to 11 and dissolved in extreme pH conditions. At the edges of the stability range the pH-induced imbalance of charges reduced the electrostatic interactions and led to a swelling of the system. The swelling was attributed to an increased osmotic pressure of small counterions that were attracted from the bulk to compensate for the charge excess of the polymers. The swollen PAH/PMA capsules could be stabilized when attractive forces counteracted the electrostatic destabilization between the layers in the acidic or basic pH range. Such attractive forces were found when the entanglement of polymers was increased by using PMA of a higher molecular weight or when the stabilization by H-bonding and hydrophobic interactions between uncharged PMA was high enough. This was achieved by increasing the amount of adsorbed material when using a porous core. When a stable swollen state was observed, it was possible to reversibly swell and shrink the capsules by varying the solution pH. Furthermore, the pH-dependent stability of PAH/PMA capsules was influenced by the ionic strength of the solution. When the ionic strength was increased,

the stability of the capsules in the acidic and basic pH range was reduced and at a given pH the capsule diameter was increased to a new equilibrium value compared to the one without additional electrolyte.

Moreover, free carboxylate groups that emerged during the post-assembly pH treatment could be used for the pH-dependent complexation of calcium ions. The calcium-binding reduced the stability of the shells at low pH and led to a shrinking of the capsules in the basic pH region. The pH-dependent binding of the carboxylate groups to calcium showed the versatility of the system to be used for selective reactions that are restricted to free functional groups within multilayer thin films.

The two polyelectrolytes used in the second pH-sensitive system are known for their hydrophobic properties, poly(4-vinylpyridine) (P4VP) is insoluble in water in its uncharged form and PMA exhibits H-bonding stabilization and hydrophobic interactions at low pH. Capsules of P4VP and PMA templated on silica particles were stabilized by a combination of hydrogen-bonding and electrostatic interactions over a broad pH range and showed a reversible swelling at pH 2 and pH 8.1. The size of the swollen capsules increased when more polymeric material was adsorbed, and the swelling was reversible, independent of the number of adsorbed layers. The stable swollen states were attributed to the competition between repulsive electrostatic interactions and attractive hydrophobic or H-bonding interactions. The stabilizing effect of hydrophobic interactions on the swollen state was investigated by exchanging the aqueous solution to a solvent mixture of 1:1 water and methanol that reduced the hydrophobic stabilization. In this case no stable swelling was observed. In addition to the pH-dependent stability of P4VP/PMA capsules, the ionic strength of the solution had an influence on the swelling behavior, too. With increasing ionic strength, the stability range of the capsules was slightly decreased and at a given pH the capsule diameter was increased.

To investigate the effect of pH-dependent electrostatic interactions on modifications within the capsule shell, the permeability of P4VP/PMA capsules for glucose was studied at various pH values. Over a broad pH-range from pH 2.1 to pH 7.9, (P4VP/PMA)<sub>4</sub> capsules showed a permeability for glucose of  $2 \cdot 10^{-8}$  to  $4 \cdot 10^{-8}$  m/s. Only at the edges of the stability range, at which a swelling of the capsules was observed, the permeability increased at least one order of magnitude to values higher than  $5.5 \cdot 10^{-7}$  m/s. Capsules that were swollen and then shrunk back to their original size showed a slightly increased permeability of  $4 \cdot 10^{-8}$  to  $7 \cdot 10^{-8}$  m/s. The reversible permeability changes with pH were used for the encapsulation of FITC-dextran at pH 8.

The equilibrium swelling of PAH/PMA and P4VP/PMA capsules was modeled with a micromechanical scaling theory that included an elastic restoring force and an osmotic expanding force. The expanding force takes into account the osmotic pressure of the counterions

that are attracted from the bulk to the shell to compensate for the charge excess of the polymers. In this model, ions within the shell are neglected and only those in the two diffuse layers on each side of the shell are considered. With this model, the essential experimental features could be described, the wide pH plateau in which the size remained close to the initial value, the sharp increases in size at the edges of the pH plateau and the increasing capsule size with increasing ionic strength. The model takes into account that the polymer charge depends on the local electrostatic potential, which is essential for the description of the wide pH plateau and of the influence of the ionic strength on the swelling behavior.

The increase in capsule size with ionic strength both in theory and experiment is not typically observed for polyelectrolyte systems. However, swelling with increasing ionic strength has been shown and predicted for polyelectrolyte brushes, at low ionic strength, when the polyelectrolyte is ionizable and is usually referred to as the osmotic brush regime. Thus, it is suggested that at the edges of the stability plateau, multilayer capsules consisting of two ionizable polyelectrolytes are another example of the osmotic regime found in weak polyelectrolyte systems.

In conclusion, it was shown that weak polyelectrolyte capsules are an interesting example of pH-sensitive microstructures. These capsules exhibit a pH-tunable charge density and can exist in a swollen state, when the electrostatic repulsion is counteracted by stabilizing forces like hydrogen-bonding, hydrophobic interactions and entanglement. Weak polyelectrolyte shells do not only show pH-sensitivity but the stability of these capsules also depends on the ionic strength of the solution. The reversible swelling is accompanied by reversible permeability changes that can be used for the encapsulation of polymeric material.

Another stimuli-responsive system that was investigated consisted of carbohydrate-sensitive thin films. These multilayers were not assembled by electrostatic interactions but instead they were stabilized by the formation of a reversible covalent ester-bond between a boronic acid moiety and the diols of a polysaccharide. For this purpose the polysaccharide mannan was assembled with poly(acrylic acid) that was modified by phenylboronic acid. The LbL assembly was followed on flat substrates in dependence of pH. Below pH 9, no film formation could be observed, and the stability of multilayers assembled at higher pH values increased with increasing pH. These findings could be related to the pH-dependent stability of the ester-bond between boronic acid and diol compounds.

The resulting mannan/PAA-BOH multilayers could be dissolved upon exposure to carbohydrates in aqueous solution. This behavior originated from the competitive binding of small molecular weight carbohydrates and mannan with the boronic acid groups within the film, resulting in a destabilization of the multilayer. Multilayer thin films of mannan/PAA-BOH were stable in fructose concentrations below  $1 \cdot 10^{-3}$  M and in solutions containing glu-



cose, mannose or galactose in a concentration below  $1 \cdot 10^{-2}$  M. Thus, the sensitivity of mannan/PAA-BOH multilayers for fructose was one order of magnitude higher than for all other saccharides studied.

It was also possible to assemble mannan/PAA-BOH multilayers on  $\text{CaCO}_3$  particles, because the negative surface charge that was maintained throughout the entire self-assembly process prevented particle aggregation. Upon dissolution of the template, hollow capsules could be obtained. The sugar-dependent stability of these capsules was investigated by following the release of encapsulated TRITC-BSA and the observed stability of the capsule shell in different carbohydrate solutions was in the same range as the one observed for flat multilayers.

In conclusion, novel sugar-responsive multilayers were assembled using the reversible covalent ester formation between a polysaccharide and phenylboronic acid moieties. The resulting multilayer films were sensitive to several carbohydrates, with high selectivity for fructose. The response to carbohydrates was observed as a fast dissolution of the multilayers, when they were brought into contact with the sugar-containing solution above a critical concentration. Thus, these multilayers have a potential in the design of carbohydrate-sensing systems and sugar-sensitive delivery systems with the capsule content as a chemical amplifier.

# Bibliography

- [1] Decher, G.; Hong, J.D.; Schmitt, J. *Thin Solid Films* (1992) **210-211**, 831-835.
- [2] Stockton, W.B.; Rubner, M.F. *Macromolecules* (1997) **30**, 2717-2725.
- [3] Hong, J.D.; Lowack, K.; Schmitt, J.; Decher, G. *Progr. Colloid Polymer Sci.* (1993) **93**, 98-102.
- [4] Lvov, Y.; Ariga, K.; Ichinose, I.; Kunitake, T. *J. Chem. Soc., Chem. Commun.* (1995) **22**, 2313-2314.
- [5] Sukhorukov, G.B.; Donath, E.; Davis, S.; Lichtenfeld, H.; Caruso, F.; Popov, V.I.; Möhwald, H. *Polym. Adv. Technol.* (1998) **9**, 759-767.
- [6] Donath, E., Sukhorukov, G.B.; Caruso, F.; Davis, S.A.; Möhwald, H. *Angew. Chem. Int. Ed.* (1998) **37**, 2202-2205.
- [7] Sukhishvili, S.A. *Curr. Opin. Colloid Interface Sci.* (2005) **10**, 37-44.
- [8] Déjugnat, C.; Sukhorukov, G.B. in *Responsive Polymer Materials: Design and Applications*, Ed. Minko, S., Blackwell Publishing Professional, Ames, IA, 2006.
- [9] Fler, G.J.; Cohen Stuart, M.A.; Scheutjens, J.M.H.M.; Cosgrove, T.; Vincent, B. *Polymers at Interfaces* Chapman & Hall, London, 1993.
- [10] Netz, R.R.; Andelman, D. *Physics Reports* (2003) **380**, 1-95.
- [11] Förster, S.; Schmidt, M. *Adv. Polymer Sci.* (1995) **120**, 51-133.
- [12] Dautzenberg, H.; Jaeger, W.; Kötz J.; Phillip, B.; Seidel, C.; Stscherbina, D. *Polyelectrolytes: Formation, Characterization and Application* Hanser, Munich, 1994.
- [13] Katchalsky, A.; Spitnik, P. *J. Polymer Sci.* (1947) **2**, 432-446.
- [14] Leyte, J.C.; Mandel, M. *J. Polymer Sci. A* (1964) **2**, 1879-1891.
- [15] Thuenemann, A.F.; Mueller, M.; Dautzenberg, H.; Joanny, J.-F.; Loewen, H. *Adv. Polymer Sci.* (2004) **166**, 113-171.
- [16] Kabanov, V. in *Multilayer Thin Films*, p. 47-86, Ed. Decher, G.; Schlenoff, J.B., Wiley-VCH, Weinheim, 2003.
- [17] Joanny, J.-F.; Castelnovo, M. in *Multilayer Thin Films*, p. 87-97, Ed. Decher, G.; Schlenoff, J.B., Wiley-VCH, Weinheim, 2003.
- [18] Blaakmeer, J.; Böhmer, M.R.; Cohen Stuart, M.A.; Fler, G.J. *Macromolecules* (1990) **23**, 2301-2309.

- [19] Iler, R.K. *J. Colloid Interface Sci.* (1966) **21**, 569-594.
- [20] Hammond, P.T. *Curr. Opin. Colloid Interface Sci.* (1999) **4**, 430-442.
- [21] Decher, G.; Schlenoff, J.B. (Ed.) *Multilayer Thin Films: Sequential Assembly of Nanocomposite Materials* Wiley-VCH, Weinheim, 2003.
- [22] Decher, G. *Science* (1997) **277**, 1232-1237.
- [23] Kotov, N.A. *Nanostructured Materials* (1999) **12**, 789-796.
- [24] Bertrand, P.; Jonas, A.; Laschewsky, A.; Legras, R. *Macromol. Rapid Commun.* (2000) **21**, 319-348.
- [25] Lvov, Y.; Decher, G.; Möhwald, H. *Langmuir* (1993) **9**, 481-486.
- [26] Schmitt, J.; Grünwald, T.; Decher, G.; Pershan, P.S.; Kjaer, K.; Lösche, M. *Macromolecules* (1993) **26**, 7058-7063.
- [27] Korneev, D.; Lvov, Y.; Decher, G.; Schmitt, J.; Yaradaikin, S. *Physica B* (1995) **213-214**, 954-956.
- [28] Ruths, J.; Essler, F.; Decher, G.; Riegler, H. *Langmuir* (2000) **16**, 8871-8878.
- [29] McAloney, R.A.; Sinyor, M.; Dudnik, V.; Goh, M.C. *Langmuir* (2001) **17**, 6655-6663.
- [30] Picart, C.; Lavalle, P.; Hubert, P.; Cuisinier, F.J.G.; Decher, G.; Schaaf, P.; Voegel, J.-C. *Langmuir* (2001) **17**, 7414-7424.
- [31] Boulmedais, F.; Ball, V.; Schwinte, P.; Frisch, B.; Schaaf, P.; Voegel, J.-C. *Langmuir* (2003) **19**, 440-445.
- [32] Lavalle, P.; Picart, C.; Mutterer, J.; Gergely, C.; Reiss, H.; Voegel, J.-C.; Senger, B.; Schaaf, P. *J. Phys. Chem. B* (2004) **108**, 635-648.
- [33] Sukhorukov, G.B.; Donath, E.; Lichtenfeld, H.; Knippel, E.; Knippel, M.; Budde, A.; Möhwald, H. *Colloids Surfaces A* (1998) **137**, 253-266.
- [34] Voigt, A.; Lichtenfeld, H.; Sukhorukov, G.B.; Zastrow, H.; Donath, E.; Bäuml, H.; Möhwald, H. *Ind. Eng. Chem. Res.* (1999) **38**, 4037-4043.
- [35] Peyratout, C.S.; Dähne, L. *Angew. Chem. Int. Ed.* (2004) **43**, 3762-3783.
- [36] Gao, C.; Moya, S.; Donath, E.; Möhwald, H. *Macromol. Chem. Phys.* (2002) **203**, 953-960.
- [37] Gao, C.; Moya, S.; Lichtenfeld, H.; Casoli, A.; Fiedler, H.; Donath, E.; Möhwald, H. *Macromol. Mater. Eng.* (2001) **286**, 355-361.
- [38] Déjugnat, C.; Sukhorukov, G.B. *Langmuir* (2004) **20**, 7265-7269.
- [39] Antipov, A.A.; Shchukin, D.; Fedutik, Y.; Petrov, A.I.; Sukhorukov, G.B.; Möhwald, H. *Colloids Surfaces A* (2003) **224**, 175-183.

- [40] Adalsteinsson, T.; Dong, W.-F.; Schönhoff, M. *J. Phys. Chem. B* (2004) **108**, 20056-20063.
- [41] Itoh, Y.; Matsusaki, M.; Kida, T.; Akashi, M. *Chem. Lett.* (2004) **33**, 1552-1553.
- [42] Köhler, K.; Shchukin, D.G.; Möhwald, H.; Sukhorukov, G.B. *J. Phys. Chem. B* (2005) **109**, 18250-18259.
- [43] Yang, S.; Zhang, Y.; Yuan, G.; Zhang, X.; Xu, J. *Macromolecules* (2004) **37**, 10059-10062.
- [44] Zhang, Y.; Guan, Y.; Yang, S.; Xu, J.; Han, C.C. *Adv. Mater.* (2003) **15**, 832-835.
- [45] Sukhorukov, G.B.; Volodkin, D.V.; Günther, A.M.; Petrov, A.I.; Shenoy, D.B.; Möhwald, H. *J. Mater. Chem.* (2004) **14**, 2073-2081.
- [46] Steitz, R.; Jaeger, W.; von Klitzing, R. *Langmuir* (2001) **17**, 4471-4474.
- [47] Schöler, B.; Kumaraswamy, G.; Caruso, F. *Macromolecules* (2002) **35**, 889-897.
- [48] Glinel, K.; Moussa, A.; Jonas, A.M.; Laschewsky, A. *Langmuir* (2002) **18**, 1408-1412.
- [49] Voigt, U.; Jaeger, W.; Findenegg, G.H.; von Klitzing, R. *J. Phys. Chem. B.* (2003) **107**, 5273-5280.
- [50] Schöler, B.; Poptoshev, E.; Caruso, F. *Macromolecules* (2003) **36**, 5258-5264.
- [51] Fischer, P.; Laschewsky, A.; Wischerhoff, E.; Arys, X.; Jonas, A.; Legras, R. *Macromol. Symp.* (1999) **137**, 1-24.
- [52] Schlenoff, J.B.; Ly, H.; Li, M. *J. Am. Chem. Soc.* (1998) **120**, 7626-7634.
- [53] Decher, G.; Schmitt, J. *Progr. Colloid Polymer Sci.* (1992) **89**, 160-164.
- [54] Dubas, S.T.; Schlenoff, J.B. *Macromolecules* (1999) **32**, 8153-8160.
- [55] Dubas, S.T.; Schlenoff, J.B. *Langmuir* (2001) **17**, 7725-7727.
- [56] Sukhorukov, G.B.; Schmitt, J.; Decher, G. *Berichte der Bunsen-Gesellschaft* (1996) **100**, 948-953.
- [57] Georgieva, R.; Dimova, R.; Sukhorukov, G.B.; Ibarz, G.; Möhwald, H. *J. Mater. Chem.* (2005) **15**, 4301-4310.
- [58] Heuvingh, J.; Zappa, M.; Fery, A. *Langmuir* (2005) **21**, 3165-3171.
- [59] Cochin, D.; Laschewsky, A. *Macromol. Chem. Phys.* (1999) **200**, 609-615.
- [60] Wang, L.Y.; Wang, Z.Q.; Zhang, X.; Shen, J.C.; Chi, L.; Fuchs, H. *Macromol. Rapid Commun.* (1997) **18**, 509-514.
- [61] Pontes, R.S.; Raposo, M.; Camilo, C.S.; Dhanabalan, A.; Ferreira, M.; Oliveira, O.N., *Physica Status Solidi A* (1999) **173**, 41-50.

- [62] He, P.-G.; Takahashi, T.; Hoshi, T.; Anzai, J.-i.; Suzuki, Y.; Osa, T. *Mater. Sci. Eng. C* (1994) **2**, 103-106.
- [63] Anzai, J.-i.; Kobayashi, Y.; Nakamura, N.; Nishimura, M.; Hoshi, T. *Langmuir* (1999) **15**, 221-226.
- [64] von Klitzing, R.; Möhwald, H. *Langmuir* (1995) **11**, 3554-3559.
- [65] Rmaile, H.H.; Schlenoff, J.B. *Langmuir* (2002) **18**, 8263-8265.
- [66] Kharlampieva, E.; Sukhishvili, S.A. *Langmuir* (2003) **19**, 1235-1243.
- [67] Petrov, A.I.; Antipov, A.A.; Sukhorukov, G.B. *Macromolecules* (2003) **36**, 10079-10086.
- [68] Choi, J.; Rubner, M.F. *Macromolecules* (2005) **38**, 116-124.
- [69] Xie, A.F.; Granick, S. *J. Am. Chem. Soc.* (2001) **123**, 3175-3176.
- [70] Xie, A.F.; Granick, S. *Macromolecules* (2002) **35**, 1805-1813.
- [71] Shiratori, S.S.; Rubner, M.F. *Macromolecules* (2000) **33**, 4213-4219.
- [72] Yoo, D.; Shiratori, S.S.; Rubner, M.F. *Macromolecules* (1998) **31**, 4309-4318.
- [73] Mendelsohn, J.D.; Barrett, C.J.; Chan, V.V.; Pal, A.J.; Mayes, A.M.; Rubner, M.F. *Langmuir* (2000) **16**, 5017-5023.
- [74] Fery, A.; Schöler, B.; Cassagneau, T.; Caruso, F. *Langmuir* (2001) **17**, 3779-3783.
- [75] Zhai, L.; Nolte, A.J.; Cohen, R.E.; Rubner, M.F. *Macromolecules* (2004) **37**, 6113-6123.
- [76] Bruening, M.L.; Sullivan, D.M. *Chem. Eur. J.* (2002) **8**, 3833-3837.
- [77] Wang, T. C.; Rubner, M.F.; Cohen, R.E. *Langmuir* (2002) **18**, 3370-3375.
- [78] Schuetz, P.; Caruso, F. *Chem. Mater.* (2004) **16**, 3066-3073.
- [79] Joly, S.; Kane, R.; Radzilowski, L.; Wang, T.; Wu, A.; Cohen, R.E.; Thomas, E.L.; Rubner, M.F. *Langmuir* (2000) **16**, 1354-1359.
- [80] Burke, S.E.; Barrett, C.J. *Biomacromolecules* (2005) **6**, 1419-1428.
- [81] Burke, S.E.; Barrett, C.J. *Langmuir* (2003) **19**, 3297-3303.
- [82] Kato, N.; Schuetz, P.; Fery, A.; Caruso, F. *Macromolecules* (2002) **35**, 9780-9787.
- [83] Gao, C.; Möhwald, H.; Shen, J. *Adv. Mater.* (2003) **15**, 930-933.
- [84] Schuetz, P.; Caruso, F. *Adv. Funct. Mater.* (2003) **13**, 929-937.
- [85] Hiller, J.; Rubner, M.F. *Macromolecules* (2003) **36**, 4078-4083.
- [86] Itano, K.; Choi, J.; Rubner, M.F. *Macromolecules* (2005) **38**, 3450-3460.

- [87] Vinogradova, O.I.; Andrienko, D.; Lulevich, V.V.; Nordschild, S.; Sukhorukov, G.B. *Macromolecules* (2004) **37**, 1113-1117.
- [88] Sukhishvili, S.A.; Granick, S. *Macromolecules* (2002) **35**, 301-310.
- [89] Sukhishvili, S.A.; Granick, S. *J. Am. Chem. Soc.* (2000) **122**, 9550-9551.
- [90] Yang, S.Y.; Rubner, M.F. *J. Am. Chem. Soc.* (2002) **124**, 2100-2101.
- [91] Kharlampieva, E.; Sukhishvili, S.A. *Langmuir* (2004) **20**, 9677-9685.
- [92] Lee, D.; Rubner, M.F.; Cohen, R.E. *Chem. Mater.* (2005) **17**, 1099-1105.
- [93] Fu, Y.; Bai, S.; Cui, S.; Qiu, D.; Wang, Z.; Zhang, X. *Macromolecules* (2002) **35**, 9451-9458.
- [94] Kozlovskaya, V.; Ok, S.; Sousa, A.; Libera, M.; Sukhishvili, S.A. *Macromolecules* (2003) **36**, 8590-8592.
- [95] Kozlovskaya, V.; Yakovlev, S.; Libera, M.; Sukhishvili, S.A. *Macromolecules* (2005) **38**, 4828-4836.
- [96] Kozlovskaya, V.; Kharlampieva, E.; Mansfield, M.L.; Sukhishvili, S.A. *Chem. Mater.* (2006) **18**, 328-336.
- [97] Yang, S.Y.; Lee, D.; Cohen, R.E.; Rubner, M.F. *Langmuir* (2004) **20**, 5978-5981.
- [98] Izumrudov, V.; Sukhishvili, S.A. *Langmuir* (2003) **19**, 5188-5191.
- [99] Izumrudov, V.; Kharlampieva, E.; Sukhishvili, S.A. *Macromolecules* (2004) **37**, 8400-8406.
- [100] Kharlampieva, E.; Sukhishvili, S.A. *Macromolecules* (2003) **36**, 9950-9956.
- [101] Cho, J.; Caruso, F. *Macromolecules* (2003) **36**, 2845-2851.
- [102] Li, Q.; Quinn, J.F.; Caruso, F. *Adv. Mater.* (2005) **17**, 2058-2062.
- [103] Onda, M.; Lvov, Y.; Ariga, K.; Kunitake, T. *J. Fermentation Bioeng.* (1996) **82**, 502-506.
- [104] Anzai, J.-i.; Kobayashi, Y.; Nakamura, N. *J. Chem. Soc., Perkin Trans.* (1998) **2**, 461-462.
- [105] Schüller, C.; Caruso, F. *Macromol. Rapid Commun.* (2000) **21**, 750-753.
- [106] Caruso, F.; Schüller, C. *Langmuir* (2000) **16**, 9595-9603.
- [107] Sato, K.; Imoto, Y.; Sugama, J.; Seki, S.; Inoue, H.; Odagiri, T.; Hoshi, T.; Anzai, J.-i. *Langmuir* (2005) **21**, 797-799.
- [108] Chinnayelka, S.; McShane, M.J. *J. Fluorescence* (2004) **14**, 585-595.

- [109] De Geest, B.G.; Jonas, A.M.; Demeester, J.; De Smedt, S.C. *Langmuir* (2006) **22**, 5070-5074.
- [110] Lorand, J.P.; Edwards, J.O. *J. Organic Chem.* (1959) **24**, 769-774.
- [111] Springsteen, G.; Wang, B. *Tetrahedron* (2002) **58**, 5291-5300.
- [112] Norrild, J.C.; Eggert, H. *J. Am. Chem. Soc.* (1995) **117**, 1479-1484.
- [113] Shoji, E.; Freund, M.S. *J. Am. Chem. Soc.* (2002) **124**, 12486-12493.
- [114] Striegler, S. *Curr. Organic Chem.* (2003) **7**, 81-102.
- [115] Davis, A.P.; Wareham, R.S. *Angew. Chem. Int. Ed.* (1999) **38**, 2979-2996.
- [116] James, T.D.; Samankumara Sandanayake, K.R.A.; Shinkai, S. *Angew. Chem. Int. Ed.* (1996) **35**, 1911-1922.
- [117] Wang, W.; Gao, X.; Wang, B. *Curr. Organic Chem.* (2002) **6**, 1285-1317.
- [118] Fang, H.; Kaur, G.; Wang, B. H. *J. Fluorescence* (2004) **14**, 481-489.
- [119] Shiino, D.; Kataoka, K.; Koyama, Y.; Yokoyama, M.; Okano, T.; Sakurai, Y. *J. Controlled Release* (1994) **28**, 317-318.
- [120] Kataoka, K.; Miyazaki, H.; Bunya, M.; Okano, T.; Sakurai, Y. *J. Am. Chem. Soc.* (1998) **120**, 12694-12695.
- [121] Antipov, A.A.; Sukhorukov, G.B. *Adv. Colloid Interface Sci.* (2004) **111**, 49-61.
- [122] Sukhorukov, G.B.; Fery, A.; Brumen, M.; Möhwald, H. *PCCP* (2004) **6**, 4078-4089.
- [123] Sukhorukov, G.B.; Brumen, M.; Donath, E.; Möhwald, H. *J. Phys. Chem. B* (1999) **103**, 6434-6440.
- [124] Ibarz, G.; Dähne, L.; Donath, E.; Möhwald, H. *Adv. Mater.* (2001) **13**, 1324-1327.
- [125] Ibarz, G.; Dähne, L.; Donath, E.; Möhwald, H. *Macromol. Rapid Commun.* (2002) **23**, 474-478.
- [126] von Klitzing, R.; Möhwald, H. *Macromolecules* (1996) **29**, 6901-6906.
- [127] Ibarz, G.; Dähne, L.; Donath, E.; Möhwald, H. *Chem. Mater.* (2002) **14**, 4059-4062.
- [128] Antipov, A.A.; Sukhorukov, G.B.; Donath, E.; Möhwald, H. *J. Phys. Chem. B* (2001) **105**, 2281-2284.
- [129] Antipov, A.A.; Sukhorukov, G.B.; Möhwald, H. *Langmuir* (2003) **19**, 2444-2448.
- [130] Moya, S.; Donath, E.; Sukhorukov, G.B.; Auch, M.; Bäumlner, H.; Lichtenfeld, H.; Möhwald, H. *Macromolecules* (2000) **33**, 4538-4544.
- [131] Georgieva, R.; Moya, S.E.; Bäumlner, H.; Möhwald, H.; Donath, E. *J. Phys. Chem. B* (2005) **109**, 18025-18030.

- [132] Lvov, Y.; Antipov, A.A.; Mamedov, A.; Möhwald, H.; Sukhorukov, G.B. *Nano. Lett.* (2001) **1**, 125-128.
- [133] Antipov, A.A.; Sukhorukov, G.B.; Leporatti, S.; Radtchenko, I.L.; Donath, E.; Möhwald, H. *Colloids Surfaces A* (2002) **198-200**, 535-541.
- [134] Sukhorukov, G.B.; Antipov, A.A.; Voigt, A.; Donath, E.; Möhwald, H. *Macromol. Rapid Commun.* (2001) **22**, 44-46.
- [135] Déjugnat, C.; Haložan, D.; Sukhorukov, G.B. *Macromol. Rapid Commun.* (2005) **26**, 961-967.
- [136] Tong, W.; Gao, C.; Möhwald, H. *Macromolecules* (2006) **39**, 335-340.
- [137] Kozlovskaya, V.; Sukhishvili, S.A. *Macromolecules* (2006) **39**, 5569-5572.
- [138] Qiu, X.; Donath, E.; Möhwald, H. *Macromol. Mater. Eng.* (2001) **286**, 591-597.
- [139] Caruso, F.; Yang, W.; Trau, D.; Renneberg, R. *Langmuir* (2000) **16**, 8932-8936.
- [140] Balabushevitch, N.G.; Sukhorukov, G.B.; Moroz, N.A.; Volodkin, D.V.; Larionova, N.I.; Donath, E.; Möhwald, H. *Biotechnol. Bioeng.* (2001) **76**, 207-213.
- [141] Volodkin, D.V.; Petrov, A.I.; Prevot, M.; Sukhorukov, G.B. *Langmuir* (2004) **20**, 3398-3406.
- [142] Volodkin, D.V.; Larionova, N.I.; Sukhorukov, G.B. *Biomacromolecules* (2004) **5**, 1962-1972.
- [143] Petrov, A.I.; Volodkin, D.V.; Sukhorukov, G.B. *Biotechnol. Progr.* (2005) **21**, 918-925.
- [144] Radtchenko, I.L.; Sukhorukov, G.B.; Leporatti, S.; Khomutov, G B.; Donath, E.; Möhwald, H. *J. Colloid Interface Sci.* (2000) **230**, 272-280.
- [145] Radtchenko, I.L.; Sukhorukov, G.B.; Möhwald, H. *Colloids Surfaces A* (2002) **202**, 127-133.
- [146] Dähne, L.; Leporatti, S.; Donath, E.; Möhwald, H. *J. Am. Chem. Soc.* (2001) **123**, 5431-5436.
- [147] Hesse, M.; Meier, H.; Zeeh, B. *Spektroskopische Methoden in der organischen Chemie* Georg Thieme Verlag, Stuttgart, 1995.
- [148] Atkins, P.W. *Physikalische Chemie* VCH, Weinheim, 1996.
- [149] Skoog, D.A.; Leary, J.J. *Instrumentelle Analytik: Grundlagen - Geräte - Anwendungen* Springer, Berlin, 1996.
- [150] Sheppard, J.R.; Shotton, D.M. *Confocal Laser Scanning Microscopy* Bios Scientific Publishers, Oxford, 1997.
- [151] Israelachvili, J.N. *Intermolecular and Surface Forces* Academic Press, London, 2002.



- [152] Lichtenfeld, H.; Stechemesser, H.; Möhwald, H. *J. Colloid Interface Sci.* (2004) **276**, 97-105.
- [153] Sauerbrey, G. *Zeitschrift f. Physik* (1959) **155**, 206-222.
- [154] Rodahl, M.; Kasemo, B. *Sensors Actuators A* (1996) **54**, 448-456.
- [155] Rodahl, M.; Höök, F.; Fredriksson, C.; Keller, C.A.; Krozer, A.; Brzezinski, P.; Voinova, M.; Kasemo, B. *Faraday Discuss.* (1997) **107**, 229-246.
- [156] Johannsmann, D. *Macromol. Chem. Phys.* (1999) **200**, 501-516.
- [157] Binnig, G.; Quate, C.F.; Gerber, C. *Physical Rev. Lett.* (1986) **56**, 930-933.
- [158] Garcia, R.; Perez, R. *Surface Sci. Rep.* (2002) **47**, 197-301.
- [159] Magonov, S.N.; Reneker, D.H. *Ann. Rev. Mater. Sci.* (1997) **27**, 175-222.
- [160] Kanayama, N.; Kitano, H. *Langmuir* (2000) **16**, 577-583.
- [161] Ramsden, J.J.; Lvov, Y.M.; Decher, G. *Thin Solid Films* (1995) **254**, 246-251.
- [162] Leporatti, S.; Voigt, A.; Mitlöhner, R.; Sukhorukov, G.B; Donath, E.; Möhwald, H. *Langmuir* (2000) **16**, 4059-4063.
- [163] Dubas, S.T.; Schlenoff, J.B. *Macromolecules* (2001) **34**, 3736-3740.
- [164] Arnold, R. *J. Colloid Sci.* (1957) **12**, 549-556.
- [165] Perrin, D.D. *Ionization Constants of Inorganic Acids and Bases in Aqueous Solution* 2nd ed.; Pergamon, Oxford, 1982.
- [166] Ahrens, H.; Foerster, S.; Helm, C.A. *Physical Rev. Lett.* (1998) **81**, 4172-4175.
- [167] Currie, E.P.K.; Sieval, A.B.; Fleer, G.J.; Cohen Stuart, M.A. *Langmuir* (2000) **16**, 8324-8333.
- [168] Biesalski, M.; Johannsmann, D.; Rühle, J. *J. Chem. Phys.* (2002) **117**, 4988-4994.
- [169] Biesheuvel, P.M. *J. Colloid Interface Sci.* (2004) **275**, 97-106.
- [170] Dai, J.; Jensen, A.W.; Mohanty, D.K.; Erndt, J.; Bruening, M.L. *Langmuir* (2001) **17**, 931-937.
- [171] Satoh, M.; Yoda, E.; Hayashi, T.; Komiyama, J. *Macromolecules* (1989) **22**, 1808-1812.
- [172] Schulz, S.F., Gislser, T.; Borkovec, M.; Sticher, H. *J. Colloid Interface Sci.* (1994) **164**, 88-98.
- [173] Tanchak, O.M.; Barrett, C.J. *Chem. Mater.* (2004) **16**, 2734-2739.
- [174] Sokrates, G. *Infrared and Raman Characteristic Group Frequencies* 3rd ed., John Wiley & Sons Ltd., Chichester, 2001.

- 
- [175] Wang, L.; Fu, Y.; Wang, Z.; Fan, Y.; Zhang, X. *Langmuir* (1999) **15**, 1360-1363.
- [176] Abe, K.; Senoh, S. *J. Polymer Sci. A* (1986) **24**, 3461-3474.
- [177] Gao, C.; Donath, E.; Moya, S.; Dudnik, V.; Möhwald, H. *Eur. Phys. J. E* (2001) **5**, 21-27.
- [178] Gao, C.; Leporatti, S.; Moya, S.; Donath, E.; Möhwald, H. *Langmuir* (2001) **17**, 3491-3495.
- [179] Wang, Q. *J. Phys. Chem. B* (2006) **110**, 5825-5828.
- [180] Lulevich, V.V.; Vinogradova, O.I. *Langmuir* (2004) **20**, 2874-2878.
- [181] Jaber, J.A.; Schlenoff, J.B. *J. Am. Chem. Soc.* (2006) **128**, 2940-2947.
- [182] Biesheuvel, P.M. *J. Colloid Interface Sci.* (2001) **238**, 362-370.
- [183] Biesheuvel, P.M.; Cohen Stuart, M.A. *Langmuir* (2004) **20**, 4764-3770.
- [184] Elsner, N. *dissertation MPI-KG*, Potsdam (2006), p.59, p. 105.
- [185] Müller, R.; Köhler, K.; Weinkamer, R.; Sukhorukov, G.B.; Fery, A. *Macromolecules* (2005) **38**, 9766-9771.
- [186] Ochiai, H.; Anabuki, Y.; Kojima, O.; Tominaga, K.; Murakami, I. *J. Polymer Sci. B* (1990) **28**, 233-240.
- [187] Jones, G.H.; Ballou, C.E. *J. Biological Chem.* (1969) **244**, 1043-1051.
- [188] Kath, F.; Kulicke, W.M. *Angew. Makromol. Chem.* (1999) **268**, 69-80.

## List of publications

Mauser, T.; Déjugnat, C.; Sukhorukov, G.B. *Reversible pH-dependent properties of multilayer microcapsules made of weak polyelectrolytes*, *Macromol. Rapid Commun.* (2004) **25**, 1781-1785.

Mauser, T.; Déjugnat, C.; Möhwald, H.; Sukhorukov, G.B. *Microcapsules made of weak polyelectrolytes: templating and stimuli-responsive properties*, *Langmuir* (2006) **22**, 5888-5893.

Mauser, T.; Déjugnat, C.; Sukhorukov, G.B. *Balance of hydrophobic and electrostatic forces in the pH response of weak polyelectrolyte capsules*, *J. Phys. Chem. B* (2006) **accepted**.

Biesheuvel, P.M.; Mauser, T.; Sukhorukov, G.B.; Möhwald, H. *Micromechanical theory for pH-dependent polyelectrolyte multilayer capsule swelling*, *Macromolecules* (2006) **submitted**.

# I would like to thank

Prof. H. Möhwald for giving me the opportunity to do my PhD at the MPI-KGF under excellent working conditions and for his continuing interest and support.

My supervisor, Prof. G. B. Sukhorukov for providing me with an interesting topic and for his support and many helpful discussions.

Dr. Christophe Déjугnat and Dr. Radostina Georgieva for their help in solving scientific problems and for many new ideas.

Dr. Maarten Biesheuvel for many interesting discussions and for the development of a theoretical model for the swelling behavior of weak polyelectrolyte capsules.

Annemarie Heilig for her great support with the AFM measurements, Heidi Zastrow for her help with the SPLS measurements, Dr. J. Hartmann for the EDX data, Dr. Michelle Prevot and Dr. Dmitry Shchukin for providing me with SEM pictures and Annegret Praast for her assistance in the lab.

All members of Gleb's group for the nice working atmosphere and their help and support in everyday life.

All colleges at the MPI-KGF, who made my time there unforgettable.

My family and Gregor for their continuing support.

Finally, I gratefully acknowledge the financial support by the Sofja Kovalevskaja program of the Alexander von Humboldt foundation and the 6th FP EU-project STREP001428 "Nanocapsules for Targeted Controlled Delivery of Chemicals".